INVESTIGATION ON TARGET DESIGN FOR PERPENDICULAR MAGNETIC RECORDING CHANNELS

CHEN LI
(*B. Eng., Shanghai Jiaotong Univ., P. R. China*)

A THESIS SUBMITTED

FOR THE DEGREE OF MASTER OF ENGINEERING

DEPARTMENT OF ELECTRICAL AND COMPUTER ENGINEERING

NATIONAL UNIVERSITY OF SINGAPORE

2004

Acknowledgements

I would like to express my most sincere and heartfelt gratitude to Dr. George Mathew for his invaluable guidance, patience and support over the entire course of my master project. Dr. Mathew has always been ready to offer his assistance and expertise to my research work. Without his judicious advice and support, my completion of this project would not be possible. It is my utmost honor to be under his supervision.

I would like to extend my gratitude to Dr. Lin Yu, Maria, Ms Cai Kui, Mr. Zou Xiaoxin, and Mr. Lim Beng Hwa, who have been kindly sharing their knowledge and research experiences with me. My appreciation also goes to all the staff and students in Data Storage Institute, who have helped me in one way or another.

I also wish to thank all of my friends for their encouragement and assistance to my study and living in Singapore.

On a personal note, I am truly grateful to my family, whose solid support has accompanied me all the time.

Table of Contents

Summary

The partial-response maximum-likelihood (PRML) receiver is the indispensable signal detection technique for high-performance digital magnetic recording systems. Currently, perpendicular recording is receiving increasing interest, as it promises to achieve much higher storage densities than the commercially used longitudinal recording technology. The receiver design strategies need to be re-investigated for perpendicular recording, since its channel response is different from that of longitudinal recording. In this thesis, we focus on the design of PRML detection strategy for perpendicular recording channel at high densities.

To optimize the performance of PRML systems, the partial-response (PR) target should be well designed to reduce noise enhancement at the input of Viterbi detector (VD). The minimum mean square error (MMSE) and noise-predictive maximum-likelihood (NPML) approaches are widely used for designing generalized PR (GPR) target. However, the MMSE criterion does not account for the noise correlation that can badly degrade the performance of VD, and the performance of NPML system may be limited if the primary target in system is not well optimized.

In this thesis, we design GPR target by maximizing the effective detection signal-to-noise ratio (SNR_{eff}), which is an equivalent measure of the bit-error-rate (BER) performance of VD. Hence, it is reasonable to claim that the target designed by the SNR_{eff} criterion achieves the optimum performance of VD. In this thesis, we develop a

novel approach for finding the optimum targets based on SNR_{eff} and show that all these optimum targets take the same magnetic frequency response. This thesis is the first to report closed-form analytical solutions for optimum targets based on SNR_{eff} and the characterization of the performance surface of SNR_{eff}. Numerical and simulation results are provided to corroborate the analytical results.

We also investigate the target design problem with emphasis on combating media noise, which is data-dependant and highly correlated. There have been a few methods proposed to adjust the branch metrics of VD according to the data-dependent correlation, variance and/or mean of media noise. In this thesis, we propose to tune VD to the targets designed by the modified SNR_{eff} criterion, which incorporates the noise statistics conditioned on each data pattern. Simulation results show that in the channel with high media noise, this approach yields a gain of about 0.5 dB at a BER of 10^{-4} over the existing approaches that aim to deal with media noise.

List of Symbols and Abbreviations

a_k	input data bit
$\hat{a}_k$	detected data bit
b_k	transition data
k_0	sampling phase delay
L_s	oversampling factor
w_k	coefficients/tap weights of equalizer
g_k	coefficients/tap weights of target response
Δ_k	transition position jitter
ϖ_k	transition pulse width variation
$G(D)$	D transform of target
$W(D)$	D transform of equalizer
$P_r(x)$	probability of x
$p_r(\cdot)$	probability density function
$x\|y$	x conditioned on y
$Q(\cdot)$	tail integration of Gaussian probability density function
$W_H(x)$	Hamming weight of x

$E[\cdot]$	expectation operator
$f(t)$	isolated transition response of magnetic recording channel
$h(t)$	pulse/dibit response of magnetic recording channel
T_c	channel bit period
T_u	user bit period
K_c	normalized channel linear density
K_u	normalized user density
R_c	code-rate
T_{50}	pulse-width of isolated transition response at 50% amplitude
$\mathrm{P}_a\left(e^{j2\pi\Omega}\right)$	power spectral density of input data
$\mathrm{P}_n\left(e^{j2\pi\Omega}\right)$	power spectral density of noise
SNR_{eff}	effective detection signal-to-noise ratio
BER	bit-error-rate
SNR	signal-to-noise ratio
PSD	power spectral density
PDF	probability density function
ECC	error control coding
PAM	pulse-amplitude-modulation
NRZI	non-return to zero inverse
MTR	maximum transition run
MAP	maximum *a posteriori* probability
PR	partial response
GPR	generalized partial response
ML	maximum-likelihood

SBS	symbol-by-symbol
MLSD	maximum-likelihood sequence detection
NPML	noise-predictive maximum-likelihood
VA	Viterbi algorithm
AWGN	additive white Gaussian noise
ISI	inter-symbol interference
NLTS	Nonlinear transition shift
HTS	hard transition shift
DFE	decision feedback equalization
RAM	random access memory
MMSE	minimum mean square error
ZF	zero-forcing
LPF	low-pass filter
IIR	infinite impulse response
FIR	finite impulse response

List of Figures

List of Tables

Chapter 1

Introduction

In this chapter, we first give a description of the overall magnetic recording system, and briefly introduce perpendicular recording technology and characteristics of noises in magnetic recording systems. Then, a survey of the existing literature on detection techniques for magnetic recording systems is presented. Thereafter, the motivation and summary of the work reported in this thesis are given. Finally, the organization of the thesis is outlined.

1.1 Magnetic Recording System

The advent of digital computer spurred the development of magnetic data storage systems (for example, hard disk drives) capable of storing large amounts of digital information. To accommodate the growing demand for the storage of digital data, improvements in storage density and data transfer rate capabilities are continuously being done since the beginning of magnetic recording technology. As a result, this technology has been making progress in leaps and bounds. Over the past five decades, breakthroughs in head and media technologies have been the major contributing

factors to the spectacular growth in storage capacity. However, signal processing and coding techniques are recognized as important and cost-efficient means for supporting as well as enhancing the storage capacity of a given head-medium combination [1]. Hence, the field of coding and signal processing has been playing an important role in modern magnetic storage systems.

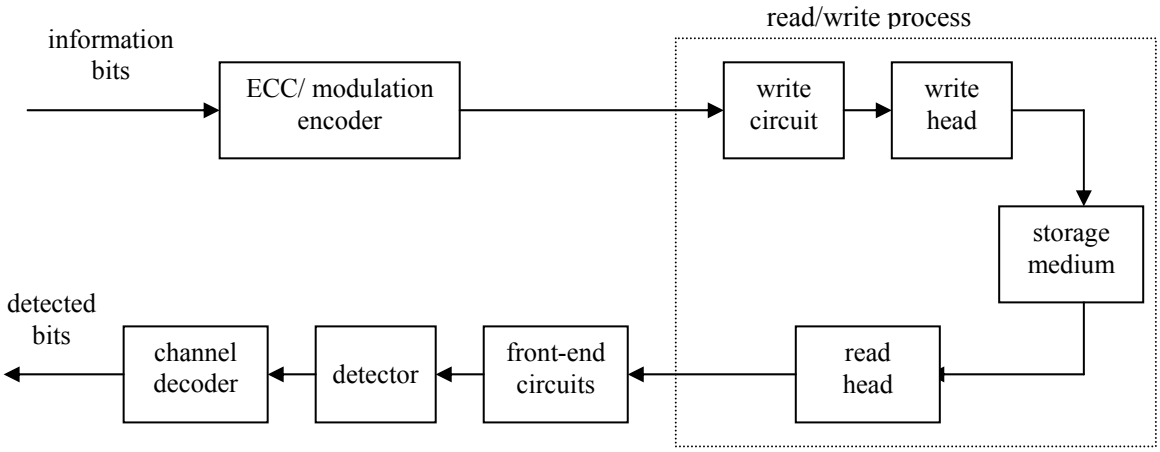

Figure 1.1: Block diagram of a digital magnetic recording system.

Figure 1.1 depicts the block diagram of a general digital magnetic recording system. The binary information bits (i.e. user data) are first fed to a two-stage channel encoder. The ECC (error control coding) encoding introduces error detection and correction capability, while the modulation coding on the second stage helps to maintain channel linearity and sufficient excitation for the control loops (e.g. gain, timing recovery) at the receiver. Following the channel encoder, the write circuit converts the coded data into a rectangular current waveform (write current) by NRZI (non-return-to-zero inverse) modulation technique [2]. The write current then drives the write head to magnetize the storage medium to saturation in the direction, which is determined by the polarity of the write current waveform in each bit interval. In the readback process, the read head converts the magnetic flux to a voltage output signal,

which reflects the transitions in the pattern of magnetization stored on the medium. Usually, the read head circuit is embedded with a preamplifier that magnifies the read voltage by several hundred times. The front-end circuits in general consist of a low-pass filter for band-limiting the readback signal, a sampler, timing recovery and gain control circuits, and an equalizer for shaping the channel response to facilitate better detection of the data bits. The detector recovers the encoded data and passes them to the decoder for recovering the original information bits.

The signal path starting from the input of write circuit to the output of read head in Figure 1.1 is called the magnetic recording channel. This channel represents the main features of the read/write process in any recording system. The readback voltage pulse corresponding to an isolated transition in the data pattern stored on the medium is usually referred to as the isolated transition response or just transition response. Successive transition responses along the recording track alternate in polarity and partly cancel each other when spaced closely. Under reasonable recording conditions, the readback signal (noiseless) can be modeled as linear superposition of transition responses. Since the bit response of the channel (i.e. response to an isolated bit at the input) is linearly related to transition response, we can say that the magnetic recording channel resembles a base-band digital communication channel with pulse-amplitude-modulation (PAM).

Retrieving the stored data from magnetic recording systems would be effortless if the output of the recording channel were clean signals as the input. Unfortunately, the readback signals are always corrupted by channel noises, interferences and non-linear distortions, all of which particularly increase with recording density. The main purpose of detector is to combat these corruptions, and recover the stored data with a very stringent level of reliability. During the past decade, several digital detection

techniques were developed for disk drives to improve the reliability in view of the ever increasing density. In particular, the partial-response maximum-likelihood (PRML) detection [3], which was introduced in early 1990s in place of analog peak detection, significantly raised storage density capability and paved the way for applications of advanced coding and signal processing in disk drives. Extensive research work has been done in designing detection strategies for longitudinal recording, since commercial disk drives use this recording technology. In recent years, perpendicular recording has attracted increasing interest, as it promises to achieve much higher recording densities than the longitudinal one [4, 5]. Consequently, the detection strategies need to be re-investigated for perpendicular recording channels, whose transition response is much different from that of longitudinal recording channels. Further, most detection techniques that have been developed so far assume that the channel noise is an additive white Gaussian random process. However, this assumption is not true on high-density recording channels, because the media noise, which is a correlated, data-dependent and non-Gaussian random process, becomes the dominant noise source at high densities [6]. In this thesis, we focus on PRML detection strategy for perpendicular recording at high densities, with and without emphasis on combating media noise.

1.2 Introduction to Perpendicular Recording

In magnetic recording systems, most of the gain in areal density (number of bits per square inch) has been achieved by proportionally reducing all physical dimensions relevant to the recording process, including head size, bit length and the thickness of granular medium. Meanwhile, the refining of the medium microstructure, in

particular, reducing the size of ferromagnetic grains in the media, is of paramount importance to support the required "magnetic" resolution and to suppress noises. In the current longitudinal magnetic recording media, use of scaling to achieve even smaller bits and grain sizes, however, may cause serious thermal instability [7], thereby limiting the achievable areal density. However, perpendicular recording proposed by Iwasaki and Nakamura [4] is expected to extend the super-paramagnetic limit to a further point because of the intrinsic merits of this recording approach.

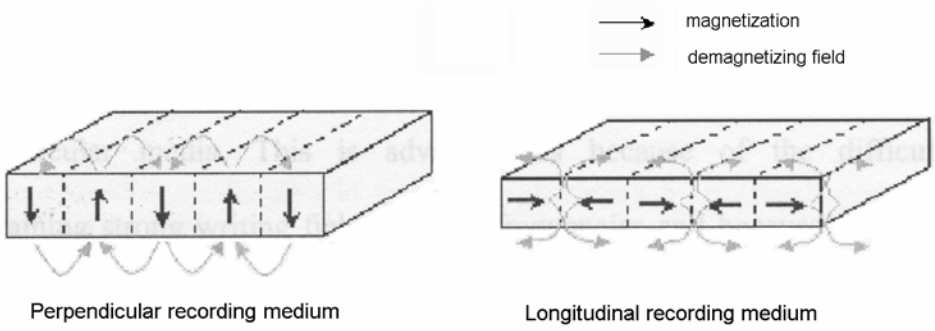

Figure 1.2: Demagnetizing fields in perpendicular and longitudinal recording media. The 'dark solid' arrows indicate the magnetization of each bit bell and the 'grey' arrows indicate the demagnetizing fields.

Due to the vertical magnetization pattern in perpendicular recording, the magnetic 'charges', which are the effective sources of demagnetizing fields, are distributed on the top and bottom of the medium layer (see Figure 1.2). In contrast, in longitudinal recording where the medium is magnetized horizontally along the track, the magnetic 'charges' are concentrated at the transitions of magnetization. As a result, the demagnetizing fields drop to zero at transitions in perpendicular recording, while they reach maxima right at the transitions in longitudinal recording. In addition, as shown in Figure 1.2, the demagnetizing fields work to reduce the strength of head-on magnetization at the transitions in longitudinal recording, thereby resulting in decrease

of output signal amplitude. In contrast to this, in perpendicular recording the demagnetizing fields assist to enhance neighboring magnetization coupling with each other at the transitions. Hence, perpendicular recording may use thicker medium than longitudinal one to realize similar recording resolution. The operation with thicker media can be translated into 'relaxed' thermal stability requirement [7]. Further, in perpendicular recording, the magnetization stability favored by demagnetizing fields increases with storage density, while longitudinal recording shows fatal thermal decay of written signals with repulsive demagnetization forces, especially at high densities. Therefore, perpendicular magnetic recording technology is considered to promote ultra-high density recording.

Besides promising ultra-high densities, perpendicular recording has other advantages, including strong head fields, sharp transitions and track edges, short wavelengths etc., as summarized in [8]. Along with these advantages, however, are also the challenges to the medium, read/write heads and signal processing for realizing perpendicular recording.

Although the storage industry has not started making products using perpendicular recording, the recent demonstrations of this technology boasted areal densities of about 100 Gbits/inch^2 [9, 10] by Seagate Technology and 146 Gbits/inch^2 by Read-Rite (now bankrupt) in November 2002 [10, 11]. These densities are comparable with or even higher than the highest densities reported for longitudinal recording [10, 12]. With further study and improvement in media and read/write head combinations, ultra-high areal densities in perpendicular recording can be expected [13].

1.3 Characteristics of Noises, Interferences and Non-linear Distortions in Magnetic Recording

The signals read from the magnetic recording channel are inevitably hampered by interferences, non-linear distortions and noises. In order to achieve as high recording densities as possible with acceptable reliability in signal detection, we first need to know the characteristics of noises, interferences and distortions in magnetic recording.

Interferences correspond to the presence of signals other than those intended in the readback signal. In magnetic recording systems, except for extremely low linear densities (number of bits per inch along the track), the isolated transition response spans several bits adjacent to the bit at the transition. This leads to overlapping of the successive transition responses along the recording track. The resulting interference is known as inter-symbol interference (ISI). At high linear densities, the transition response becomes even 'wider' with respect to a single bit period, and thereby results in more severe ISI. Nevertheless, this interference is deterministic, and in principle, may be reduced to an arbitrarily small level by proper design of detection strategy. The residual ISI (i.e. ISI that cannot be eliminated) adds to the noises in the magnetic recording systems.

Nonlinear distortions in magnetic recording systems refer to the phenomena that violate the linear superposition principle used to reconstruct the readback signal. As density increases, closely spaced magnetic transitions start to interact, and result in significant nonlinear effects, including transition shifts, transition broadening, partial erasure, overwrite etc [14]. The shift in transition positions is an important manifestation of nonlinearities. Nonlinear transition shift (NLTS) occurs when the write head field is influenced by the demagnetizing field from the previous transitions.

Another type of transition shift is called hard transition shift (HTS). In longitudinal recording, the cause of HTS is the demagnetizing field of the secondary transition, which is instantaneously formed at the leading edge of the head field opposing the residual media magnetization therein. In perpendicular recording, HTS is caused by the demagnetizing field at the leading side of the head that results from the background magnetization, irrespective of whether it is for or against the head field. Besides the effect of transition shift, the transition is broadened simultaneously if the influencing demagnetizing field is adverse to the head field. The broadening of transition results in a transition response with reduced amplitude and larger width. Overwrite effect refers to the nonlinear distortion caused by erasing old data on the medium with direct overwrite of new data. The residual magnetization left from previously stored data causes HTS in the transitions recorded for new data, which is the main manifestation of the overwrite effect. Another form of nonlinearities is partial erasure of adjacent transitions when they approach very close to each other at high linear densities. In the readback signal, this effect appears as a sudden reduction of the signal amplitude. Nonlinear distortions are deterministic and data dependant. Therefore, it is possible to control and minimize nonlinearities. In practice, the transition shift can be minimized to a large extent by using appropriate "write pre-compensation" techniques [15]. The partial erasure can be mitigated to a certain extent by using appropriate constrained codes, such as maximum transition run (MTR) codes that limit the maximum number of consecutive transitions, and write pre-compensation schemes [16].

Unlike interferences and nonlinear distortions, noises arise from the uncertainties in physical phenomena and need to be treated statistically. Noise in a digital magnetic recording system is a combination of thermal noise generated in the preamplifier, head noise, and media noise. In general, these three noise sources are mutually uncorrelated.

Head noise and thermal noise, which are the sources of electronics noise in magnetic recording, are well modeled as additive white Gaussian random processes. Media noise, which arises from irregularities and imperfections of the medium, is another major noise source in magnetic recording. In advanced disks using thin-film medium, media noise can be classified into modulation noise and transition noise [13, 17]. The former is generally due to unfavorably reversed magnetization domains at regions in between transitions. Full saturation of the medium throughout the bit-cells is necessary to reduce the modulation noise. This noise is independent of transitions, and tends to decrease with increasing densities because there are less non-transition areas at higher densities. The latter, i.e. the transition noise, comes from disordered transitions due to large magnetic domains and their size distribution, or due to easily moving domain walls. The transition noise is non-stationary in nature because it depends on the recording data pattern, and strictly speaking, cannot be modeled as additive noise. A simple, yet fairly general, model for transition noise is obtained by introducing random position jitter and width variation to the readback transition pulses [18][1]. It is indicated that, both in longitudinal and perpendicular recording, transition noise increases with recording density [19, 20], and becomes the dominant noise in high-density recording.

Thus far, considerable research has been done to investigate signal processing techniques for combating interferences, nonlinear distortions and noises in magnetic recording systems. Since nonlinear distortions can be effectively controlled during the writing process, we emphasize in this thesis on the detection methods applied to the magnetic recording channels corrupted by ISI, electronics noise and media noise. A brief review of the existing techniques in this area is provided in the next section.

[1] The work done in [18] was originally for longitudinal magnetic recording. However, the general model of transition noise proposed by [18] is also widely applied to perpendicular magnetic recording now, as the mechanisms of transition noise in both recording media are similar.

1.4 Literature Survey

The detectors that have been considered for digital recording systems can be classified into symbol-by-symbol (SBS) detector and sequence detector. The SBS detectors simply map the multilevel outputs of the channel into binary detected bits, usually with aid of suitable precoding and equalization as described in [21]. The sequence detectors make a symbol decision based on observation of channel outputs over many symbol intervals. In spite of their inherent decision delay and relatively high complexity, the sequence detectors are desirable because they significantly outperform SBS detectors in combating signal interferences. The prominent example of sequence detectors is the maximum-likelihood sequence detector (MLSD), which yields the optimum detection quality in the presence of ISI [22]. When the channel noise is additive and white Gaussian, MLSD can be efficiently implemented by using the Viterbi algorithm (VA) based on Euclidean distance metrics [22, 23, 24]. In practice, the VA detector is preceded by a partial-response (PR) equalizer that reduces the span of ISI. This technique is called partial-response maximum-likelihood (PRML) detection. In this section, we briefly survey the existing PRML detection strategies for digital magnetic recording channels. The review first focuses on typical PRML schemes developed with no regard to the data-dependence of noise. Thereafter, the review focuses on PRML detection techniques that take into account the data-dependence of media noise.

1.4.1 Typical PRML Detection Techniques

PRML detection is currently the predominant signal processing technique used in high-performance digital recording systems. The PR equalization typically uses a linear filter to shape the original channel bit response into a pre-determined PR target

response of reasonably short length. Following the equalizer, the VA detector tuned to this PR target performs sequence detection of the stored data bits. The key design problem in PRML scheme is about the choice of a suitable PR target, which is required to be a good match to the natural channel response to avoid mis-equalization and noise enhancement. More importantly, since the assumption of additive white Gaussian noise (AWGN) at the detector input is essential for the VA detector to be optimum (in the sense of maximum-likelihood) [22], the target design should particularly aim to minimize noise correlation at PR equalizer output.

Conventional PRML schemes, as proposed in [3, 25], employ standard PR targets with integer coefficients, which are chosen by simple inspection of their match to the natural channel response. The well-known example of targets for longitudinal recording is PR Class 4 (PR4) targets in the form of $(1-D)(1+D)^n$, where D denotes the 1-bit delay operator and n is a positive integer. With the recent interest in perpendicular recording, several studies have been carried out investigating the PR targets, for instance, PR2 and MEPR2, whose characteristics are similar to those of perpendicular magnetic recording channels [26, 27]. Although several standard PR targets have been investigated and proposed, these targets are quite different from the natural channel responses due to the integer constraint, especially at high linear densities. Therefore, the performances of standard PR targets based PRML systems may be quite limited.

At the cost of a minor increase in the complexity of VA detector, the generalized PR (GPR) targets with real-valued coefficients can provide close match to the natural channel, and thereby, achieve good performance. Several approaches have been considered to design GPR targets with finite length. The most widely used method is to jointly optimize the target and equalizer by the minimum mean square error

(MMSE) criterion, which minimizes the total power of residual ISI and noises at the output of the equalizer [28, 29, 30, 31]. To avoid trivial solutions, a constraint needs to be imposed on the target in the MMSE approach. Among the different constraints investigated for MMSE approach, the monic constraint, which restricts the first tap of target to be unity, outperforms other constraints [31]. In addition, the monic constrained MMSE criterion results in target and equalizer equivalent to the solutions of forward and backward filters in MMSE based decision feedback equalization (MMSE-DFE) system. In fact, the DFE system [32, 33] can be viewed as a special case of PRML receiver using a one-state VA detector with a minimum phase GPR target. It should be remarked that the MMSE method does not consider noise correlation at the equalizer output that may significantly impair the performance of VA detector. To whiten the correlated noise, a noise predictor may be used at the output of PR equalizer, which gives rise to noise-predictive maximum-likelihood (NPML) method [34]. NPML system is also a special case of PRML receiver, in which the VA detector is tuned to an effective GPR target that is obtained as the convolution of the primary PR target and the noise prediction-error filter. The performance of NPML may be limited as well, if the primary PR target used in the system is not well optimized.

Another method proposed to design GPR target is by minimizing the probability of the dominant error event in VA detector [31, 35], which is proportional to the bit-error-rate (BER) of PRML systems at medium-to-high signal-to-noise ratios (SNRs). As reported in [31], however, numerical search for optimum targets based on this approach costs large computational load, and whether the search leads to global optima is not clear. Further, to make the receiver structure more practical, adaptive algorithms

for optimizing the coefficients of target and equalizer are proposed in [29, 36, 45], since the channel characteristics are often unknown or slowly varying.

Other than the widely used linear PR equalization, nonlinear equalization by means of neural networks combined with VA detector has been proposed [37, 38] to mitigate the problems caused by non-additive transition noise and nonlinear distortions. The principle behind this approach is to use neural network as a nonlinear function approximator. The neural network is trained to minimize the output mean squared error.

1.4.2 PRML Detection with Modified VA Detector

At high recording densities, highly correlated and signal-dependant media noise becomes substantial, and it badly degrades the performance of VA detector designed for channels with AWGN [39, 40, 41]. Recently, researchers have attempted to remedy this problem by modifying the Euclidian distance metric computations in the VA to account for the correlation and data-dependence of media noise [42, 43, 44, 45, 58]. By modeling media noise as a finite-order Markov process [42], the branch metrics in VA are computed using the conditional second-order noise statistics, and result in a signal-dependent and correlation-sensitive MLSD. The same detector structure has been derived in [43] from the viewpoint of linear prediction of noise, by using the same noise model as in [42]. Regardless of the noise correlation, some studies have proposed to modify the branch metrics in VA according to the data-dependant power and/or mean of the noise, as described in [44, 58] and [45, 46], respectively. In short, these approaches address the signal-dependent nature of media noise by allowing each branch in VA to independently account for the noise associated with the corresponding state transition. The resulting VA in each case either requires

more states and branches or utilizes feedback to reduce the number of states required. In particular, the complexity of signal-dependent VA exponentially increases with the length of data pattern considered in the design. An advantage of these schemes is that they assume the usual PR equalization, and hence they can be easily integrated into existing PRML systems.

It has also been proposed to use a modified adaptive random access memory DFE (RAM-DFE) to compensate for the channel nonlinearities caused by media noise, which cannot be accurately anticipated or eliminated in a fixed design. In RAM-DFE, the usual linear feedback path is replaced by a look-up-table or RAM as described in [48]. The proposed method [47] is to implicitly adjust the threshold of the RAM-DFE by adding a constant to each memory location in RAM. This constant is automatically determined by the adaptive algorithm proposed in [48].

1.5 Motivation and Summary of the Present Work

In this thesis, we propose a novel analytical approach for designing optimum GPR targets for high-density perpendicular recording channels, based on the cost function that is closely related to the BER performance of PRML systems. We also propose the approach for designing targets to combat media noise. The motivation and summary of the current work reported in this thesis are briefly presented in two parts. The first part is about designing optimum GPR targets for PRML systems using the conventional VA detector. The second part is about designing optimum GPR targets that account for the data-dependence of media noise, and subsequently developing a modified VA with the proposed data-dependent targets.

1.5.1 Design of Data-Independent Optimum GPR Target

PRML detection is widely used in modern magnetic recording systems. Design of PR target is critical to the performance of PRML scheme. The target should well match the natural channel response so as to reduce mis-equalization, noise enhancement and noise coloration, which impair the performance of VA detector. On the other hand, the target should help to increase the noise immunity of VA detector by enhancing the minimum Euclidean distance between any two distinct noiseless signal sequences at the output of PR equalized channel [49]. Most of the existing approaches for designing target do not take all of these factors into account.

In this thesis, we design GPR target by maximizing effective detection SNR (SNR_{eff}), which is an equivalent measure of the BER performance of VA detector at medium-to-high channel SNRs. Therefore, it is reasonable to expect the optimum target based on the SNR_{eff} criterion to achieve the optimum BER performance in PRML receivers. This criterion was investigated in [31] and [35]. However, the complete analytical solution of the optimum target based on this criterion is not yet available and the characterization of the stationary points of SNR_{eff} has not been reported so far. In this thesis, we propose a novel approach for designing optimum targets based on the SNR_{eff} criterion. Using a frequency-domain approach, we first show that the optimum target that maximizes SNR_{eff} is unique in its magnitude frequency response. Then, we derive closed-form analytical solutions for the optimum magnitude frequency response of the GPR target. Using our analytical approach, we clarify that all the optima of SNR_{eff} are global optima and take the same magnitude frequency response. These analytical results are corroborated by the numerical results

obtained through an iterative algorithm that we developed to search for the maximum of SNR_{eff} .

We evaluate the BER performance of PRML systems for perpendicular magnetic recording channels using the optimum GPR target designed by our approach, and compare with targets from existing approaches. Simulation results show that our approach achieves the best performance compared to the rest. In addition, our investigation of the performances of different targets shows that noise correlation is the major cause for the degradation of performance in PRML systems.

1.5.2 Design of Data-Dependent Optimum GPR Target

In order to better combat media noise, which is highly correlated and data-dependent, the detector needs to be data-dependant too. There have been a few methods proposed to modify the branch metrics of VA detector with emphasis on data-dependent correlation, variance or mean of the noise. However, these statistics of noise do not fully govern the performance of VA detector. In this thesis, we derive a modified SNR_{eff} criterion for target design by incorporating the conditional correlation of media noise. Therefore, the resulting target accounts for the data-dependent nature of media noise, and is expected to produce the optimum performance for any particular data pattern. We also propose to compute the branch metrics of VA detector with the data-dependent target designed by the modified SNR_{eff} criterion. Note that media noise is highly correlated, and thus its conditional statistics depend on a large span of the input data. For the sake of convenience and practical implementation, we have to restrict to a short span of data pattern when designing the target based on the modified SNR_{eff} criterion. We also note that longer span of data pattern leads to more accurate

estimation of the noise statistics, which may improve the performance of the proposed target. However, the size of VA trellis (or, complexity of VA) increases with the length of data pattern. A compromising approach that allows the use of long span of data patterns is to use the data bits from the survivor paths in the VA trellis. Simulation results show that the proposed modified VA detector yields performance gains when applied to the perpendicular recording channels with media noise.

1.6 Organization of the Thesis

The rest of the thesis is organized as follows. Chapter 2 presents a detailed description of magnetic recording channel models and PRML detection technique. Chapter 3 gives the development of the proposed approaches for designing optimum targets based on the SNR_{eff} criterion. Performance comparison of the proposed approach with existing approaches is also presented in this chapter. Chapter 4 is devoted to the characterization of the performance surface defined by SNR_{eff}. In Chapter 5, the method of designing optimum target to deal with data-dependant media noise is proposed. Finally, Chapter 6 concludes the work reported in this thesis and lists some possible directions of future work.

Chapter 2

Background on Signal Processing for Digital Magnetic Recording

As we have introduced in Chapter 1, PRML approach is currently the most widely used technique for signal detection in high-performance digital magnetic recording systems. To further improve the performance of PRML receiver in magnetic recording channels, we first need to have good understanding of the two blocks that constitute a PRML receiver: PR equalizer and Viterbi algorithm (VA) detector. In this Chapter, the model of digital magnetic recording channel with electronics noise and media noise is described in Section 2.1. Subsequently, Viterbi algorithm and typical linear PR equalization methods are detailed in Sections 2.2 and 2.3, respectively.

2.1 Digital Magnetic Recording Channel Model

In this section, we introduce a widely used approach of modeling digital magnetic read/write processes. Then, we describe the equivalent discrete-time models of the digital magnetic recording channel with and without media noise.

2.1.1 Magnetic Recording Channel with Electronics Noise

Figure 2.1 depicts the functional schematic of the read/write process in a conventional digital magnetic recording system, which consists of write-circuit, write-head/medium/read-head assembly and associated pre-processing circuitry. We start to mathematically develop a model of the magnetic read/write process in the presence of electronics noise only. Electronics noise is usually considered as AWGN. The modeling of media noise will be detailed in Section 2.1.2.

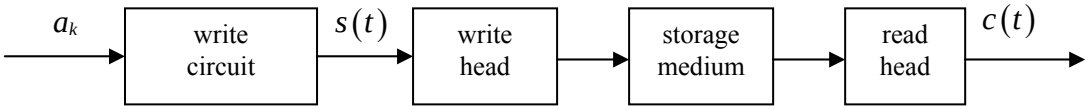

Figure 2.1: Functional schematic of the magnetic read/write process.

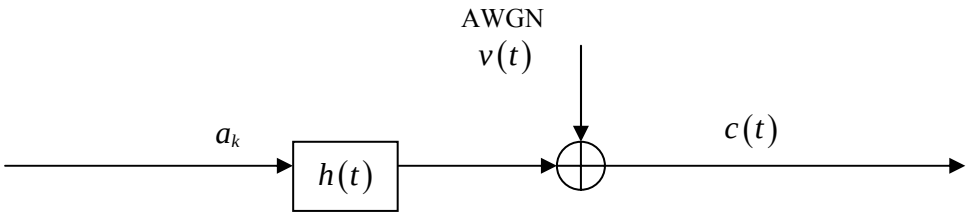

Figure 2.2: Continuous-time model of digital magnetic recording channel.

As shown in Figure 2.1, a binary data sequence $a_k \in \{+1, -1\}$ is first fed into the write circuit at the rate of $1/T$ (T denotes the channel bit period). The write circuit is a linear pulse modulator, and its impulse response is given by an ideal rectangular pulse of duration T and amplitude 1.0. Consequently, it converts the bit sequence a_k into a rectangular current waveform $s(t)$, whose amplitude swings between +1 and -1, corresponding to the bit sequence a_k. This current waveform drives the write

head to magnetize the bit-cell in the storage medium to saturation in a certain direction when $s(t)=+1$ and in the reverse direction when $s(t)=-1$. Clearly, the magnetization directions in the medium reflect the data sequence a_k.

In the readback process, the read head, either an inductive head or a magneto-resistive (MR) head, performs the flux-to-voltage conversion. The read head responds to the magnetic flux emanating from the transitions of magnetization in the medium. For an isolated magnetization transition corresponding to the data transition from -1 to $+1$, the read head produces a voltage pulse, $f(t)$, while for an inverse transition it outputs $-f(t)$. This readback voltage pulse $f(t)$, which is usually referred to as isolated transition response, is a low-pass type of response due to the combined effect of (head) gap loss, (thin-film) thickness loss, and write-process loss [50]. Assuming that the linearity of channel is maintained in the course of read/write process, the readback signal can be reconstructed by the superposition of all transition responses resulting from the stored data pattern. We may introduce a sequence $b_k \in \{+1, 0, -1\}$ where '$+1$' and '-1' indicate the presence of positive and negative transitions, respectively, and '0' indicates the absence of transition. Therefore, the noiseless readback signal can be expressed as $d(t)=\sum_k b_k f(t-kT)$. Noting that electronics noise is added at the output of the read head, the readback waveform is modeled as

$$c(t)=d(t)+v(t)=\sum_k b_k f(t-kT)+v(t), \tag{2.1}$$

where $v(t)$ represents the electronics noise. It is easy to find that

$$b_k=(a_k-a_{k-1})/2. \tag{2.2}$$

Therefore, the readback waveform may be re-written as

$$c(t)=\sum_k a_k h(t-kT)+v(t), \tag{2.3}$$

where $h(t)=\frac{1}{2}[f(t)-f(t-T)]$ is bit response or pulse response or dibit response. Eqn. (2.3) shows that the overall read/write process is mathematically modeled as a pulse-amplitude modulated channel with input data sequence a_k, effective symbol response $h(t)$, and additive noise $v(t)$. Figure 2.2 depicts the channel model represented by (2.3).

Based on experimental data, the isolated transition response in longitudinal recording is well modeled by the Lorentzian pulse given by [17, 50]

$$f(t)=\frac{2V_p}{1+\left(\frac{2t}{T_{50}}\right)^2}, \tag{2.4}$$

where V_p is half of the base-to-peak amplitude, and T_{50} refers to the temporal width of the pulse at its 50% amplitude level. In perpendicular recording channel, where giant MR read head and double-layered medium are employed, the isolated transition response is widely approximated either by an arctangent function [27, 30] defined as

$$f(t)=\frac{2V_p}{\pi}\arctan\left(\frac{2t}{T_{50}}\right), \tag{2.5a}$$

or by a hyperbolic tangent function [26, 51] defined as

$$f(t)=V_p\tanh\left(\frac{\ln 3}{T_{50}}t\right). \tag{2.5b}$$

Different from its definition in Lorentzian function, T_{50} used in (2.5a) and (2.5b) refers to the time duration required for $f(t)$ to rise from $-V_p/2$ to $V_p/2$. We may take T_{50} as a measure of the channel linear density by defining the normalized linear density as $K_c=T_{50}/T$. Denoting the duration of user input data[1] bit by T_u, the quantity defined as $K_u=T_{50}/T_u$ is called the normalized user density, which is a measure of the linear

[1] The data bits before and after channel encoding (see Figure 1.1) are called user data and channel data, respectively.

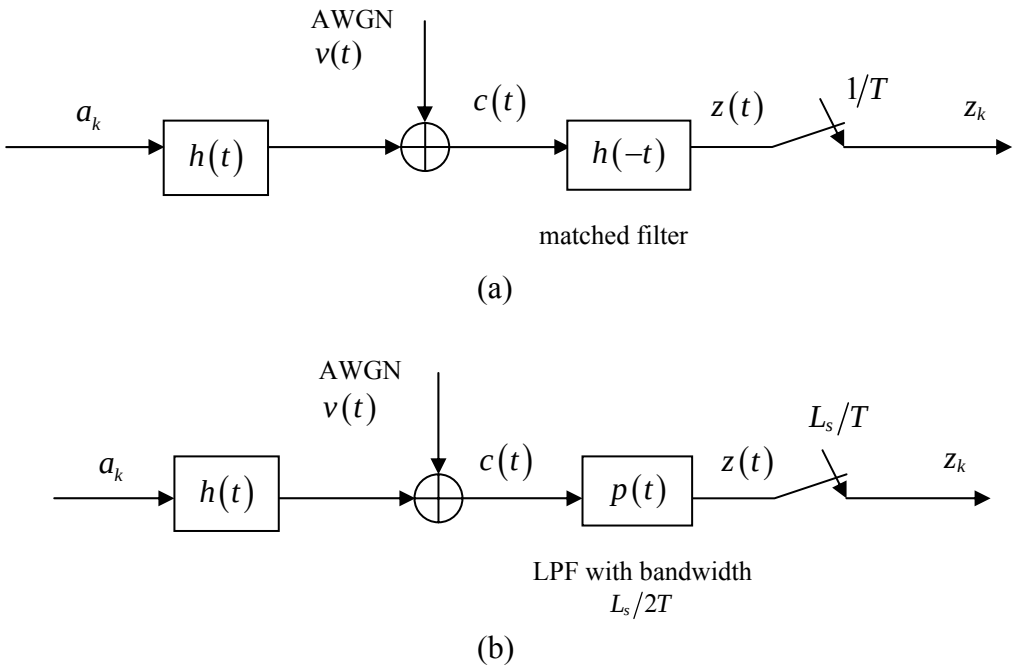

Figure 2.3: Extracting sufficient statistics. (a) application of the matched filter, (b) application of low-pass filter and over-sampling with over-sampling factor L_s.

density from the user's point of view. Assuming R_c to be the code-rate of the channel encoder, we have $T = R_c T_u$, and consequently $K_c = K_u / R_c$. Hence, the use of channel code will cause increase in linear density. This increase in the density, though unavoidable, is undesirable since detection becomes difficult as density increases.

To obtain the digital information from the continuous-time readback signal $c(t)$, a matched filter $h(-t)$ and a symbol-rate sampler can be employed at the channel output, as shown in Figure 2.3(a). It is well known that when the channel noise is AWGN, the matched filter is information lossless as its sampled outputs are a set of sufficient statistics for estimation of the input data bits [22]. In practice, it is common to replace the matched filter with a low-pass filter (LPF) that does not require the knowledge of channel response (Figure 2.3(b)). For a perfectly band-limited channel wherein all of the signal energy is confined within $|f| \le 1/2T$, a low-pass front-end filter also provides sufficient statistics [50]. To accommodate channels with

bandwidths wider than $1/2T$, the configuration shown in Figure 2.3(b) can be used. The over-sampling factor L_s is chosen large enough so that the LPF bandwidth is greater or equal to the channel bandwidth. Therefore, the equalizer that follows the over-sampler in Figure 2.3(b) should have its taps spaced at T/L_s (i.e. fractionally spaced equalizer). We may also remark that the noise power at the sampler is proportional to the bandwidth of the LPF. At high linear densities, the energy of the channel bit response $h(t)$ beyond the bandwidth $1/2T$ will be negligible. Therefore, over-sampling is not necessary (i.e. $L_s = 1$) at high densities.

Let $n(t)$ and $r(t)$ denote the filtered versions of noise $v(t)$ and channel bit response $h(t)$, respectively, with the filter being either matched filter or LPF. Then, a convenient discrete-time model arises from Figures 2.3(a) and 2.3(b) by observing that (assuming $L_s = 1$, i.e. high densities)

$$\begin{aligned} z_k \triangleq z(kT) &= \sum_i a_i r(t - iT) + n(t)\Big|_{t=kT} = \sum_i a_i r(kT - iT) + n(kT) \\ &= \sum_i a_i r_{i-k} + n_k = a_k \otimes r_k + n_k, \end{aligned} \tag{2.6}$$

where $\otimes$ denotes the convolution operator, $n_k = n(kT)$ and $r_k = r(kT)$. Let $q(t)$ be the impulse response of the filter (either matched filter or LPF) before the sampler. Then, r_k and n_k are given by

$$r_k = \int_{-\infty}^{+\infty} h(\tau) q(kT - \tau)\, d\tau \tag{2.7}$$

and

$$n_k = \int_{-\infty}^{+\infty} v(\tau) q(kT - \tau)\, d\tau, \tag{2.8}$$

respectively. In the case where the recording channel is perfectly band-limited and an ideal 'brick-wall' LPF is assumed, r_k can be directly obtained as

$$r_k = h(t)\big|_{t=kT} = h(kT) \tag{2.9}$$

and the resulting sampled noise n_k is a discrete-time AWGN if $v(t)$ is AWGN. Figure 2.4 gives a block diagram of the equivalent discrete-time model of a magnetic recording channel, where the transfer function $R(D)$ is the D transform of $\{r_k\}$.

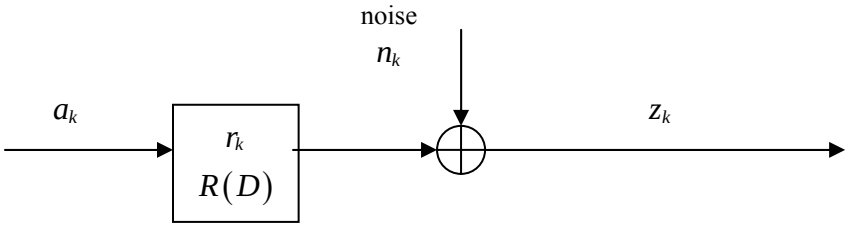

Figure 2.4: Equivalent discrete-time model of a magnetic recording channel.

In the discrete-time channel model given by (2.6), the noise is additive due to the nature of electronics noise. Unlike electronics noise, media noise is correlated, non-stationary, and causes nonlinear distortions. In the next subsection, we introduce media noise into the magnetic recording channel model.

2.1.2 Media Noise Model

Media noise is one of the dominant noise sources, especially at high linear densities, in magnetic recording channel. The major effect of media can be decomposed into two orthogonal noise modes: transition position jitter and transition pulse width variation [18]. Based on the linear channel model presented in (2.1), a simple and accurate nonlinear model of the magnetic recording channel including media noise effect is provided as

$$c(t) = \sum_k b_k f\left(t + \Delta_k - kT, T_{50} + \varpi_k\right) + v(t), \tag{2.10}$$

where $f(t,T_{50})$ is the nominal isolated transition response given by (2.4) or (2.5), Δ_k and ϖ_k are the random variables representing the amounts of position jitter and variation in T_{50}, respectively, and $v(t)$ is the electronics noise. The two types of jitters, Δ_k and ϖ_k are usually assumed independent from each other.

For the sake of convenience in doing linear equalization and performance analysis, a first-order derivative model of position jitter and width variation is proposed in [52, 53]. From (2.1) and (2.10), the media noise $m(t)$ in the readback signal is obtained as

$$m(t)=\sum_k b_k f\left(t-kT+\Delta_k,T_{50}+\varpi_k\right)-\sum_k b_k f\left(t-kT,T_{50}\right). \tag{2.11}$$

With small enough position jitter Δ_k and width jitter ϖ_k, the distorted isolated transition response can be approximated using first-order Taylor's series expansion as

$$f\left(t+\Delta_k,T_{50}+\varpi_k\right)\approx f\left(t,T_{50}\right)+\Delta_k \tilde{f}^{\,p}(t)+\varpi_k \tilde{f}^{\,w}(t), \tag{2.12}$$

where $\tilde{f}^{\,p}(t)=\dfrac{\partial f\left(t,T_{50}\right)}{\partial t}$ and $\tilde{f}^{\,w}(t)=\dfrac{\partial f\left(t,T_{50}\right)}{\partial T_{50}}$. Substituting (2.12) into (2.11), we get an approximate model of media noise as

$$\tilde{m}(t)=\sum_k b_k\Delta_k f^{\,p}(t-kT)+\sum_k b_k\varpi_k f^{\,w}(t-kT). \tag{2.15}$$

Consequently, an approximate linear model of magnetic recording channel with media noise and electronics noise is obtained as

$$\tilde{c}(t)=\sum_k b_k f\left(t-kT\right)+v(t)+\tilde{m}(t)=\sum_k a_k h(t-kT)+v(t)+\tilde{m}(t), \tag{2.16}$$

where $\tilde{c}(t)$ is the approximate readback waveform. (Note that in (2.15) and (2.16) the variable T_{50} is not explicitly indicated as an argument of the functions $f(\bullet)$, $f^{\,p}(\bullet)$ and $f^{\,w}(\bullet)$, since it is considered as a constant.) The first-order model presented in (2.15) clearly indicates the data-dependence and correlation features of media noise.

Digital information is extracted from the channel readback waveform by passing $\tilde{c}(t)$

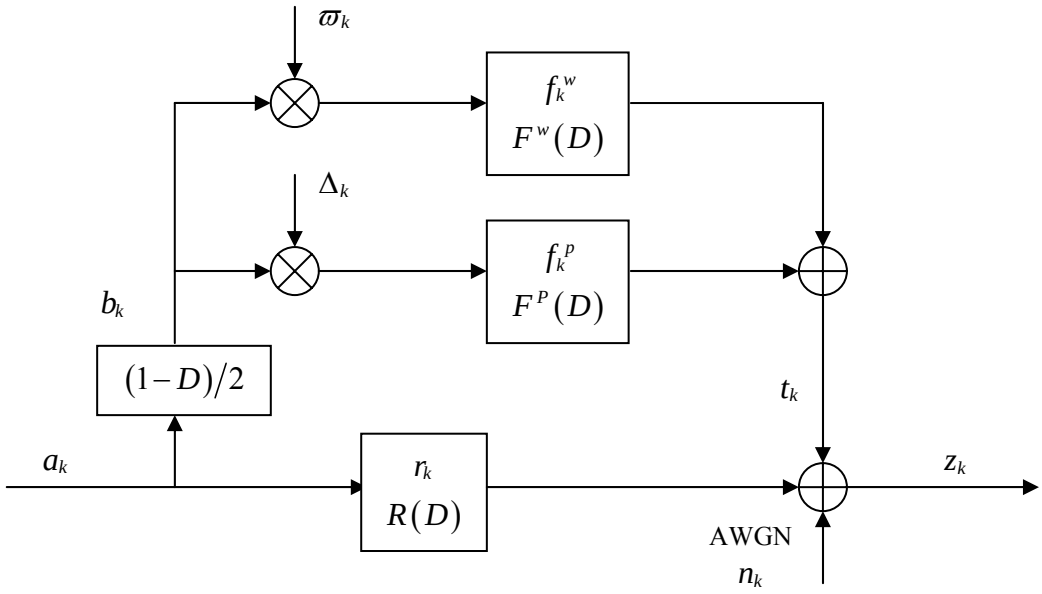

Figure 2.5: Equivalent discrete-time model of a magnetic recording channel with electronics noise and media noise.

through a front-end filter $q(t)$ (either a matched filter or a LPF[2]) and a symbol-rate sampler. Similar to the derivation in Section 2.1.1, the equivalent discrete-time model of the channel is obtained as

$$z_k = a_k \otimes r_k + n_k + t_k , \tag{2.17}$$

where z_k is the output of the sampler, r_k represents the sampled bit response of the channel as given by (2.7), n_k denotes the electronics noise as in (2.8), and t_k represents the sampled version of media noise filtered by $q(t)$. From (2.15), it is easy to find that

$$t_k = \sum_i b_{k-i}\Delta_{k-i} f_i^p + \sum_i b_{k-i}\varpi_{k-i} f_i^w , \tag{2.18}$$

where $f_k^p = \int_{-\infty}^{+\infty} \tilde{f}^p(\tau) q(kT-\tau)\, d\tau$ and $f_k^w = \int_{-\infty}^{+\infty} \tilde{f}^w(\tau) q(kT-\tau)\, d\tau$. Figure 2.5 gives a block diagram of the equivalent discrete-time model of a magnetic recording

[2] Strictly speaking, the matched filter or LPF is not an optimum front-end filter for the channel under consideration because media noise is not AWGN.

channel with electronics noise and media noise as presented in (2.17). In the figure, the input data sequence $\{a_k\}$ passes through a differentiator $(1-D)/2$ to form the transition data sequence $\{b_k\}$; $F^p(D)$ and $F^w(D)$ are the D transforms of $\{f_k^p\}$ and $\{f_k^w\}$, respectively.

From (2.4), (2.5a) and (2.5b), we see that with increase in normalized linear density K_c, the duration of the channel bit response $h(t)$ increases as well, which results in a long span of ISI. Therefore, the magnetic recording channel at high linear densities is subject to severe ISI, and a detector that is powerful enough to deal with large ISI is required at high densities.

2.2 Viterbi Algorithm

It is well known that maximum-likelihood sequence detection (MSLD) provides optimum performance for channels with ISI [22]. It is also known that the Viterbi algorithm (VA) is an efficient implementation of MLSD when the channel noise is AWGN [23]. In this section, we present a brief description of MLSD and VA. For this, we consider the linear channel model shown in Figure 2.4. We wish to design a signal detector that makes a decision on input data sequence $\mathbf{a} = [\cdots, a_k, a_{k-1}, a_{k-2}, \cdots]$ based on the channel output sequence $\mathbf{z} = [\cdots, z_k, z_{k-1}, z_{k-2}, \cdots]$ such that the probability of correct decision is maximized. This goal leads to a decision rule based on the computation of the *posterior* probabilities defined as

$$P_r(\mathbf{a} \mid \mathbf{z}), \qquad \mathbf{a} \in \Lambda$$

where Λ is the set of all possible input data patterns or sequences. The data pattern belonging to Λ is taken as the detected output $\hat{\mathbf{a}}$ if it maximizes the *posterior*

probability $P_r(\mathbf{a}|\mathbf{z})$ over all $\mathbf{a} \in \Lambda$. This decision criterion is called the maximum *a posteriori* probability (MAP) criterion [54]. Using Bayes' rule, the *posterior* probabilities can be expressed as

$$P_r(\mathbf{a}|\mathbf{z}) = \frac{p_r(\mathbf{z}|\mathbf{a})P_r(\mathbf{a})}{p_r(\mathbf{z})}, \tag{2.19}$$

where $p_r(\mathbf{z}|\mathbf{a})$ is the joint probability function (PDF) of $\mathbf{z}$ conditioned on $\mathbf{a}$, $p_r(\mathbf{z})$ represents the joint PDF of $\mathbf{z}$, and $P_r(\mathbf{a})$ denotes the 'prior probability' that the data pattern $\mathbf{a}$ is sent into the channel.

Note that the denominator in (2.19) is independent of which data sequence $\mathbf{a}$ is under consideration, and thus it can be omitted while comparing the posterior probabilities. Further simplification can be achieved for the MAP criterion when all the possible input data patterns have equal prior probabilities. Then, the sequence detection rule based on the MAP criterion is equivalent to estimating the input data sequence that maximizes $p_r(\mathbf{z}|\mathbf{a})$, i.e.

$$\hat{\mathbf{a}} = \arg\max_{\mathbf{a}\in\Lambda} \{ p_r(\mathbf{z}|\mathbf{a}) \}. \tag{2.20}$$

The conditional PDF $p_r(\mathbf{z}|\mathbf{a})$ is usually referred to as likelihood function, and the decision criterion given by (2.20) is called the maximum-likelihood (ML) criterion. Sequence detection based on the ML criterion is referred to as maximum-likelihood sequence detection (MLSD).

As shown in Figure 2.4, the channel output is given by

$$z_k = a_k \otimes r_k + n_k = \sum_i a_{k-i} r_i + n_k. \tag{2.21}$$

Assuming that the noise n_k in (2.21) is AWGN with zero mean and variance σ^2, the likelihood function can be computed as

$$
\begin{aligned}
p_r(\mathbf{z}\,|\,\mathbf{a}) &= \prod_k p(z_k\,|\,\mathbf{a}) \\
&= \prod_k \frac{1}{\sqrt{2\pi\sigma^2}}\ \exp\left(-(d_k - z_k)^2 \big/ 2\sigma^2\right) \\
&= \left(\frac{1}{\sqrt{2\pi\sigma^2}}\right)^{L_1}\ \exp\left(-\sum_k (d_k - z_k)^2 \Big/ 2\sigma^2\right),
\end{aligned} \tag{2.22}
$$

where L_1 is the number of samples in the vector $\underline{z}$ and $d_k = a_k \otimes r_k = \sum_i a_{k-i} r_i$ represents the noiseless signal at channel output for the given input data pattern $\mathbf{a}$. Since σ^2 is independent of $\mathbf{a}$, we can see from (2.20) and (2.22) that the ML detection criterion in AWGN channel is equivalent to

$$
\hat{\mathbf{a}} = \arg\min_{\mathbf{a}\in\Lambda}\left\{\sum_k (z_k - d_k)^2\right\} = \arg\min_{\mathbf{a}\in\Lambda}\left\{\sum_k \left(z_k - \sum_i a_{k-i} r_i\right)^2\right\}. \tag{2.23}
$$

The quantity defined by $\sum_k (z_k - d_k)^2$ is actually the squared Euclidean distance between the received channel output sequence $\underline{z}$ and the noiseless signal sequence $\mathbf{d} = [\cdots d_k, d_{k-1}, d_{k-2}, \cdots]$ for the given data pattern $\mathbf{a}$.

It is almost impossible to implement MLSD in its original form given by (2.23). For L bits binary input sequence $\mathbf{a}$ under consideration, one must search over 2^L possible input data sequences by computing 2^L Euclidean distances required by (2.23). The underlying computational load exponentially grows with L and becomes impractically large even for moderate values of L.

The Viterbi algorithm (VA) is an efficient implementation of the search implied by (2.23). Assuming that the channel bit response is causal and given by $\{r_0, r_1, \cdots, r_M\}$, we may rewrite (2.21) as

$$
z_k = \sum_{i=0}^{M} a_{k-i} r_i + n_k = a_k r_0 + \sum_{i=1}^{M} a_{k-i} r_i + n_k\,. \tag{2.24}
$$

Since the channel has a memory (or, ISI) of M bits, the VA forms a trellis with 2^M states per bit interval. At instant k, for example, the 2^M states represent 2^M possible

patterns of M data bits $\{a_{k-1}, a_{k-2}, \cdots, a_{k-M}\}$. Clearly, the bits that were sent into the channel during the instants $\{k-1, k-2, \cdots, k-M\}$ will be one among these 2^M possibilities. A branch connecting a state at instant k and a state at instant $k+1$ represents the data bit a_k that results in the state transition. For binary input, each state has two incoming and two outgoing branches. Any path composed by a sequence of branches from the beginning to the end of the trellis represents a possible input data sequence. An example of a 4-state trellis is illustrated in Figure 2.6. The four states at any instant k are given by $S_1 = \langle -1, -1 \rangle$, $S_2 = \langle -1, +1 \rangle$, $S_3 = \langle +1, -1 \rangle$, and $S_4 = \langle +1, +1 \rangle$, which represent the four possible patterns of the input data bits $\{a_{k-2}, a_{k-1}\}$.

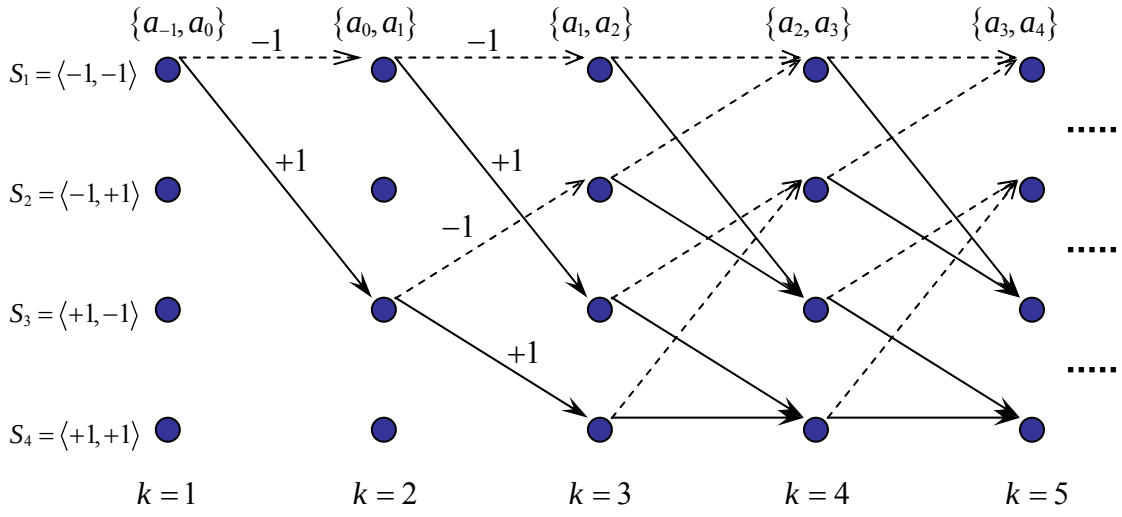

Figure 2.6: The trellis for a channel with memory of 2 bits.

Assume that L bits binary data $\{a_1, a_2, \cdots, a_L\}$ were sent into the channel (i.e. stored on the medium) during the instants $\{1, 2, \cdots, L\}$. Therefore, there are 2^L possible paths through the trellis. Let $\mathbf{a}_l = [a_{l,1}, a_{l,2}, \cdots, a_{l,L}]$ denote the data sequence corresponding to the l^{th} $(1 \le l \le 2^L)$ path in the trellis and $\mathbf{d}_l = [d_{l,1}, d_{l,2}, \cdots, d_{l,L_2}]$, where

$d_{l,k} = \sum_{i=0}^{M} a_{l,k-i} r_i$ and $L_2 = L + M$, denote the noiseless signal sequence at the channel output for the given input data sequence $\mathbf{a}_l$. Further, let $\mathbf{z} = [z_1, z_2, \cdots, z_{L_2}]$ denote the received channel output sequences, where z_k is given by (2.24). The Euclidean distance between $\mathbf{z}$ and $\mathbf{d}_l$ can be computed as

$$\begin{aligned} PM(\mathbf{a}_l) &= \sum_{i=1}^{L_2} (z_i - d_{l,i})^2 = \sum_{i=1}^{L_2-1} (z_i - d_{l,i})^2 + (z_{L_2} - d_{l,L_2})^2 \\ &= PM_{L_2-1}(\mathbf{a}_l) + BM_{L_2}(\mathbf{a}_l) = PM_{k-1}(\mathbf{a}_l) + \sum_{i=k}^{L_2} BM_i(\mathbf{a}_l), \end{aligned}$$

where $PM(\mathbf{a}_l) = \sum_{k=1}^{L_2} (z_k - d_{l,k})^2$ is usually referred to as the path metric associated with the l^{th} path, $PM_k(\mathbf{a}_l) = \sum_{i=1}^{k} (d_{l,i} - z_i)^2$ (for $1 \le k < L_2$) is the partial path metric for the partial data path $[a_{l,1}, a_{l,2}, \cdots, a_{l,k}]$, and $BM_k(\mathbf{a}_l) = (z_k - d_{l,k})^2$ is known as the branch metric associated with the state transition at instant k on the l^{th} path. Assume that the paths $\mathbf{a}_m$ and $\mathbf{a}_l$ ($m \ne l$) pass through the same state S at instant $k-1$, i.e. the partial paths $[a_{l,1}, a_{l,2}, \cdots, a_{l,k-1}]$ and $[a_{m,1}, a_{m,2}, \cdots, a_{m,k-1}]$ both end at that state. If $PM_{k-1}(\mathbf{a}_l) < PM_{k-1}(\mathbf{a}_m)$, then we can find that

$$\begin{aligned} PM(\mathbf{a}_m) &= PM_{k-1}(\mathbf{a}_m) + \sum_{i=k}^{L_2} BM_i(\mathbf{a}_m) \\ &> PM_{k-1}(\mathbf{a}_l) + \sum_{i=k}^{L_2} BM_i(\mathbf{a}_m) = PM(\mathbf{a}_n), \end{aligned}$$

where $\mathbf{a}_n = [a_{l,1}, a_{l,2}, \cdots, a_{l,k-1}, a_{m,k}, a_{m,k+1}, \cdots, a_{m,L_2}]$ ($\mathbf{a}_n \ne \mathbf{a}_m$) is also a path in the trellis passing through the state S. Cleary, all those paths in the trellis that have $[a_{m,1}, a_{m,2}, \cdots, a_{m,k-1}]$ as the first $k-1$ bits cannot be the solution to the ML criterion in (2.23), and hence these paths can be dropped. Extending this, we can conclude the following. Among all the partial paths ending at the state S at instant $k-1$, we only need to keep the one that results in the smallest partial path metric. The other partial paths, and consequently, all the paths having any of these partial paths as the first $k-1$

bits can be dropped. This retained partial path is called the survivor path and the corresponding partial path metric is called the survivor metric associated with the state S at instant $k-1$. Doing this for every state throughout the trellis, we find that only one survivor path needs to be retained for each state at any instant. Further, the survivor path and metric for any state at instant k can be determined by finding which of the partial paths ending at that state has the smallest partial path metric. These candidate partial paths are obtained by extending the survivor paths at instant $k-1$ with all possible branch transitions to that state at instant k. At the end, the solution to the ML solution in (2.23) at any instant is given by the survivor path associated with the state having minimum survivor metric at that instant. The above described 'path dropping' mechanism results in halving the total number of paths at every instant. This leads to significant saving in storage and computational requirements.

Note that the Viterbi algorithm described above performs MLSD only if the channel noise is AWGN. Once this assumption is violated, the performance of VA detector will no longer be optimum, or may be badly degraded. From Figure 2.6, we can see that the complexity of VA trellis grows exponentially with the channel length. Since the magnetic recording channel is usually long and not causal, PR equalization techniques are widely employed to shorten the channel response and make it causal, so that the complexity of VA detector based on the equalized channel is practically affordable.

2.3 Linear Partial-Response Equalization

The technique of equalization is used for mitigating ISI and channel noise. Partial-response (PR) equalization typically uses a filter to transform a long channel response

into the desired PR characteristics that only contains a few bits of ISI. The transfer function that defines the desired PR characteristics is referred to as the PR target response. Ideally, the equalizer should be designed to minimize the probability of decision error. However, such ideal design is usually hampered by mathematical difficulties and therefore simpler criteria are used instead. In this section, we briefly introduce the typical linear PR equalization by means of zero forcing and by the minimum mean square error criteria. The linear equalizer can be an analog (i.e. continuous-time) filter, a digital (i.e. discrete-time) filter, or a mixture of the two. In this thesis, we consider digital equalizer that is placed at the output of the sampler in Figure 2.3(b). Since our focus is detection techniques for high-density recording channels that are almost band-limited, hereafter we assume the over-sampling factor $L_s = 1$ in Figure 2.3(b). As a result, the equalizer that follows the sampler has its taps spaced *T* seconds apart. Figure 2.4 shows the resulting discrete-time channel model.

2.3.1 Zero-Forcing PR Equalization

Figure 2.7 depicts the system model using zero-forcing (ZF) equalizer. The discrete-time channel with transfer function $R(D)$ shown in Figure 2.4 is equalized into a target response $G(D)$. The ZF criterion requires that transmission be distortion-less, i.e. the undesirable ISI is forced to zero. In order to achieve this objective, the linear ZF equalizer $W(D)$ should have the characteristics given by

$$W\left(e^{j2\pi\Omega}\right) = \frac{G\left(e^{j2\pi\Omega}\right)}{R\left(e^{j2\pi\Omega}\right)}, \tag{2.25}$$

where Ω is the frequency normalized by the bit rate $1/T$, and $W\left(e^{j2\pi\Omega}\right)$, $G\left(e^{j2\pi\Omega}\right)$ and $R\left(e^{j2\pi\Omega}\right)$ are the discrete-time Fourier transforms of the equalizer w_k, PR target g_k

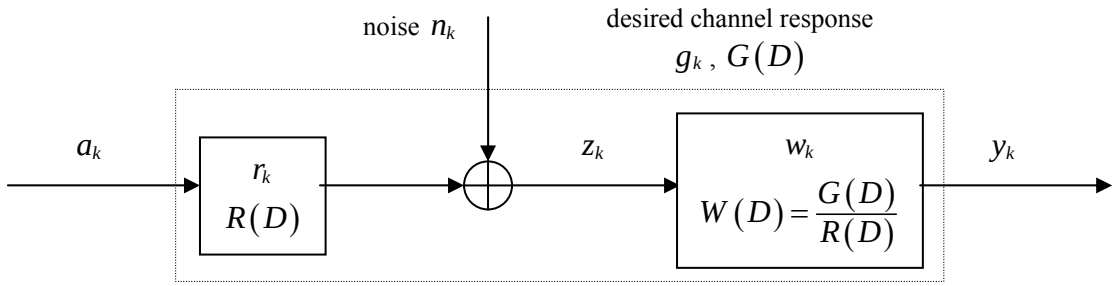

Figure 2.7: Zero-forcing PR linear equalizer operating on the output of a discrete-time channel with additive noise.

and the original channel r_k, respectively. Note that the equalizer characterized by (2.25) is in general a recursive (infinite impulse response – IIR) filter.

To assess the performance of the ZF equalizer in terms of noise enhancement, we compute the noise power at the equalizer output as

$$\xi_{ZF} \triangleq \int_{-0.5}^{0.5} \mathrm{P}_n\left(e^{j2\pi\Omega}\right) \frac{\left|G\left(e^{j2\pi\Omega}\right)\right|^2}{\left|R\left(e^{j2\pi\Omega}\right)\right|^2} d\Omega , \tag{2.26}$$

where $\mathrm{P}_n\left(e^{j2\pi\Omega}\right)$ is the power spectral density (PSD) of the channel noise n_k. When $\left|G\left(e^{j2\pi\Omega}\right)\right|$ is well selected to be small wherever $\left|R\left(e^{j2\pi\Omega}\right)\right|$ is small, the ratio $\left|G\left(e^{j2\pi\Omega}\right)\right| / \left|R\left(e^{j2\pi\Omega}\right)\right|$ will not be unreasonably large, and thus ξ_{ZF} will be reduced. The smallest noise enhancement accrues if $\left|G\left(e^{j2\pi\Omega}\right)\right|$ is selected such that the ratio $\left|G\left(e^{j2\pi\Omega}\right)\right| / \left|R\left(e^{j2\pi\Omega}\right)\right|$ is independent of frequency. In a magnetic recording channel having infinitely long response, this is, in general, not possible if the target is of finite length. Thus, noise enhancement is inevitable. In addition, we see from (2.24) that channel instabilities are amplified where $\left|R\left(e^{j2\pi\Omega}\right)\right|$ is small while $\left|G\left(e^{j2\pi\Omega}\right)\right|$ is not. Even worse, the ZF PR equalizer may not exist if $R(D)$ has spectral zeros.

2.3.2 Minimum Mean Square Error Criterion

To minimize noise enhancement, we need to drop the strict requirement that all the undesired ISI be completely eliminated. Instead, we could demand that the total power of noise and residual ISI (mis-equalization) at equalizer output be minimized. This requirement is called the minimum mean square error (MMSE) criterion. The equalizer designed by the MMSE criterion results in small noise enhancement because the noise is included in the criterion. Also, the existence of MMSE equalizer is assured since noise is always present in the channel.

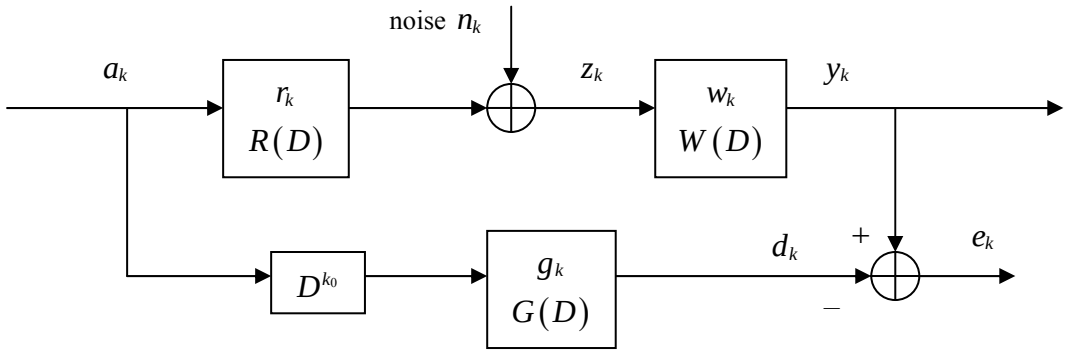

Figure 2.8: Block diagram of channel equalization based on the MMSE criterion.

In this section, the formulation of MMSE criterion and the derivation of MMSE equalizer solution are described. For this development, we first assume that the equalizer is a finite impulse response (FIR) filter. As shown in Figure 2.8, the total noise at the equalizer output, including the filtered channel noise and residual ISI, is equivalent to the estimation error e_k given by $e_k = y_k - d_k$, where y_k is the equalizer output and d_k is the desired noiseless output based on the target response. Hence, the total noise power at equalizer output can be computed as the mean of the squared estimation error, i.e.

$$\xi_{MMSE} \triangleq E\left[e_k^2\right] = E\left[\left(y_k - d_k\right)^2\right], \tag{2.27}$$

where $E[\bullet]$ denotes expectation over the data a_k and noise n_k ensembles. With N_w-tap equalizer and N-tap target response, we get

$$y_k = \sum_{i=0}^{Nw-1} z_{k-i} w_i = \mathbf{w}^T \mathbf{z}_k \text{ and } d_k = \sum_{i=0}^{N-1} a_{k-k_0-i} g_i = \mathbf{g}^T \mathbf{a}_{k-k_0},$$

where the superscript ^{T} denotes the transpose operator, the column vectors $\mathbf{w} = [w_0, w_1, \cdots, w_{N_w-1}]^T$ and $\mathbf{g} = [g_0, g_1, \cdots, g_{N-1}]^T$ represent the tap-weight vectors of the equalizer and target response, respectively, $\mathbf{z}_k = [z_k, z_{k-1}, \cdots, z_{k-N_w+1}]^T$ and $\mathbf{a}_k = [a_k, a_{k-1}, \cdots, a_{k-N+1}]^T$ denote the equalizer input vector and channel input vector, respectively, and k_0 is the delay from channel input to equalizer output. Then, we have

$$\xi_{MMSE} = E\left[\left(\mathbf{w}^T \mathbf{z}_k - \mathbf{g}^T \mathbf{a}_{k-k_0}\right)^2\right] = \mathbf{g}^T \mathbf{R}_{aa} \mathbf{g} - 2\mathbf{w}^T \mathbf{R}_{za} \mathbf{g} + \mathbf{w}^T \mathbf{R}_{zz} \mathbf{w}, \tag{2.28}$$

where $\mathbf{R}_{aa} = E\left[\mathbf{a}_{k-k_0} \mathbf{a}_{k-k_0}^T\right]$, $\mathbf{R}_{zz} = E\left[\mathbf{z}_k \mathbf{z}_k^T\right]$, and $\mathbf{R}_{za} = E\left[\mathbf{z}_k \mathbf{a}_{k-k_0}^T\right]$. Eqn. (2.28) is a quadratic function of the equalizer tap-weight vector $\mathbf{w}$ with a single minimum[3], and the optimum solution of equalizer that minimizes ξ_{MMSE} is obtained as

$$\mathbf{w}_o = \mathbf{R}_{zz}^{-1} \mathbf{R}_{za} \mathbf{g}. \tag{2.29}$$

The FIR filter with tap weights given by (2.29) is the so-called MMSE PR equalizer.

Now we consider the equalizer having infinitely long response, and derive the expression for optimum equalizer based on the MMSE criterion. Using Parseval's principle, we may rewrite (2.27) as

$$\xi_{MMSE} = \int_{-0.5}^{0.5} \left(\mathrm{P}_n |W|^2 + \mathrm{P}_a \left| RW - G e^{-j2\pi k_0} \right|^2 \right) d\Omega, \tag{2.30}$$

where P_a represents the PSD of the channel input a_k. (For notational convenience we omit the argument $\left(e^{j2\pi\Omega}\right)$ from the discrete-time Fourier transforms and PSDs in

[3] $\mathbf{R}_{zz}$ is the autocorrelation matrix of the random process z_k, and hence it is a positive definite matrix.

(2.30) and hereafter.) To find the optimum equalizer W_o that minimizes ξ_{MMSE}, we use a technique known as *calculus of variations* [55]. Let the equalizer variable be $W = W_o + \mu V$, where V is an arbitrary complex-valued variation and μ is a real scalar. Since ξ_{MMSE} is a quadratic function of the equalizer with unique minimum, the gradient of ξ_{MMSE} must approach to zero when W approaches W_o along any arbitrary direction defined by V. That is, for all V, we must have

$$\frac{\partial}{\partial \mu}\xi_{MMSE}\,|_{\mu=0} = 2\,\mathrm{Re}\int_{-0.5}^{0.5} V^*\left[\mathrm{P}_a R^* G e^{-j2\pi k_0} - \left(\mathrm{P}_a|R|^2 + \mathrm{P}_n\right)W_o\right]d\Omega = 0\,, \tag{2.31}$$

where the superscript * denotes the complex conjugation operator. In order to satisfy (2.31) for all V, the quantity in the square brackets should vanish for all Ω, which implies that W_o should have the characteristics as

$$W_o = \frac{\mathrm{P}_a R^* e^{-j2\pi\Omega k_0}}{\mathrm{P}_n + \mathrm{P}_a|R|^2} G\,. \tag{2.32}$$

The IIR filter defined by (2.31) is referred to as unconstrained MMSE PR equalizer. Substituting (2.32) in (2.30), we obtain the minimum mean square error (MMSE) as

$$\xi_{MMSE,\min} = \int_{-0.5}^{0.5} \frac{\mathrm{P}_n \mathrm{P}_a |G|^2}{\mathrm{P}_n + \mathrm{P}_a|R|^2}\, d\Omega\,. \tag{2.33}$$

Note that the integrand of (2.33) is actually the PSD of the total noise at the output of the unconstrained MMSE PR equalizer. From (2.33), we see that the spectra of the target response should be well designed to avoid enhancing the noise components at the frequencies where $\left(\mathrm{P}_n/\mathrm{P}_a + |R|^2\right)$ is small. If $|G|$ is selected such that the integrand of (2.33) is independent of frequency, the noise at the unconstrained PR equalizer output is white. Since the channel input SNR (the ratio of input signal power to the channel noise power) is normally much higher than 0 dB, the quantity defined by $\left(\mathrm{P}_n/\mathrm{P}_a + |R|^2\right)$ almost resembles $|R|^2$, where R is the original channel response. Thus,

similar to the discussion about the performance of ZF PR equalizer in Section 2.3.1, in magnetic recording channels, the noise enhancement and noise correlation (i.e. non-white noise resulting at equalizer output) cannot be avoided with a finitely long target response.

2.4 Conclusion

In this chapter, we have introduced a discrete-time model of digital magnetic recording channel at high densities. Based on this discrete-time channel model, we described the VA detector based on Euclidean distance metrics and the PR equalizers designed by means of the ZF and MMSE criteria. If a VA detector is used to perform sequence detection on the output of the PR equalized channel, the overall system is called PRML system. It should be especially noted that the noise at PR equalized channel output is usually non-white, which violates the basic AWGN assumption required to make VA optimum. Therefore, the performance of VA detector in PRML system is sub-optimum compared to MLSD. As indicated in the above discussion, target response is the key factor that controls the noise characteristics at the output of the PR equalizer. Hence, target response critically influences the performance of PRML system. In the next chapter, we provide detailed discussion on target design.

Chapter 3

Novel Analytical Approach for Optimum Target Design

In this chapter, we propose a novel analytical approach for designing optimum generalized PR target response for the PRML receiver, for application perpendicular recording channels at high densities. We start with Section 3.1 by addressing the problem of target design. Section 3.2 presents the performance analysis for the Viterbi algorithm (VA) detector, and then introduces a cost function for designing the target, which is closely related to the performance of VA detector. Thereafter, the proposed analytical approach for finding the optimum target based on this cost function is developed in Section 3.3. In Section 3.4, we investigate by simulations the performance of the targets designed by our approach and compare the performance with other target design approaches.

3.1 Problem of Target Design

As indicated in Chapter 2, in order to reduce noise enhancement, the partial-response

(PR) target for PRML detection strategy should be well designed to match the natural channel response. Standard PR targets with integer coefficients, for example the PR4 target, are conventionally considered for PRML systems. Standard PR targets are selected by inspecting the match between the target and the natural channel response, either in time domain or frequency domain. But, the search space for integer-valued tap weights becomes infinitely large to guarantee optimum BER performance. In other words, due to the integer constraint, the standard PR target usually cannot satisfactorily match the natural channel response, and thus its performance is limited. At the cost of a minor increase in the complexity of VA detector, generalized PR (GPR) targets with real-valued coefficients can provide better match to the recording channel response, and thus result in significant performance gain. In this thesis, our discussion on target design focuses on GPR targets.

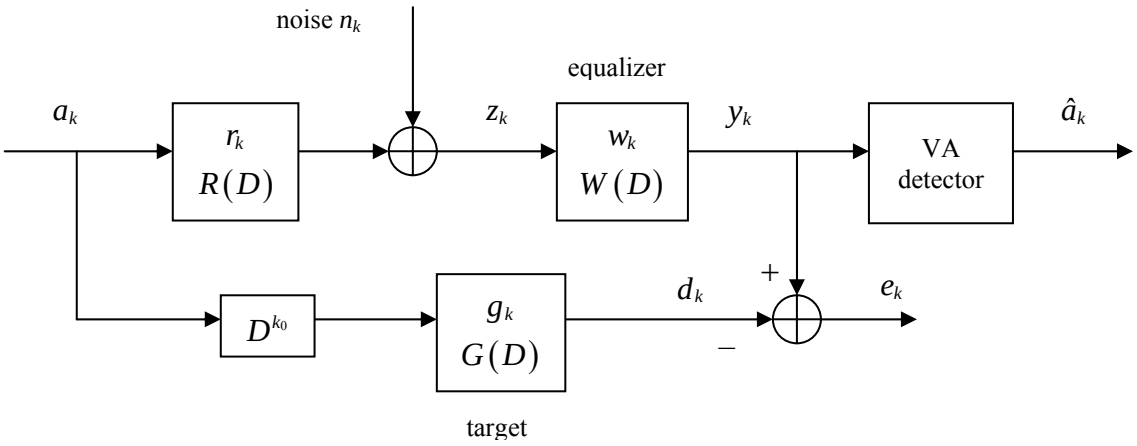

Figure 3.1: PRML system using MMSE PR equalizer and VA detector.

The most widely used method of designing GPR target is to jointly optimize target and PR equalizer based on the MMSE criterion [28, 29, 30, 31]. In the system model shown in Figure 3.1, the mean squared error (MSE) at the equalizer output is given by (2.28), i.e.

$$\xi_{MMSE} = E\left[e_k^2\right] = \mathbf{g}^T\mathbf{R}_{aa}\mathbf{g} - 2\mathbf{w}^T\mathbf{R}_{za}\mathbf{g} + \mathbf{w}^T\mathbf{R}_{zz}\mathbf{w},$$

where $\mathbf{w} = [w_0, w_1, \cdots, w_{N_w-1}]^T$ and $\mathbf{g} = [g_0, g_1, \cdots, g_{N-1}]^T$ denote the tap-weight vectors of N_w–tap equalizer and N–tap target response, respectively. As introduced in Chapter 2, the optimum equalizer minimizing ξ_{MMSE} is given by $\mathbf{w}_o = \mathbf{R}_{zz}^{-1}\mathbf{R}_{za}\mathbf{g}$. Substituting $\mathbf{w}_o$ into (2.28) yields

$$\xi_{MMSE} = \mathbf{g}^T\left(\mathbf{R}_{aa} - \mathbf{R}_{za}^T\mathbf{R}_{zz}^{-1}\mathbf{R}_{za}\right)\mathbf{g} = \mathbf{g}^T\mathbf{R}_n\mathbf{g}, \tag{3.1}$$

where $\mathbf{R}_n = \mathbf{R}_{aa} - \mathbf{R}_{za}^T\mathbf{R}_{zz}^{-1}\mathbf{R}_{za}$. Since ξ_{MMSE} is always positive for any non-zero target (Note: that ξ_{MMSE} is the total power of noise and residual ISI at equalizer output), $\mathbf{R}_n$ is a positive definite matrix. We may denote the eigenvalues of $\mathbf{R}_n$ and corresponding orthonormal eigenvectors as $\{\lambda_1, \lambda_2, \cdots, \lambda_N\}$ ($\lambda_1 \geq \lambda_2 \geq \cdots \geq \lambda_N > 0$) and $\{\mathbf{q}_1, \mathbf{q}_2, \cdots, \mathbf{q}_N\}$, respectively. To avoid the trivial solution $\mathbf{g} = \mathbf{0}$, we need to impose a constraint on $\mathbf{g}$ when solving the optimization problem (3.1). With unit energy constraint (i.e. $\mathbf{g}^T\mathbf{g} = 1$), the MMSE solution of $\mathbf{g}$ is simply the eigenvector $\mathbf{q}_N$ of $\mathbf{R}_n$, and the resulting minimum MSE, which we denote as $\xi_{\min}^{\text{En}}$, is equal to the minimum eigenvalue λ_N of $\mathbf{R}_n$ [29]. If the monic constraint (i.e. $g_0 = 1$) is used, the MMSE solution of target $\mathbf{g}$ and the resulting minimum MSE are obtained as

$$\mathbf{g}_o^{\text{monic}} = \left(\mathbf{R}_n^{-1}\mathbf{c}\right)\Big/\left(\mathbf{c}^T\mathbf{R}_n^{-1}\mathbf{c}\right) \quad \text{and} \quad \xi_{\min}^{\text{monic}} = 1\Big/\left(\mathbf{c}^T\mathbf{R}_n^{-1}\mathbf{c}\right),$$

respectively, where $\mathbf{c} = [1, 0, \cdots, 0]^T$ [31].

To investigate the effectiveness of monic constraint as compared to unit-energy constraint, we normalize $\mathbf{g}_o^{\text{monic}}$ to having unit energy, i.e. $\mathbf{g}_o^{\text{monic}} = \left(\mathbf{R}_n^{-1}\mathbf{c}\right)\Big/\sqrt{\mathbf{c}^T\mathbf{R}_n^{-2}\mathbf{c}}$, and get the resulting minimum MSE as

$$\xi_{\min}^{\text{monic}} = \frac{\mathbf{c}^T\mathbf{R}_n^{-1}\mathbf{c}}{\mathbf{c}^T\mathbf{R}_n^{-2}\mathbf{c}} = \left(\sum_{i=1}^{N}\left(v_i^2/\lambda_i\right)\right)\Big/\left(\sum_{i=1}^{N}\left(v_i^2/\lambda_i^2\right)\right),$$

where v_i is the first element of the eigenvector $\mathbf{q}_i$ ($i = 1, 2, \cdots, N$). Since λ_N is the minimum eigenvalue of $\mathbf{R}_n$, we have $\sum_{i=1}^{N} v_i^2/\lambda_i^2 \le \frac{1}{\lambda_N}\sum_{i=1}^{N} v_i^2/\lambda_i$, and thus

$$\xi_{\min}^{\text{monic}} = \left(\sum_{i=1}^{N} v_i^2/\lambda_i\right) \Bigg/ \left(\sum_{i=1}^{N} v_i^2/\lambda_i^2\right) \ge \lambda_N = \xi_{\min}^{\text{En}}. \tag{3.2}$$

As mentioned earlier, the MSE represents the total power of the noises, including channel noise and residual ISI, at the detector input. Hence, from the inequality (3.2), we may draw the conclusion that unit-energy constrained MMSE target results in better performance than the monic constrained MMSE target in the sense of suppressing noise power (i.e. MSE). Nevertheless, as indicated by existing literature, such as [31], simulation results show that the latter target always outperforms the former in terms of bit-error-rate (BER). This contradiction indicates that MSE is not a good measure of the performance of PRML systems. This is mainly because MMSE design aims to minimize MSE but puts no specific demand on how the noise correlation should be at the VA input. As a result, the direct MMSE approach may badly degrade the performance of VA detector. Clearly, in order to design optimum target leading to the best system performance, we need to find a good cost function that is closely related to the performance of VA detector.

3.2 Cost Function for Optimum Target Design

The most important step in the design of optimum GPR target for a PRML system is to find a cost function that incorporates the effect of noise enhancement, noise correlation and other factors that influence the performance of VA detector. For this purpose, we

analyze the error probability of VA detector based on the channel model shown in Figure 3.1, by following the development proposed in [55, 56].

Let $\mathbf{a} = [\cdots a_{k-n}, \cdots a_{k-1}, a_k, \cdots]$ be the data sequence actually input to the channel, which can be considered as the correct data path in the VA trellis for this channel. Then, let $\mathbf{a}' = [a'_{k-n}, \cdots, a'_k, a'_k, \cdots]$ be another data sequence, corresponding to a wrong data path (i.e. $\mathbf{a}' \neq \mathbf{a}$) in the VA trellis. The VA detector makes the wrong decision of $\mathbf{a}'$ as the input data sequence instead of $\mathbf{a}$ if

$$\sum_k \left(y_k - \sum_{i=0}^{N-1} g_i a'_{k-i-k_0} \right)^2 < \sum_k \left(y_k - \sum_{i=0}^{N-1} g_i a_{k-i-k_0} \right)^2, \tag{3.3}$$

where y_k is the input to the VA detector (see Figure 3.1). Since y_k can be written as $y_k = e_k + \sum_{i=0}^{N-1} g_i a_{k-i-k_0}$, we may rewrite (3.3) as

$$\frac{1}{2} \sum_k \left(\sum_{i=0}^{N-1} g_i \left(a_{k-i-k_0} - a'_{k-i-k_0} \right) \right)^2 + \sum_k e_k \left(\sum_{i=0}^{N-1} g_i \left(a_{k-i-k_0} - a'_{k-i-k_0} \right) \right) < 0 .$$

We describe the difference between the correct path $\mathbf{a}$ and the wrong path $\mathbf{a}'$ by defining an error sequence $\boldsymbol{\varepsilon} = \mathbf{a} - \mathbf{a}' = [\cdots, \varepsilon_k, \varepsilon_{k+1}, \cdots, \varepsilon_{k+N_\varepsilon - 1} \cdots]^T$. For binary input, $\varepsilon_{k+i} \in \{+2, -2, 0\}$. The error vector $\boldsymbol{\varepsilon}_k = [\varepsilon_k, \varepsilon_{k+1}, \cdots, \varepsilon_{k+N_\varepsilon - 1}]^T$ is said to be an error event of length N_ε if it satisfies the following conditions.

1. $\varepsilon_k \neq 0$ and $\varepsilon_{k+N_\varepsilon - 1} \neq 0$.
2. $\varepsilon_{k+i} = 0$ for $-N+1 < i < 0$ and $N_\varepsilon \leq i \leq N_\varepsilon + N - 2$.
3. The length of strings of zeros, if any, in $\underline{\varepsilon}$ must not exceed $N-1$.

The quantity '$N-1$' is called the 'error-free interval'. If the noise at the detector input is not white, then the error-free interval required to separate two error events must be larger than $N-1$ so as to account for the increase in channel memory induced by the noise correlation.

Assuming that the error sequence $\boldsymbol{\varepsilon}$ contains only one error event $\boldsymbol{\varepsilon}_k$ given above, we can derive the probability of this error event $\boldsymbol{\varepsilon}$ (Note: since $\boldsymbol{\varepsilon}$ and $\boldsymbol{\varepsilon}_k$ are equivalent here, we drop the index 'k' from $\boldsymbol{\varepsilon}_k$) conditioned on the underlying data path $\mathbf{a}$ as

$$P_r(\boldsymbol{\varepsilon}|\mathbf{a}) = P_r\left(\frac{1}{2}\sum_{j=k_0}^{N_\varepsilon+N-2+k_0}\left(\sum_{i=0}^{N-1} g_i\varepsilon_{k-i-k_0+j}\right)^2 + \sum_{j=k_0}^{N_\varepsilon+N-2+k_0} e_{k+j}\left(\sum_{i=0}^{N-1} g_i\varepsilon_{k-i-k_0+j}\right) < 0\middle|\mathbf{a}\right)$$
$$= P_r\left(\frac{1}{2}\sum_{j=0}^{N_\varepsilon+N-2}\tilde{\varepsilon}_{k+j}^2 + \sum_{j=0}^{N_\varepsilon+N-2} e_{k+j+k_0}\tilde{\varepsilon}_{k+j} < 0\middle|\mathbf{a}\right) = P_r\left(\frac{1}{2}d_{\boldsymbol{\varepsilon}}^2 + u_k < 0\middle|\mathbf{a}\right),$$

where $\tilde{\varepsilon}_k = \sum_{i=0}^{N-1} g_i\varepsilon_{k-i}$, $d_{\boldsymbol{\varepsilon}}^2 = \sum_{i=0}^{N_\varepsilon+N-2}\tilde{\varepsilon}_{k+i}^2$ and $u_k = \sum_{j=0}^{N_\varepsilon+N-2} e_{k+j+k_0}\tilde{\varepsilon}_{k+j}$. We assume that the estimation error e_k is a stationary Gaussian random process with zero mean[1], Consequently, u_k is zero-mean random variable with conditional variance $\sigma_{u,\boldsymbol{\varepsilon}}^2 = E\left[{u_k}^2|\mathbf{a}\right] = \sum_{i=0}^{N_\varepsilon+N-2}\sum_{j=0}^{N_\varepsilon+N-2}\tilde{\varepsilon}_{k+j}\tilde{\varepsilon}_{k+i}r_{e|\mathbf{a}}(|j-i|)$ where $r_{e|\mathbf{a}}(m) = E\left[e_k e_{k+m}|\mathbf{a}\right]$ is the conditional autocorrelation of e_k. Therefore, we get

$$P_r(\boldsymbol{\varepsilon}|\mathbf{a}) = Q\left(\frac{d_{\boldsymbol{\varepsilon}}^2}{2\sigma_{u,\boldsymbol{\varepsilon}}}\right), \tag{3.4}$$

where $Q(\beta) \triangleq \frac{1}{2\pi}\int_{\beta}^{+\infty} e^{-x^2/2}dx$ denotes the tail integral of the Gaussian density function.

The probability of the error event $\boldsymbol{\varepsilon}$ can be predicted by averaging (3.4) over all possible data paths that support this error event pattern. If no coding scheme is used, we get this probability as [55]

$$P_r(\boldsymbol{\varepsilon}) = \sum_{\{\mathbf{a}\}} P_r(\boldsymbol{\varepsilon}|\mathbf{a})P_r(\mathbf{a}) = 2^{-W_H(\boldsymbol{\varepsilon})}Q\left(\frac{d_{\boldsymbol{\varepsilon}}^2}{2\sigma_{u,\boldsymbol{\varepsilon}}}\right), \tag{3.5}$$

where $W_H(\boldsymbol{\varepsilon})$ indicates the number of the non-zero elements of $\boldsymbol{\varepsilon}$. Let Ψ denote the set of all possible error events. An upper bound for the BER of VA detector is given

[1] It is safe to make this assumption because the non-Gaussian distributed residual ISI present in the e_k is rather a small quantity compared to channel noises, which are usually modeled as Gaussian random processes.

by summing up the probability of every error event belonging to Ψ, i.e.

$$P_b \le \sum_{\boldsymbol{\varepsilon}\in\Psi} W_H(\boldsymbol{\varepsilon}) 2^{-W_H(\boldsymbol{\varepsilon})} Q\left(\frac{d_{\boldsymbol{\varepsilon}}^2}{2\sigma_{u,\boldsymbol{\varepsilon}}}\right).$$

This bound becomes tight at medium-to-high channel SNRs, and thus we have

$$P_b \approx \sum_{\boldsymbol{\varepsilon}\in\Psi} W_H(\boldsymbol{\varepsilon}) 2^{-W_H(\boldsymbol{\varepsilon})} Q\left(\frac{d_{\boldsymbol{\varepsilon}}^2}{2\sigma_{u,\boldsymbol{\varepsilon}}}\right). \tag{3.6}$$

Let $\mathbf{R}_{ee}$ denote the $(N+N_\varepsilon-1)\times(N+N_\varepsilon-1)$ autocorrelation matrix of e_k with element $R_{ee}(i,j)=r_e(|i-j|)$, and the column vector $\tilde{\boldsymbol{\varepsilon}}=[\tilde{\varepsilon}_k,\tilde{\varepsilon}_{k+1},\cdots,\tilde{\varepsilon}_{k+N+N_\varepsilon-2}]^T$ represent the error event $\boldsymbol{\varepsilon}$ filtered by the target, where $\tilde{\varepsilon}_k=\sum_{i=0}^{N-1} g_i\varepsilon_{k+j-i}$. Then, we may express (3.6) using matrix notation as

$$P_b \approx \sum_{\boldsymbol{\varepsilon}\in\Psi} W_H(\boldsymbol{\varepsilon}) 2^{-W_H(\boldsymbol{\varepsilon})} Q\left(\frac{\tilde{\boldsymbol{\varepsilon}}^T\tilde{\boldsymbol{\varepsilon}}}{2\sqrt{\tilde{\boldsymbol{\varepsilon}}^T\mathbf{R}_{ee}\tilde{\boldsymbol{\varepsilon}}}}\right),$$

since $d_{\boldsymbol{\varepsilon}}^2=\tilde{\boldsymbol{\varepsilon}}^T\tilde{\boldsymbol{\varepsilon}}$ and $\sigma_{u,\boldsymbol{\varepsilon}}^2=\tilde{\boldsymbol{\varepsilon}}^T\mathbf{R}_{ee}\tilde{\boldsymbol{\varepsilon}}$. As the $Q(\bullet)$ function exponentially decreases with its argument, at media-to-high channel SNRs, the bit-error-rate can be estimated by

$$P_b \approx 2^{1-W_H(\boldsymbol{\varepsilon}^d)} W_H(\boldsymbol{\varepsilon}^d) Q\left(\frac{(\tilde{\boldsymbol{\varepsilon}}^d)^T\tilde{\boldsymbol{\varepsilon}}^d}{2\sqrt{(\tilde{\boldsymbol{\varepsilon}}^d)^T\mathbf{R}_{ee}\tilde{\boldsymbol{\varepsilon}}^d}}\right), \tag{3.7}$$

where $\boldsymbol{\varepsilon}^d$ and its sample-by-sample reversed version, $-\boldsymbol{\varepsilon}^d$ are the pair of the dominant error events that minimize the argument of $Q(\bullet)$ function in (3.6), and $\tilde{\boldsymbol{\varepsilon}}^d$ is obtained by filtering $\boldsymbol{\varepsilon}^d$ by the target. Without loss of generality, we set the first error bit of $\boldsymbol{\varepsilon}^d$ to be positive.

With the BER prediction given by (3.7), we can define the squared argument of the $Q(\bullet)$ function in (3.7) as the cost function for target design, i.e.

$$SNR_{eff}=\frac{1}{4}\frac{\left((\tilde{\boldsymbol{\varepsilon}}^d)^T\tilde{\boldsymbol{\varepsilon}}^d\right)^2}{(\tilde{\boldsymbol{\varepsilon}}^d)^T\mathbf{R}_{ee}\tilde{\boldsymbol{\varepsilon}}^d}. \tag{3.8}$$

The quantity defined by (3.8) is usually referred to as the 'effective detection SNR'

(SNR_{eff}) for VA detector, which is an equivalent measure of the BER performance of PRML systems. Different from mean squared error, SNR_{eff} accounts for noise correlation and the noise power in its denominator, while its numerator reflects the effective signal energy felt by the VA detector from the error event $\boldsymbol{\varepsilon}^d$. It is natural to expect that the GPR target that maximizes SNR_{eff} can achieve the optimum performance of the PRML system. However, this cost function is so complicated that directly deriving the optimum solution for the target response does not seem possible. One may search the optimum target based on (3.8) by numerical methods, which, as indicated in [31], is a very expensive computational effort. Further, since SNR_{eff} is not a quadratic function of the target, whether the search will result in a global optimum is not clear.

In the next section, we will propose a novel analytical approach for finding the optimum GPR target based on the SNR_{eff} criterion.

3.3 Novel Analytical Approach for Designing Optimum Target of Finite Length

In this section, we develop an analytical approach for designing GPR target based on the effective detection SNR criterion. An early attempt to solve this optimization problem by a frequency-domain approach was reported in [35], but the complete analytical solution was not provided. In this thesis, we derive the closed-form analytical solution of the optimum magnitude frequency response of target of finite length based on the SNR_{eff} criterion. We also discuss the necessary constraints to ensure that the optimized target response have real coefficients.

3.3.1 Optimization in Frequency Domain

As mentioned in Section 3.2, effective detection SNR defined by (3.8) can be used as a cost function for designing optimum GPR target. The equivalent expression of SNR_{eff} in frequency domain is given by

$$SNR_{eff} = \frac{\frac{1}{4}\left(\int_{-0.5}^{0.5} \left|GE^d\right|^2 d\Omega\right)^2}{\int_{-0.5}^{0.5} \left|GE^d\right|^2 \left(\mathrm{P}_n \left|W\right|^2 + \mathrm{P}_a \left|WR - Ge^{-j2\pi\Omega k_0}\right|^2\right) d\Omega}, \tag{3.9}$$

where Ω is the frequency normalized by bit rate, G, E^d, R and W represent the Fourier transforms of the target response g_k, dominant error event $\boldsymbol{\varepsilon}^d$ channel bit response r_k and equalizer w_k, respectively, k_0 is the delay from channel input to equalizer output, and P_a and P_n denote the PSDs of the input data a_k and overall channel noise e_k, respectively. In the case where channel noise is not actually stationary due to the presence of media noise, we estimate an effective PSD of channel noise by time averaging (i.e. we ignore the non-stationary induced by the data-dependence of media noise). However, when the first-order approximation of media noise shown in Figure 2.5 is valid (i.e. for sufficiently small transition jitter and pulse variation), the expression for the overall noise PSD can be obtained as

$$\mathrm{P}_n = E\left[b_k{}^2\right]\left(E\left[\Delta_k{}^2\right]\left|F^p\right|^2 + E\left[\varpi_k{}^2\right]\left|F^w\right|^2\right) + E\left[n_k{}^2\right],$$

where Δ_k and ϖ_k denote the random transition position jitter and the transition pulse width variation, respectively, n_k represents the electronics noise, F^w and F^p are the Fourier transforms of first-order jitter path and pulse width variation path, respectively, as shown in Figure 2.5, and $\{b_k\}$ represents the transition data sequence.

For a given dominant error event E^d, the equalizer W is only related to the denominator in (3.9). Equivalently by minimizing the denominator, we can obtain the

optimum solution of W that maximizes SNR_{eff}. Since $|GE^d|$ cannot have region(s) of continuous zeros in frequncy domain when dominant error event and target are of finite length, the denominator of (3.9) is essentially a quadratic function of W with a unique minimum. Using the method of *calculus of variations* introduced in Section 2.3.2, we obtain the optimum solution of W as

$$W_o = \frac{\mathrm{P}_a R^* e^{-j2\pi\Omega k_0}}{\mathrm{P}_n + \mathrm{P}_a |R|^2} G . \tag{3.10}$$

From (3.10) and (2.32), we see that the optimum equalizer based on the SNR_{eff} criterion is same as the solution of unconstrained MMSE equalizer.

Substituting (3.10) in (3.9) yields

$$SNR_{eff} = \frac{1}{4} \frac{\left(\int_{-0.5}^{0.5} |G|^2 |E^d|^2 d\Omega \right)^2}{\int_{-0.5}^{0.5} \left[|G|^4 |E^d|^2 \mathrm{P}_a \mathrm{P}_n \Big/ \left(\mathrm{P}_n + \mathrm{P}_a |R|^2 \right) \right] d\Omega} . \tag{3.11}$$

Eqn. (3.11) shows that the optimal effective detection SNR is determined by $|G|^2$ instead of G. In other words, the performance of PRML system in terms of SNR_{eff} is related only to the magnitude frequency response of target and is independent of its phase response. This observation agrees with the fact that the path metrics in VA detector do not depend on target phase. To simplify the fourth power optimization problem given by (3.11), we define $X \triangleq |G|^2$ and change (3.11) into a function of X given by

$$J(X) = \frac{1}{4} \frac{\left(\int_{-0.5}^{0.5} X |E^d|^2 d\Omega \right)^2}{\int_{-0.5}^{0.5} \left[X^2 |E^d|^2 \mathrm{P}_a \mathrm{P}_n \Big/ \left(\mathrm{P}_n + \mathrm{P}_a |R|^2 \right) \right] d\Omega} . \tag{3.12}$$

The numerator and denominator of (3.12) are both quadratic functions of X. The analytical solution for the optimum X that maximizes $J(X)$ can be derived.

Since $X = |G|^2$, the inverse Fourier transform of X is the correlation function of the target. For N–tap GPR target $G(D) = g_0 + g_1 D + \cdots + g_{N-1} D^{N-1}$ (g_i is real-valued), the expression for X can be given as

$$X = |G|^2 = x_0 + 2\sum_{i=1}^{N-1} x_i \cos(i2\pi\Omega) = x_0\left(1 + 2\sum_{i=1}^{N-1} \frac{x_i}{x_0}\cos(i2\pi\Omega)\right), \qquad (3.13)$$

where $x_i = g_i \otimes g_{-i}$ and $x_i = x_{-i}$ ($\otimes$ denotes convolution operator) for $i = 0,1\cdots, N-1$. We see from (3.12) and (3.13) that $J(X)$ is only determined by the ratios x_i/x_0. Hence, without loss of generality, we may set $x_0 = 1$, i.e. normalize the energy of target to unity, when optimizing $J(X)$ given by (3.12). Then, we can rewrite (3.12) as a function of $\mathbf{x} = [x_1, \ldots, x_{N-1}]^T$ given by

$$J(X) \equiv J(\mathbf{x}) = \frac{1}{4}\frac{p_0^2 + 4p_0\mathbf{x}^T\mathbf{p} + 4\mathbf{x}^T\mathbf{B}\mathbf{x}}{t_0 + 4\mathbf{x}^T\mathbf{t} + 4\mathbf{x}^T\mathbf{U}\mathbf{x}}, \qquad (3.14)$$

where $\mathbf{p} = [p_1, \ldots, p_{N-1}]^T$, $\mathbf{t} = [t_1, \ldots, t_{N-1}]^T$, $p_i = \int_{-0.5}^{0.5} |E^d|^2 \cos(i2\pi\Omega)\, d\Omega$ and $t_i = \int_{-0.5}^{0.5} \left[|E^d|^2 \mathrm{P}_a \mathrm{P}_n / \left(\mathrm{P}_n + \mathrm{P}_a |R|^2\right)\right] \cos(i2\pi\Omega)\, d\Omega$ for $i = 0,1,\cdots, N-1$, $\mathbf{B} = \mathbf{p}\mathbf{p}^T$, and $\mathbf{U}$ is a $(N-1)\times(N-1)$ matrix with element $U_{i,j} = \frac{1}{2}(t_{i+j} + t_{|i-j|})$ for $i, j = 1, 2, \cdots, N-1$.

In the case where the single-bit error event dominates the BER performance of the VA detector (i.e. $|E^d|^2$ is a constant, and thus $\mathbf{p} = \mathbf{0}$ and $\mathbf{B} = \mathbf{0}$), the numerator of (3.14) becomes the constant p_0^2. Hence, the optimum solution of $\mathbf{x}$ that maximizes (3.14) can be obtained by simply minimizing its denominator. Since $\mathbf{U}$ is a symmetric positive definite matrix due to its definition (unless $X \equiv 0$, the denominator of (3.12) is always positive for any X), we can easily find the optimum solution of $\mathbf{x}$ as

$$\mathbf{x}_o = [x_{o,1}, x_{o,2}, \cdots, x_{o,N-1}]^T = -\frac{1}{2}\mathbf{U}^{-1}\mathbf{t}. \qquad (3.15)$$

In the case where a multi-bit error event is the dominant event, the square matrix $\mathbf{B}$ in the numerator of (3.14) is non-zero. There must exist a unitary matrix $\mathbf{Q}=[\mathbf{q}_1,\ldots,\mathbf{q}_{N-1}]$ such that $\mathbf{QBQ}^T = diag\left(\lambda_d^2, 0.\ldots 0\right)$ where $\lambda_d = \mathbf{p}^T\mathbf{q}_1$ ($\lambda_d \neq 0$). Then, defining $\mathbf{y}=\left[y,\mathbf{z}^T\right]^T=\mathbf{Q}^T\mathbf{x}$ yields

$$J(\mathbf{x}) \equiv J(y,\mathbf{z}) = \frac{\lambda_d{}^2 (y+c)^2}{t_0 + 4s_1 y + 4\mathbf{v}^T\mathbf{z} + 4ay^2 + 8y\boldsymbol{\alpha}^T\mathbf{z} + 4\mathbf{z}^T\mathbf{A}\mathbf{z}}, \tag{3.16}$$

where $c = p_0 \big/ 2\lambda_d$, $\mathbf{s}=\begin{bmatrix} s_1 \\ \mathbf{v}\end{bmatrix}=\mathbf{Q}^T\mathbf{t}$ and $\mathbf{S}=\begin{pmatrix} a & \boldsymbol{\alpha}^T \\ \boldsymbol{\alpha} & \mathbf{A}\end{pmatrix}=\mathbf{Q}^T\mathbf{U}\mathbf{Q}$. Note that $\mathbf{A}$ is a positive definite matrix, since $\mathbf{U}$ is positive definite. Apparently, $J(y,\mathbf{z})$ given by (3.16) reaches its zero-valued minimum when $y=-c$. Hence, by setting the derivative of $J(y,\mathbf{z})$ with respect to y and every element of $\mathbf{z}$ to zero, and disregarding the solution $y=-c$, we obtain the optimum solution that maximizes $J(y,\mathbf{z})$ as $y_o = \dfrac{\left(t_0 - \mathbf{v}^T\mathbf{A}^{-1}\mathbf{v}\right) - 2c\left(s_1 - \boldsymbol{\alpha}^T\mathbf{A}^{-1}\mathbf{v}\right)}{4c\left(a - \boldsymbol{\alpha}^T\mathbf{A}^{-1}\boldsymbol{\alpha}\right) - 2\left(s_1 - \boldsymbol{\alpha}^T\mathbf{A}^{-1}\mathbf{v}\right)}$ and $\mathbf{z}_o = -\frac{1}{2}\mathbf{A}^{-1}\left(\mathbf{v} + 2y_o\boldsymbol{\alpha}\right)$. With $\mathbf{y}_o = \left[y_o,\ \mathbf{z}_o{}^T\right]^T$, the optimum solution of $\mathbf{x}$ is obtained as

$$\mathbf{x}_o = \begin{bmatrix} x_{o,1} \\ x_{o,2} \\ \vdots \\ x_{o,N-1}\end{bmatrix} = \mathbf{Q}\begin{bmatrix} \dfrac{\left(t_0 - \mathbf{v}^T\mathbf{A}^{-1}\mathbf{v}\right) - 2c\left(s_1 - \boldsymbol{\alpha}^T\mathbf{A}^{-1}\mathbf{v}\right)}{4c\left(a - \boldsymbol{\alpha}^T\mathbf{A}^{-1}\boldsymbol{\alpha}\right) - 2\left(s_1 - \boldsymbol{\alpha}^T\mathbf{A}^{-1}\mathbf{v}\right)} \\ -\frac{1}{2}\mathbf{A}^{-1}\left(\mathbf{v} + 2\dfrac{\left(t_0 - \mathbf{v}^T\mathbf{A}^{-1}\mathbf{v}\right) - 2c\left(s_1 - \boldsymbol{\alpha}^T\mathbf{A}^{-1}\mathbf{v}\right)}{4c\left(a - \boldsymbol{\alpha}^T\mathbf{A}^{-1}\boldsymbol{\alpha}\right) - 2\left(s_1 - \boldsymbol{\alpha}^T\mathbf{A}^{-1}\mathbf{v}\right)}\boldsymbol{\alpha}\right)\end{bmatrix}. \tag{3.17}$$

Consequently, the optimum X is formed as $X_o = 1 + 2\sum_{i=1}^{N-1} x_{o,i}\cos(i2\pi\Omega)$.

Having found the optimum X_o, the corresponding optimum target G can be obtained by spectral factorization, i.e.

$$X(D) = G(D)G^*\left(D^{-*}\right),$$

where $X(D)$ is the D transform of X given by $X(D)=\sum_{-N+1}^{N-1} x_i D^i$. The spectral factorization will result in $G(D)$ with real coefficients, if all the complex-valued zeros

of $X(D)$ appear in groups as $\{D_0, D_0^*, D_0^{-1}, D_0^{-*}\}$ and all the real-valued zeros of $X(D)$ are in pairs as $\{D_0, D_0^{-1}\}$. In our problem, since the coefficients of $X(D)$ are symmetric (i.e. $x_i = x_{-i}$) and real-valued, if D_0 is a zero of $X(D)$, then D_0^*, D_0^{-*} and D_0^{-1} must be the zeros of $X(D)$ too. Hence, as long as $X(D)$ has no zeros on the unit circle $|D|=1$ or its zeros on the unit circle are evenly repeated, the target $G(D)$ obtained by spectral factorization has real-valued coefficients, i.e. the de-convolution of **x** into a valid target response **g** is guaranteed. Unfortunately, this is not naturally guaranteed by the optimum solution $\mathbf{x}_o$ given by (3.15) or (3.17). Consequently, the target response obtained by spectral factorization may have complex-valued coefficients, which is not permissible. This problem arises because we do not account for the fact that **x** is the auto-correlation of the target **g** while deriving (3.15) and (3.17). In the next sub-section, we will discuss the region of feasible **x**, which guarantees **x** to be de-convoluted into valid target response with real-valued coefficients.

3.3.2 Characterization of the Region of Feasible Solutions

For $X(D)$ with real-valued and symmetric coefficients (i.e. $x_i = x_{-i}$), spectral factorization of $X(D)$ results in target $G(D)$ with real-valued coefficients only if $X(D)$ has no odd times repeated zeros on the unit circle. This is equivalent to requiring that $X = 1 + 2\sum_{i=1}^{N-1} x_i \cos(i2\pi\Omega) \geq 0$, or

$$\min_{\Omega\in[0,0.5]} \{F(\mathbf{x},\Omega)\} \geq -0.5, \tag{3.18}$$

where $F(\mathbf{x},\Omega) = \sum_{i=1}^{N-1} x_i \cos(i2\pi\Omega)$. In this section, we present a characterization of

the feasible region $\tilde{R}$ of $\mathbf{x}$ that satisfies (3.18).

Obviously, the origin $\mathbf{x}=[0,0,\cdots,0]^T$ lies inside the region $\tilde{R}$. Let $\mathbf{x}=[x_1,x_2,\cdots,x_{N-1}]^T$ change along a radial direction defined by $\mathbf{k}=[k_1,k_2,\cdots,k_{N-1}]^T$ ($\mathbf{k}\neq\mathbf{0}$), i.e. $x_1=k_1t,\ x_2=k_2t,\cdots,\ x_{N-1}=k_{N-1}t$ for $t\in[0,+\infty)$. When $\mathbf{x}=\mathbf{k}$, i.e. $t=1$, let ρ ($\rho<0$) be the minimum value of $F(\mathbf{k},\Omega)$ over all Ω. Therefore, we get

$$\min_{\{\Omega\}}\{F(t\mathbf{k},\Omega)\}=t\rho\quad\begin{cases}\geq -0.5 & 0\leq t\leq -\dfrac{1}{2\rho}\\ <-0.5 & t>-\dfrac{1}{2\rho}\end{cases}$$

which implies that the region $\tilde{R}$ is continuous along any given radial direction $\mathbf{k}$ with a bound specified by $t\leq -1/(2\rho)$. Since this must be true for all possible $\mathbf{k}$, we can conclude that $\tilde{R}$ is a continuous region. In addition, as ρ continuously changes with $\mathbf{k}$, the boundary of $\tilde{R}$ is also continuous. Furthermore, it also follows that the X formed from a point $\mathbf{x}$ on the boundary of $\tilde{R}$ will have zero-valued global minimum (minima), i.e. $X=0$ for some Ω and $X>0$ elsewhere. Note that any zero-valued global minimum of X in frequency domain must correspond to an evenly repeated zero of $X(D)$ on the unit circle; otherwise it would be a saddle point of X.

Let $\mathbf{x}^a$ and $\mathbf{x}^b$ represent any two distinct points on the boundary of $\tilde{R}$. Then, the line segment $\overset{\frown}{ab}$ joining $\mathbf{x}^a$ and $\mathbf{x}^b$ can be expressed as

$$x_1=\left(x_1^a-x_1^b\right)t+x_1^b,\ \ x_2=\left(x_2^a-x_2^b\right)t+x_2^b,\cdots,\ x_{N-1}=\left(x_{N-1}^a-x_{N-1}^b\right)t+x_{N-1}^b,\quad t\in[0,\,1].$$

It is found that all the points on $\overset{\frown}{ab}$ belong to the region $\tilde{R}$, because

$$\begin{aligned}F(\mathbf{x},\Omega)\big|_{\mathbf{x}\in\overset{\frown}{ab}}&=\sum_{i=1}^{N-1}\left[t\left(x_i^a-x_i^b\right)+x_i^b\right]\cos(i2\pi\Omega)\\&=\sum_{i=1}^{N-1}\left[t\,x_i^a+(1-t)\,x_i^b\right]\cos(i2\pi\Omega)\\&=t\,F\left(\mathbf{x}^a,\Omega\right)+(1-t)\,F\left(\mathbf{x}^b,\Omega\right)\geq -0.5\end{aligned}$$

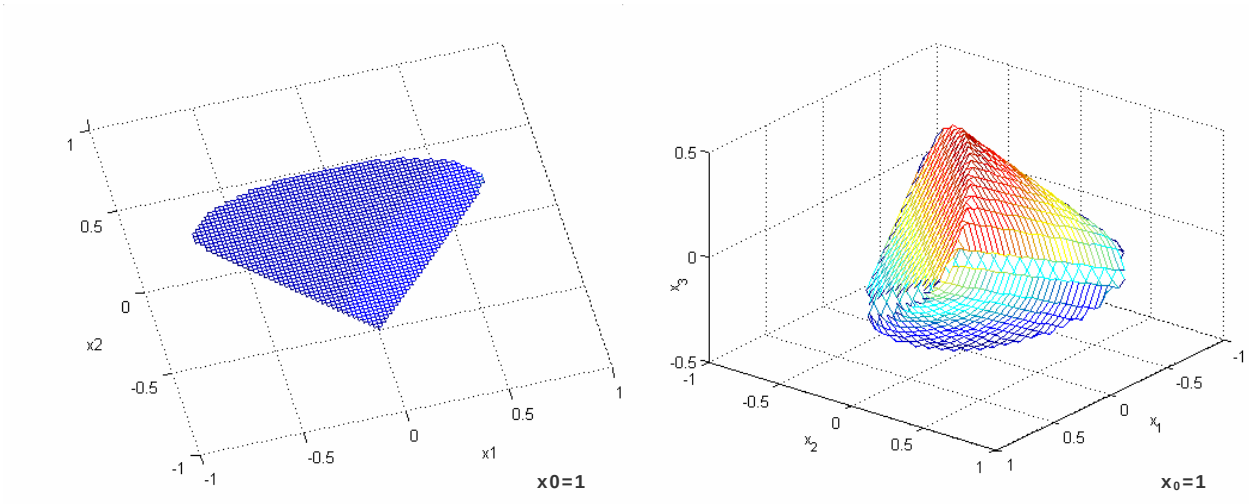

(a) (b)

Figure 3.2: Region $\tilde{R}$ in which $\mathbf{x}$ can be de-convoluted into real-valued target response. (a) example with 3-tap unit-energy target, (b) example with 4-tap unit-energy target.

for $0 \le t \le 1$. Hence, $\tilde{R}$ is a continuous and convex region.

Figure 3.2 illustrates examples of the region $\tilde{R}$ of $\mathbf{x}$ satisfying (3.18) based on 3-tap and 4-tap targets having unit energy.

3.3.3 Approach for Finding Feasible Optimum Solution

The region $\tilde{R}$ defines the feasible space of solution for the underlying optimization problem of $J(\mathbf{x})$ given by (3.14). That is,

$$SNR_{eff} \equiv J(\mathbf{x}) \quad \text{for } \mathbf{x} \in \tilde{R}.$$

In Section 3.3.1, we showed that $J(\mathbf{x})$ given by (3.14) has a unique maximum given by (3.15) or (3.17). Further, the analysis in Section 3.3.2 shows that the region $\tilde{R}$ of feasible $\mathbf{x}$ is continuous and convex. From these facts, we can conclude that if the solution given by (3.15) or (3.17) lies outside the region $\tilde{R}$, then the feasible solution

$\mathbf{x}$ that maximizes SNR_{eff} must be located on the boundary of $\tilde{R}$ and it is unique[2]. To find such a solution that lies on the boundary of $\tilde{R}$, we may use the constraint that X formed from the solution $\mathbf{x}$ must be non-negative and has spectral zero(s), when optimizing (3.14). This constraint is equivalent to making the global minimum (minima) of X to be zero.

Let us assume that the optimum $X_o = |G_o|^2$ based on SNR_{eff} has M zero-valued global minima at frequencies $\{\Omega_1,\ldots,\Omega_M\}$, i.e. $\sum_{i=1}^{N-1} x_i \cos(i2\pi\Omega_j) = -0.5$ for $j = 1,2,\cdots,M$. Then, we have M 'zero-constraints' given by

$$\mathbf{C}\,\mathbf{x} = [\mathbf{C}'\ \ \mathbf{C}''] \begin{bmatrix} \mathbf{x}' \\ \mathbf{x}'' \end{bmatrix} = \mathbf{C}'\,\mathbf{x}' + \mathbf{C}''\,\mathbf{x}'' = \mathbf{l},$$

or equivalently,

$$\mathbf{x}' = (\mathbf{C}')^{-1}(\mathbf{l} - \mathbf{C}''\,\mathbf{x}'') = \boldsymbol{\gamma} + \mathbf{P}\mathbf{x}'', \tag{3.19}$$

where $\mathbf{C}$ is a $M \times (N-1)$ matrix whose elements are given by $C_{i,j} = \cos(j2\pi\Omega_i)$ for $i, j = 1,2,\cdots,M$, $\mathbf{l} = [-0.5,\cdots,-0.5]^T$ is a $M \times 1$ vector, $\mathbf{x}' = [x_1, x_2, \cdots, x_M]^T$, $\mathbf{x}'' = [x_{M+1}, x_{M+2}, \cdots, x_{N-1}]^T$, $\mathbf{C}'$ and $\mathbf{C}''$ are the matrices given by

$$\mathbf{C}' = \begin{bmatrix} C_{1,1} & C_{1,2} & \cdots & C_{1,M} \\ C_{2,1} & C_{2,2} & \cdots & C_{2,M} \\ \vdots & \vdots & \ddots & \vdots \\ C_{M,1} & C_{M,2} & \cdots & C_{M,M} \end{bmatrix} \text{ and } \mathbf{C}'' = \begin{bmatrix} C_{1,M+1} & C_{1,M+2} & \cdots & C_{1,N-1} \\ C_{2,M+1} & C_{2,M+2} & \cdots & C_{2,N-1} \\ \vdots & \vdots & \ddots & \vdots \\ C_{M,M+1} & C_{M,M+2} & \cdots & C_{M,N-1} \end{bmatrix},$$

respectively, $\boldsymbol{\gamma} = (\mathbf{C}')^{-1}\mathbf{l}$, and $\mathbf{P} = -(\mathbf{C}')^{-1}\mathbf{C}''$.

We now partition the vectors $\mathbf{p}$ and $\mathbf{t}$, and matrix $\mathbf{U}$ in (3.14) as

$$\mathbf{p} = \begin{bmatrix} \mathbf{p}' \\ \mathbf{p}'' \end{bmatrix},\ \mathbf{t} = \begin{bmatrix} \mathbf{t}' \\ \mathbf{t}'' \end{bmatrix},\ \text{and}\ \mathbf{U} = \begin{bmatrix} \mathbf{U}' & \mathbf{V}^T \\ \mathbf{V} & \mathbf{U}'' \end{bmatrix},$$

[2] A rigorous analysis on the uniqueness issue is presented in Chapter 5.

respectively, where $\mathbf{p}'$ and $\mathbf{t}'$ are $M \times 1$ vectors, $\mathbf{U}'$ is a $M \times M$ matrix, and $\mathbf{U}''$ is a $(N-M-1)\times(N-M-1)$ matrix. Note that $\mathbf{U}'$ and $\mathbf{U}''$ are both symmetric and positive definite, since $\mathbf{U}$ is symmetric and positive definite. Then, substituting (3.19) and the above forms of $\mathbf{p}$, $\mathbf{t}$ and $\mathbf{U}$ into (3.14), we have

$$J(\mathbf{x}_c) = J_c(\mathbf{x}'') = \frac{\tilde{p}_0{}^2 + 4\tilde{p}_0 \mathbf{x}''^T \tilde{\mathbf{p}} + 4\mathbf{x}''^T \tilde{\mathbf{B}} \mathbf{x}''}{\tilde{t}_0 + 4\mathbf{x}''^T \tilde{\mathbf{t}} + 4\mathbf{x}''^T \tilde{\mathbf{U}}\, \mathbf{x}''}, \tag{3.20}$$

where $\mathbf{x}_c = \left[(\boldsymbol{\gamma} + \mathbf{P}\mathbf{x}'')^T,\ \mathbf{x}''^T \right]^T$ represents $\mathbf{x}$ subject to the 'zero-constraints' (3.19), $\tilde{p}_0 = p_0 + 2\boldsymbol{\gamma}^T \mathbf{p}'$, $\tilde{\mathbf{p}} = \mathbf{p}'' + \mathbf{P}^T \mathbf{p}'$, $\tilde{t}_0 = t_0 + 4\boldsymbol{\gamma}^T \mathbf{t}' + 4\boldsymbol{\gamma}^T \mathbf{U}' \boldsymbol{\gamma}$, $\tilde{\mathbf{t}} = \mathbf{t}'' + \mathbf{P}^T \mathbf{t}' + 2\left(\mathbf{V} + \mathbf{P}^T \mathbf{U}'\right)\boldsymbol{\gamma}$, $\tilde{\mathbf{B}} = \tilde{\mathbf{p}}\tilde{\mathbf{p}}^T$, and $\tilde{\mathbf{U}} = \mathbf{P}^T \mathbf{U}' \mathbf{P} + \mathbf{U}'' + \mathbf{V}\mathbf{P} + \mathbf{P}^T \mathbf{V}^T$. Note that matrix $\tilde{\mathbf{U}}$ is symmetric and positive definite too.

Observing the similarity between (3.20) and (3.14) we can find the optimum solution $\mathbf{x}_o''$ that maximizes (3.20) by following the same procedure in deriving the optimum solution for (3.14). If $\tilde{\mathbf{p}} = \mathbf{0}$, we have the solution that maximizes $J_c(\mathbf{x}'')$ as

$$\mathbf{x}_o'' = -\frac{1}{2} \tilde{\mathbf{U}}^{-1} \tilde{\mathbf{t}}, \tag{3.21}$$

If $\tilde{\mathbf{p}} \neq \mathbf{0}$ the solution $\mathbf{x}_o''$ is obtained as

$$\mathbf{x}_o'' = \tilde{\mathbf{Q}} \begin{bmatrix} \dfrac{\left(\tilde{t}_0 - \tilde{\mathbf{v}}^T \tilde{\mathbf{A}}^{-1} \tilde{\mathbf{v}}\right) - 2\tilde{c}\left(\tilde{s}_1 - \tilde{\boldsymbol{\alpha}}^T \tilde{\mathbf{A}}^{-1} \tilde{\mathbf{v}}\right)}{4\tilde{c}\left(\tilde{a} - \tilde{\boldsymbol{\alpha}}^T \tilde{\mathbf{A}}^{-1} \tilde{\boldsymbol{\alpha}}\right) - 2\left(\tilde{s}_1 - \tilde{\boldsymbol{\alpha}}^T \tilde{\mathbf{A}}^{-1} \tilde{\mathbf{v}}\right)} \\ -\dfrac{1}{2} \tilde{\mathbf{A}}^{-1} \left(\tilde{\mathbf{v}} + 2 \dfrac{\left(\tilde{t}_0 - \tilde{\mathbf{v}}^T \tilde{\mathbf{A}}^{-1} \tilde{\mathbf{v}}\right) - 2\tilde{c}\left(\tilde{s}_1 - \tilde{\boldsymbol{\alpha}}^T \tilde{\mathbf{A}}^{-1} \tilde{\mathbf{v}}\right)}{4\tilde{c}\left(\tilde{a} - \tilde{\boldsymbol{\alpha}}^T \tilde{\mathbf{A}}^{-1} \tilde{\boldsymbol{\alpha}}\right) - 2\left(\tilde{s}_1 - \tilde{\boldsymbol{\alpha}}^T \tilde{\mathbf{A}}^{-1} \tilde{\mathbf{v}}\right)} \tilde{\boldsymbol{\alpha}} \right) \end{bmatrix}, \tag{3.22}$$

where $\tilde{\mathbf{Q}}$ is a unitary eigenvector matrix of $\tilde{\mathbf{B}}$, $\tilde{\lambda}_d$ is the non-zero eigenvalue of $\tilde{\mathbf{B}}$ (Note: $\tilde{\mathbf{B}}$ is a rank-1 matrix), $\tilde{c} = \dfrac{\tilde{p}_0}{2\tilde{\lambda}_d}$, $\tilde{\mathbf{Q}}^T \tilde{\mathbf{t}} = \begin{bmatrix} \tilde{s}_1 \\ \tilde{\mathbf{v}} \end{bmatrix}$ and $\tilde{\mathbf{Q}}^T \tilde{\mathbf{U}} \tilde{\mathbf{Q}} = \begin{pmatrix} \tilde{a} & \tilde{\boldsymbol{\alpha}}^T \\ \tilde{\boldsymbol{\alpha}} & \tilde{\mathbf{A}} \end{pmatrix}$. Having obtained $\mathbf{x}_o''$, we can obtain $\mathbf{x}_o' = \boldsymbol{\gamma} + \mathbf{P}\mathbf{x}_o''$. Then, the optimum solution subject to 'zero-constraints' is given by $\mathbf{x}_{c,o} = \left[\mathbf{x}_o'^T,\ \mathbf{x}_o''^T \right]^T$.

Note the constrained optimum solution $\mathbf{x}_{c,o}$ derived above is dependent on the assumed frequencies $\{\Omega_1,\ldots,\Omega_M\}$ at which the optimum $|G_o|^2\,(=X_o)$ reaches its zero-valued global minima. However, we do not actually know the values of $\{\Omega_1,\ldots,\Omega_M\}$. We can perform a linear search over the *M*-dimensional space where $\{0\le\Omega_i\le 0.5$ for $i=1,2,\cdots,M\}$ to determine these frequencies as $\{\Omega'_1,\ldots,\Omega'_M\}$ such that the *X* formed from the resulting $\mathbf{x}_{c,o}$ has its zero-valued global minima at $\{\Omega'_1,\ldots,\Omega'_M\}$. Note that we also need to determine *M*, the number of the zero-constraints. Considering the performance loss due to constraints, we should use as few constraints as possible. Therefore, we may start the search for the number of zero-constraints with $M=0$, and increase *M*, if necessary, until we find suitable values of $\{\Omega_1,\ldots,\Omega_M\}$. In addition, it is noticed that the unconstrained (i.e. $M=0$) solution given by (3.15) or (3.17) is usually quite close to the valid optimum in $\tilde{R}$ even though the former may be outside the feasible region $\tilde{R}$. We may use this unconstrained solution, when it is invalid for de-convolution, to obtain a good initial point for searching the zero-valued global minima of the optimum $X_o=|G_o|^2$, and thus significantly reduce the computations required to determine *M* and the values of $\{\Omega_1,\ldots,\Omega_M\}$. The approach for determining the feasible optimum solution based on the SNR_{eff} criterion is concluded as a flow chart shown in Figure 3.3.

Finally, we need to check if the dominant error event assumed in the computation of the optimum target based on SNR_{eff} really dominates the bit error probability with the resulting target. Generally, we need to investigate over all the possible error events. However, we see from (3.7) that the BER is predicted by the error event probability weighted by the quantity $W_H(\boldsymbol{\varepsilon})2^{1-W_H(\boldsymbol{\varepsilon})}$, which exponentially decreases

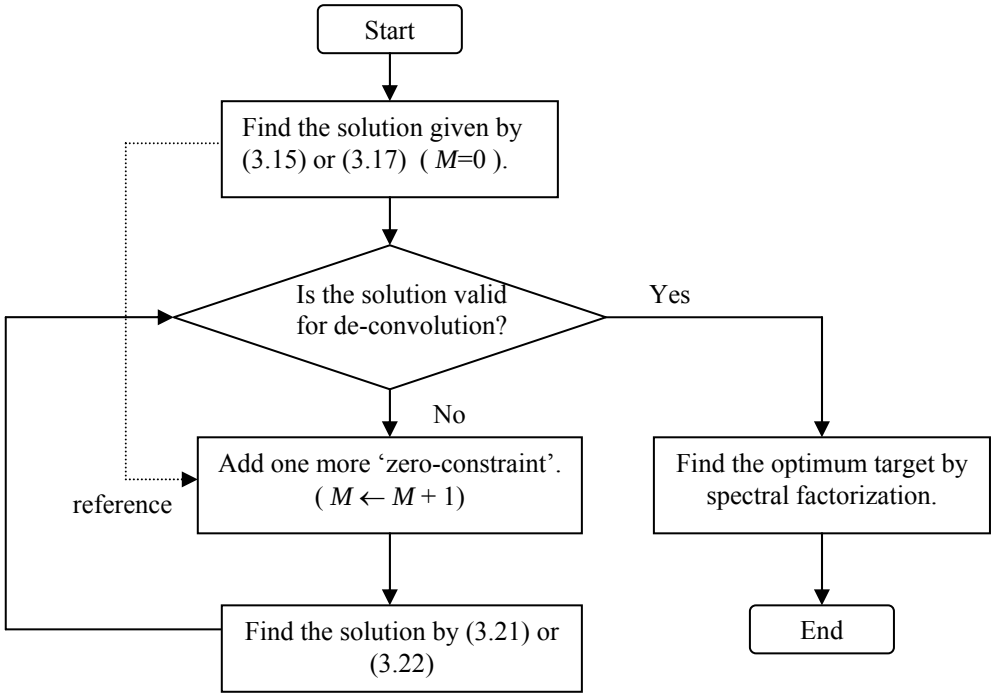

Figure 3.3: Approach for finding the optimum target based on the SNR_{eff} criterion.

with the Hamming weight of the error event. Hence, it is sufficient to determine the dominant error event over the set of the error events having small Hamming weights.

3.4 Optimum Target of Infinite Length

In this section, we derive the optimum magnitude frequency response of infinitely long target that maximizes the SNR_{eff} given by (3.11). Similar to the approach for finding the optimum target of finite length, we first derive the optimum X_o of infinite length that maximizes $J(X)$ given by (3.12), and then check whether X_o is a feasible solution that corresponds to the squared magnitude frequency response of a target G of infinite length.

The analysis in Section 3.3.1 indicates that $J(X)$ given by (3.12) has a unique maximizer X_o whose coefficients are uniquely determined by (3.15) or (3.17). This is also true when the number of the coefficients of X approaches infinity. Due to the uniqueness of the optimum X_o that maximizes $J(X)$, we can find X_o of infinite length by using the technique of *calculus of variations*. Further, we see from (3.12) that $J(X)=0$ if $\int_{-0.5}^{0.5} X\left|E^d\right|^2 d\Omega = 0$, otherwise $J(X)>0$. Let $X = X_o + \mu V$, where V is an arbitrary complex-valued variation and μ is a real scalar. Setting $\frac{\partial}{\partial \mu} J(X)|_{\mu=0} = 0$ and disregarding the case of $\int_{-0.5}^{0.5} X\left|E^d\right|^2 d\Omega = 0$, we obtain

$$\begin{aligned}\int_{-0.5}^{0.5} \mathrm{Re}[V]\left|E^d\right|^2 X Z d\Omega \int_{-0.5}^{0.5} X_o \left|E^d\right|^2 d\Omega \\ - \int_{-0.5}^{0.5} \mathrm{Re}[V]\left|E^d\right|^2 d\Omega \int_{-0.5}^{0.5} {X_o}^2 \left|E^d\right|^2 Z d\Omega = 0\end{aligned}, \tag{3.23}$$

where $Z = \mathrm{P}_a \mathrm{P}_n / \left(\mathrm{P}_n + \mathrm{P}_a |R|^2\right)$. We may rewrite (3.23) as

$$\begin{aligned}\int_{-0.5}^{0.5} \mathrm{Re}\left[V\left(e^{j2\pi\Omega}\right)\right]\left|E^d\left(e^{j2\pi\Omega}\right)\right|^2 \Bigg[X_o\left(e^{j2\pi\Omega}\right) Z\left(e^{j2\pi\Omega}\right) \int_{-0.5}^{0.5} X_o\left(e^{j2\pi\Theta}\right)\left|E^d\left(e^{j2\pi\Theta}\right)\right|^2 d\Theta \\ - \int_{-0.5}^{0.5} X_o^2\left(e^{j2\pi\Theta}\right)\left|E^d\left(e^{j2\pi\Theta}\right)\right|^2 Z\left(e^{j2\pi\Theta}\right) d\Theta \Bigg] d\Omega = 0\end{aligned} \tag{3.24}$$

where the frequencies Ω and Θ are independent of each other. Since V is arbitrary and the dominant error event E^d does not have continuous region of zeros, in order to satisfy (3.24), the quantity in the square brackets should vanish for all Ω. This implies that the optimum X_o should have the characteristics given by

$$X_o\left(e^{j2\pi\Omega}\right) = \frac{1}{Z\left(e^{j2\pi\Omega}\right)} \frac{\int_{-0.5}^{0.5} {X_o}^2\left(e^{j2\pi\Theta}\right)\left|E^d\left(e^{j2\pi\Theta}\right)\right|^2 Z d\Theta}{\int_{-0.5}^{0.5} X_o\left(e^{j2\pi\Theta}\right)\left|E^d\left(e^{j2\pi\Theta}\right)\right|^2 d\Theta}. \tag{3.25}$$

Eqn. (3.25) shows that the optimum X_o is non-negative and real-valued over all Ω, and thus X_o is the squared magnitude frequency response of a valid infinitely long

target that maximizes SNR_{eff}. Note that the quantity $\int_{-0.5}^{0.5} X_o^2 \left|E^d\right|^2 Z d\Theta \Big/ \int_{-0.5}^{0.5} X_o \left|E^d\right|^2 d\Theta$ in (3.25) is independent of Ω. Hence, we obtain the optimum solution of infinitely long target $G_{o,\inf}$ that maximizes SNR_{eff} as

$$\left|G_{o,\inf}\right|^2 = \varphi\left(\frac{1}{\mathrm{P}_a} + \frac{|R|^2}{\mathrm{P}_n}\right), \tag{3.26}$$

where φ is an arbitrary positive constant.

We see from (3.26) that the optimum squared magnitude spectral response of infinitely long target is independent of the assumed dominant error event pattern. This can be explained by examining P_e, the PSD of the estimation error e_k at equalizer output. Using the optimum equalizer W_o given by (3.10), i.e. $W_o = \dfrac{\mathrm{P}_a R^* e^{-j2\pi\Omega k_0}}{\mathrm{P}_n + \mathrm{P}_a |R|^2} G_{o,\inf}$, we get

$$\begin{aligned} \mathrm{P}_e &= \mathrm{P}_n \left|W_o\right|^2 + \mathrm{P}_a \left|W_o R - G_{o,\inf} e^{-j2\pi\Omega k_0}\right|^2 \\ &= \left|G_{o,\inf}\right|^2 \mathrm{P}_a \mathrm{P}_n \Big/ \left(\mathrm{P}_n + \mathrm{P}_a |R|^2\right) = \varphi . \end{aligned} \tag{3.27}$$

Thus, we find that the infinitely long optimum target that maximizes SNR_{eff} results in whitening the error e_k (i.e. the total noise) at the output of PR equalizer. Since we assumed e_k to be Gaussian distributed, the whitened $\{e_k\}$ becomes an AWGN process. Thus, the VA detector, tuned to the optimum infinitely long target becomes optimum in sense of MLSD, which yields optimum detection quality in ISI channels. Therefore, the optimum target of infinite length should be independent of the error event pattern.

If we restrict the optimum target in (3.26) to have minimum phase, the optimum target and the corresponding equalizer are same as the solution of the optimum infinitely long backward and forward filters in the DFE system based on the MMSE criterion [55]. It is already known that the optimum infinitely long forward and backward filters in DFE based on the zero-forcing criterion are also the optimum

equalizer and target, respectively, for VA detector [55]. But, our derivation above shows that the optimum DFE filters based on the MMSE criterion are also the optimum for VA detector if the mis-equalization error contained in e_k can be assumed to be Gaussian distributed.

3.5 Simulation Results and Discussion

In this section, we evaluate the performance of our proposed target design approach in high-density perpendicular recording channels in terms of effective detection SNRs and BER. We also compare the performance of the targets designed by our approach with existing approaches, including MMSE with unit-energy constraint, MMSE with unit-tap constraint (the position of unit tap is chosen to minimize the mean square error), MMSE with monic constraint (equivalent to finite-length MMSE-DFE) and the PR target taking the form of $(1+D)^{N-1}$, where N is the length of target. For the sake of convenience, we use the abbreviations SNR_{eff}, MMSE Unit-En, MMSE Unit-Tap, MMSE Monic and standard PR, respectively, to refer to these approaches in the rest of this section.

Before we proceed further, we would like to clarify the following. Recall that the contribution of this chapter is an analytical approach to find the optimum GPR target for VA detector based on the SNR_{eff} criterion. In other words, we are not claiming any kind of performance improvement by virtue of our analytical design approach. Therefore, the purpose of the simulation studies reported here is to assess how good the SNR_{eff} criterion is, compared to other criteria, for designing the GPR target.

3.5.1 Channel Model used in Simulations

The channel model used in simulation is shown in Figure 3.4. Un-coded data are used, i.e. $P_a\left(e^{j2\pi\Omega}\right)=1$ for all Ω. The isolated transition response of the perpendicular recording channel is modeled by arctangent function given by (2.5a):

$$f(t)=\frac{2V_p}{\pi}\arctan\left(\frac{2t}{T_{50}}\right).$$

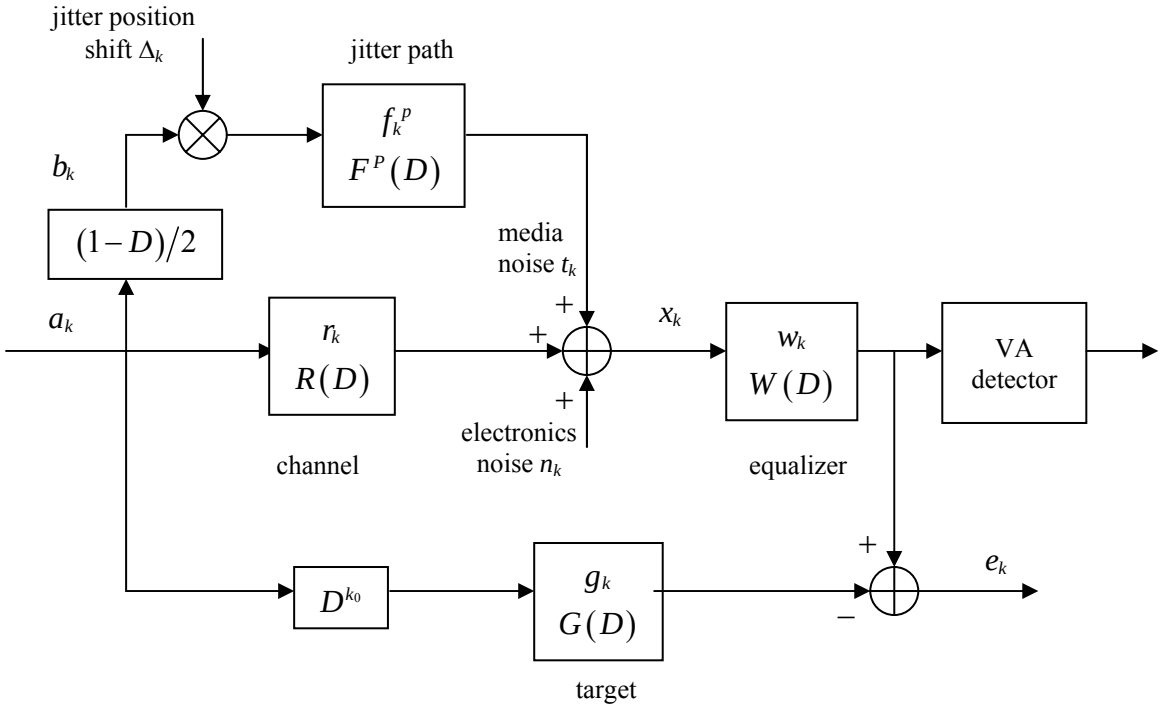

Figure 3.4: Channel model with electronics noise and media noise, and PRML receiver.

We refer to the quantity defined by $K_c=T_{50}/T$ as channel linear density, where T is the channel bit period. Since we are considering high-density recording channels, the natural channel bit response shown in Figure 3.4 can be directly obtained by

$$r_k=\frac{f(kT)-f(kT-T)}{2},$$

as stated in (2.9). As shown in Figure 3.4, we only consider the effect of position jitter

to model media noise. The position jitter Δ_k is considered as a white random process, and each Δ_k is a truncated Gaussian random variable with zero mean and variance σ_t^2 such that $|\Delta_k|$ does not exceed $T/2$. The electronics noise is modeled as AWGN with power σ_n^2 within the bandwidth of $1/2T$. In this section and hereafter, we define the channel SNR (with respect to electronics noise only) as $10\log_{10}\left(V_p^2/\sigma_n{}^2\right)$, and specify media noise in terms of the percentage jitter defined by $(100\sigma_t/T)\%$.

Three noise conditions, namely, electronics noise together with 0% jitter, 3% jitter and 6% jitter, respectively, are used in the investigation. Considering the practical complexity of VA detector, we restrict our investigation to targets of short lengths ($N=3$, 4, 5 and 6), while the linear PR equalizer contains 12 taps. High linear densities ($K_c = 1.5 \sim 4.0$) are considered in the simulations. The channel SNR with respect to electronics noise is set at 27 dB for all the cases.

3.5.2 Performance Investigation

The computed effective detection SNRs for different target lengths and different channel conditions are plotted in Figure 3.5, while the BER simulation results are plotted in Figure 3.6. Figures 3.5 and 3.6 imply that the BER results correlate well with the trends in SNR_{eff}. In other words, the simulation results show that the effective detection SNR is an equivalent measure of BER performance under the channel conditions investigated.

Form Figure 3.5, it can be seen that the target designed by the SNR_{eff} approach outperforms the other approaches in terms of effective detection SNR for all the

channel conditions considered here. Even though this is expected to happen, we must bear in mind that the conclusion from Figure 3.5 is that the BER performance of all the non-SNR_{eff} approaches are going to be worse compared to the SNR_{eff} approach. In some sense, the target based on SNR_{eff} approach results in a reasonable upper bound for the performance of PRML systems using VA detector. The SNR_{eff} approach shows evident performance gap over MMSE Unit-En, MMSE Unit-Tap and standard PR. However, its advantage over the MMSE Monic approach is considerably small, with the gain no greater than 0.024 dB over all the cases investigated. The reason for this is investigated in the next subsection.

We also observe from Figure 3.5 that the performances of SNR_{eff} and MMSE Monic approaches improve with target length in all the cases investigated, especially at high densities. At K_c=4.0, for instance, the 6-tap target outperforms the 3-tap target by about 2dB gain in SNR_{eff} with electronics noise only, and by nearly 1 dB with 6% jitter. In contrast to this, the performance of MMSE Unit-En approach worsens with target length, especially in the media noise environment. This is because for the perpendicular recording channel that is low-pass in nature, the MMSE Unit-En approach results in a target resembling a low-pass eigen-filter, whose characteristics remain almost unchanged under various channel conditions. Hence, although it is a GPR target, MMSE Unit-En target has minimum flexibility to match the natural channel, and thereby results in poor performance.

3.5.3 Analysis of Noise Correlation

We know that the correlation of noise at the VA detector input has significant effect on its detection performance. Therefore, to further illustrate the effectiveness of the

targets designed by different approaches, we plot, in Figure 3.7, the PSDs of total noise (i.e. the estimation error e_k), filtered overall channel noises (i.e. electronics noise and media noise) and the residual ISI at the equalizer output. The channel parameters are selected to result in channel SNR of 27dB, 3% jitter and linear density of 2.5. From Figures 3.7(a) and 3.7(b), we see that the MMSE Unit-En target and the standard PR target $(1+D)^4$ result in low power of the total noise and good suppression of the residual ISI at the cost of high noise correlation. On the other hand, as shown in Figures 3.7(c) and 3.7(d), even though the MMSE Monic target and the target designed by the SNR_{eff} approach result in considerable residual ISI components at high frequencies and larger power of total noise, but the PSD of the total noise turns out to be rather flat. Figures 3.8(a) and 3.8(b) illustrate the PSDs of total noise at the VA detector input for 5-tap, 8-tap and 15-tap targets from MMSE Monic and SNR_{eff} approaches, respectively, with the channel conditions same as that in Figure 3.7. The results plotted in Figures 3.8(a) and 3.8(b) show that the PSD of the total noise approaches to a flat spectrum as the target length increases. With reference to the BER performances shown in Figure 3.6, we see from Figure 3.7 that noise correlation degrades the performance of PRML systems more significantly than noise power and residual ISI. The reason that MMSE-monic target produces near optimum performance is that MMSE-monic approach is equivalent to MMSE-DFE approach. In MMSE-DFE system, the forward equalizer tends to be an all-pass phase filter, and thus avoid increasing noise correlation and noise enhancement.

3.6 Conclusion

In this chapter, we presented a novel analytical approach for finding the optimum GPR target based on the effective detection SNR, i.e. SNR_{eff} criterion, and derived the closed-form analytical solutions of the optimum targets with and without length constraint. Simulation studies show that the target from our SNR_{eff} approach results in maximum effective detection SNR, and thus produce the best BER performance, compared to the targets from MMSE based approaches and standard PR targets. Simulation studies also show that noise correlation influences the performance of VA detector more significantly than noise power and mis-equalization. In the next chapter, we are going to reinforce the analytical work of this chapter with much more extensive analysis on the global optimality of the target that maximizes SNR_{eff} .

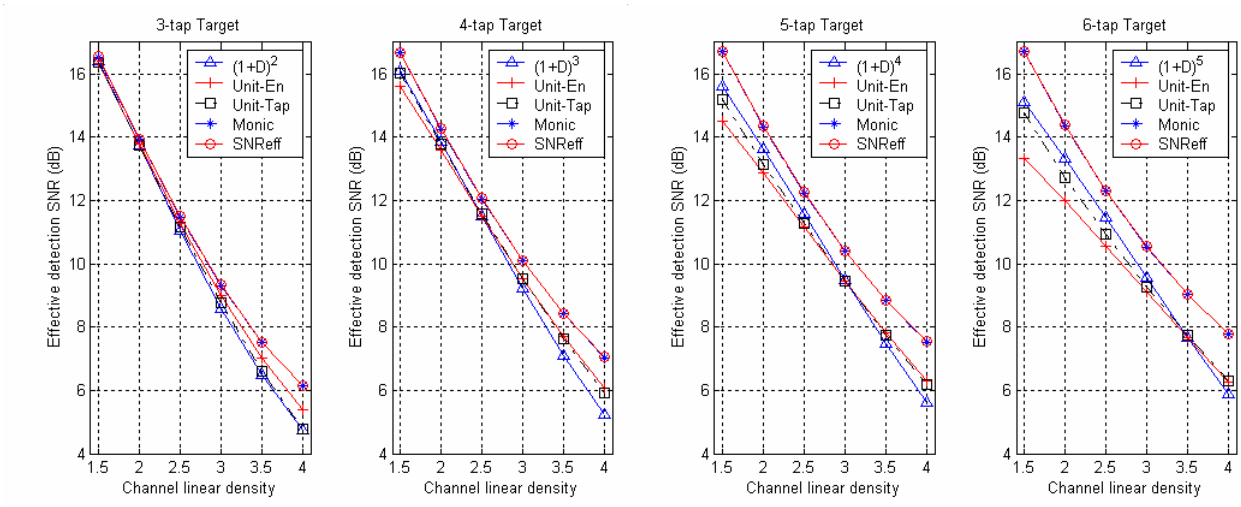

(a) electronics noise at SNR of 27 dB with 0% jitter.

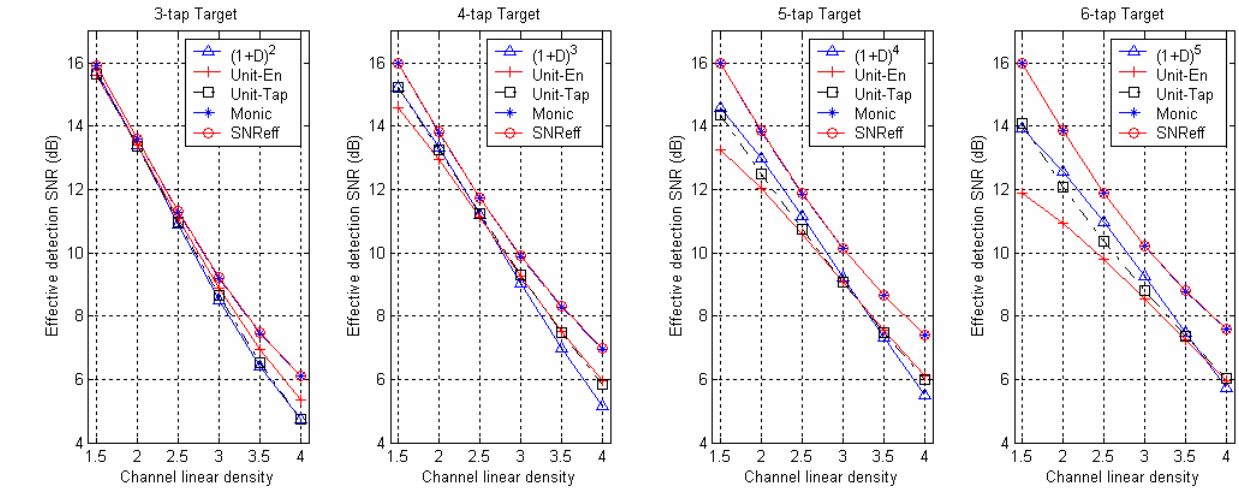

(b) electronics noise at SNR of 27 dB and 3% jitter.

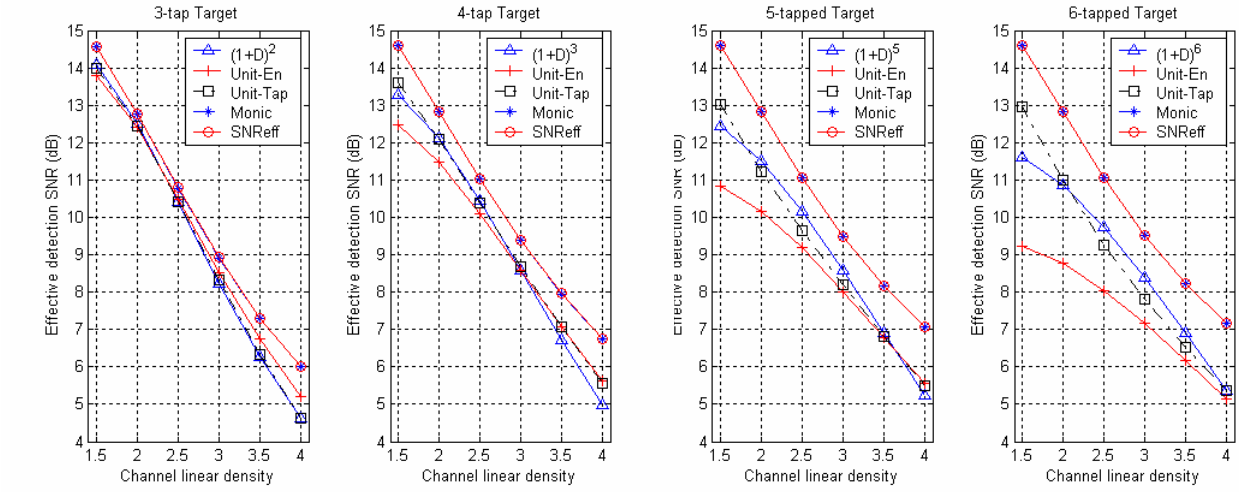

(c) electronics noise at SNR of 27 dB with 6% jitter.

Figure 3.5: Effective detection SNRs for different target design approaches.

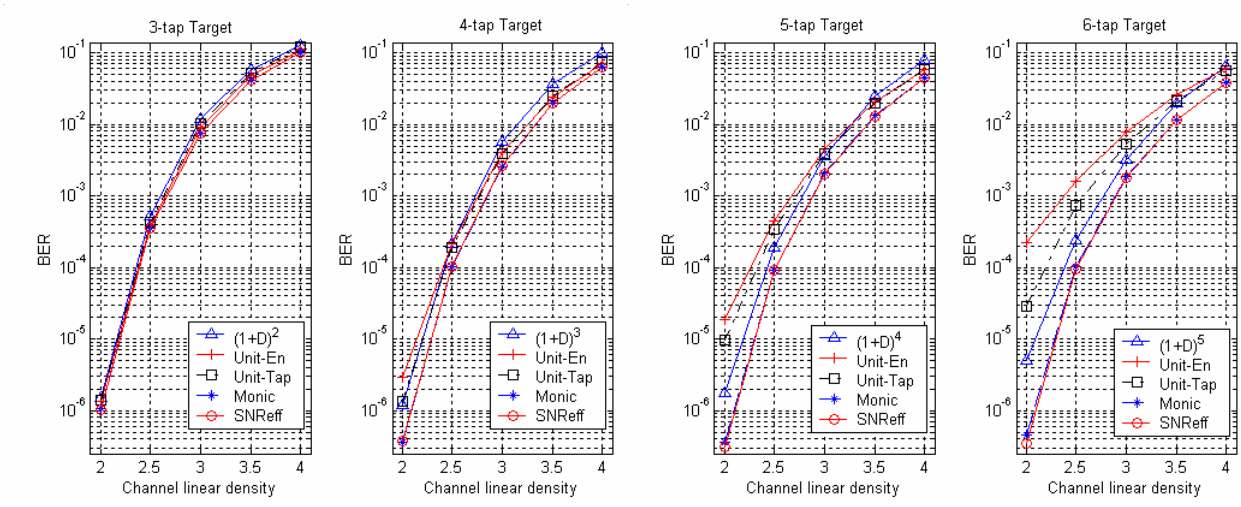

(a) electronics noise at SNR of 27 dB and 0% jitter.

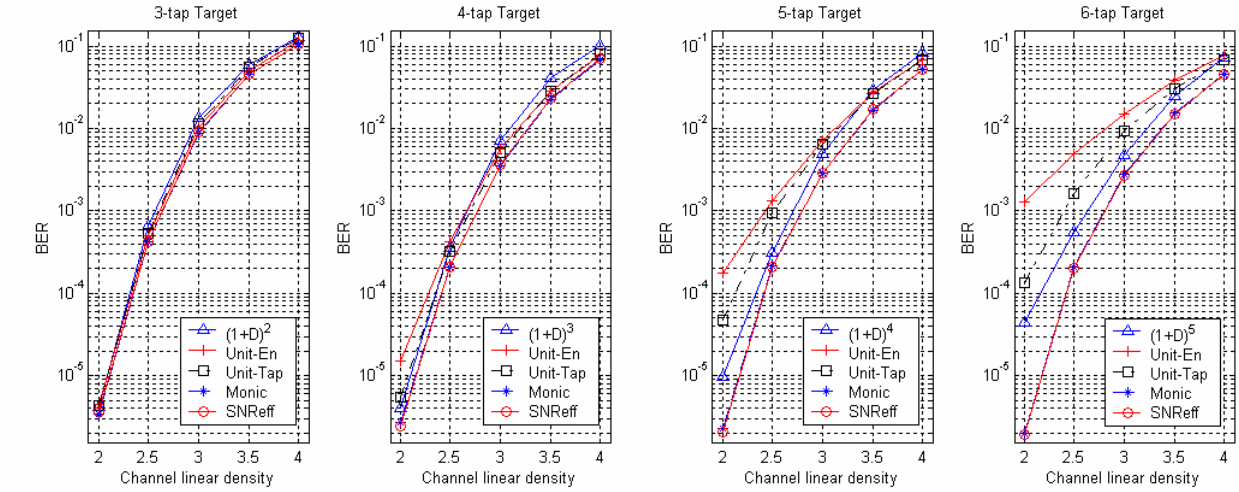

(b) electronics noise at SNR of 27 dB with 3% jitter.

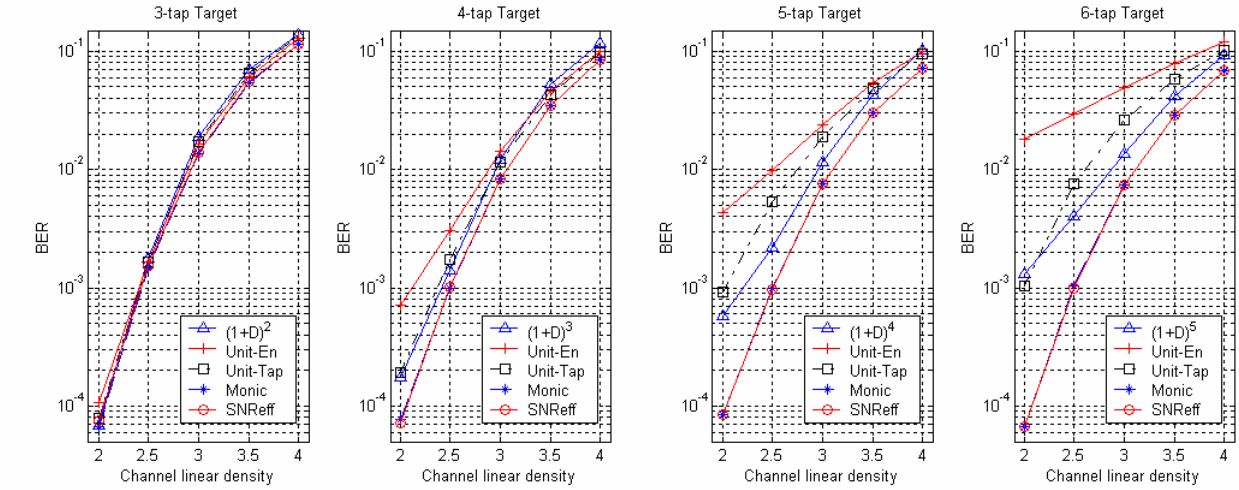

(c) electronics noise at SNR of 27 dB with 6% jitter.

Figure 3.6: BER performances for different target design approaches.

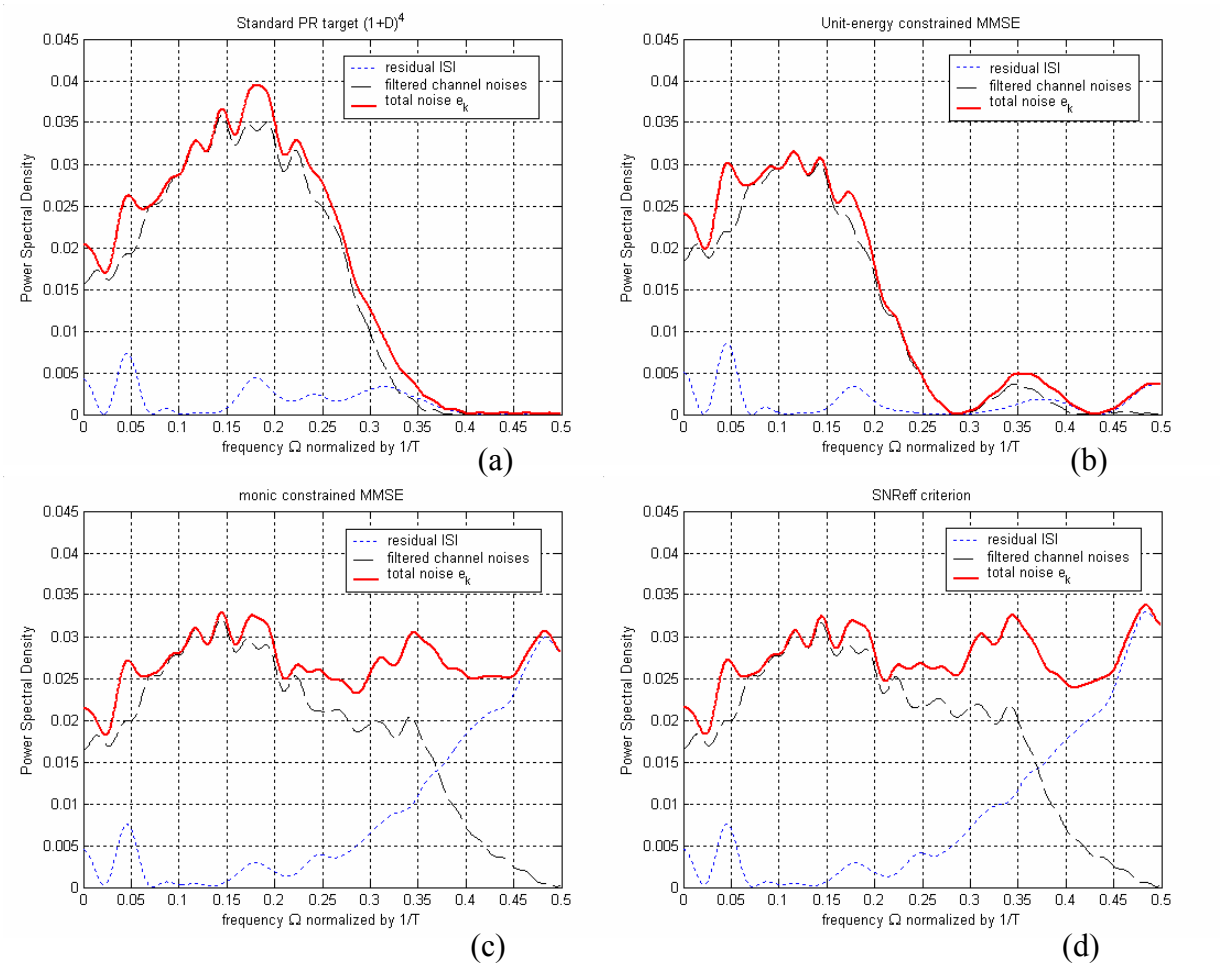

Figure 3.7: Power spectral densities of noises resulting from different targets for perpendicular recording channel at density 2.5 with electronics noise at SNR of 27dB and 3% jitter. All the targets have 5 taps and are normalized to having unit energy. (a) standard PR target $(1+D)^4$, (b) unit-energy constrained MMSE, (c) monic constrained MMSE, and (d) SNR_{eff} approach.

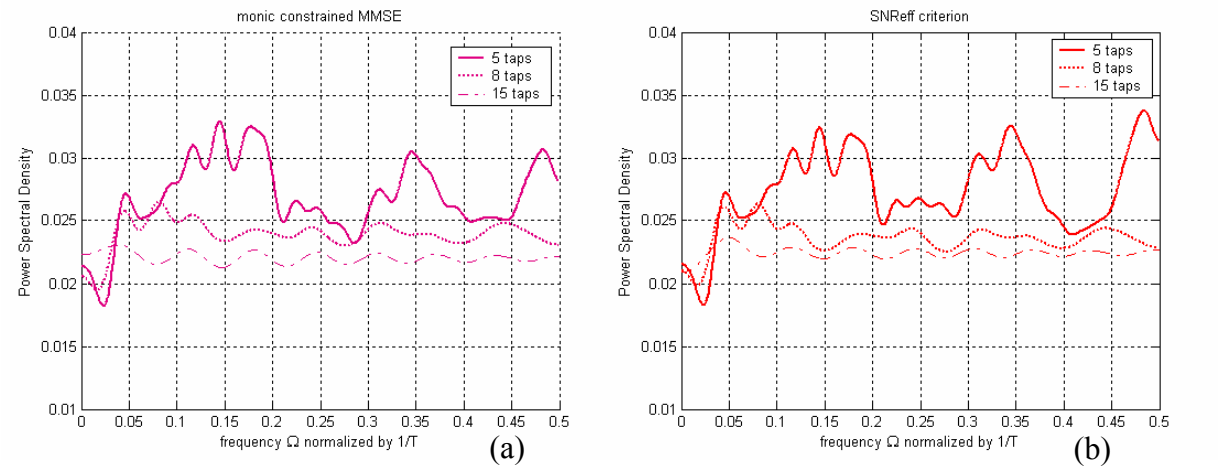

Figure 3.8: Power spectral densities of total noise resulting from 5-tap, 8-tap and 15-tap targets with unit energy for perpendicular recording channel at density 2.5 with electronics noise at SNR of 27dB and 3% jitter. (a) monic constrained MMSE and (b) SNR_{eff} approach.

Chapter 4

Characterization of the Performance Surface of Effective Detection SNR

In the last chapter, we proposed an analytical approach for finding the optimum GPR target based on effective detection SNR (SNR_{eff}). Compared to the conventional MMSE criterion that is essentially a quadratic cost function of target, the performance surface defined by SNR_{eff} is quite complicated, and may contain many optima. Furthermore, the dominant error event used in computing SNR_{eff} is not really fixed, unlike our assumption of a fixed dominant error event in Chapter 3. Instead, dominant error event pattern is an implicit function dependent on the target. In this chapter, we provide the characterization of the performance surface of SNR_{eff} by using the analytical approach presented in Chapter 3. In Section 4.1, we provide clarification of the global optima of SNR_{eff} for a given dominant error event. In Section 4.2, we discuss the issue of multiple dominant error events and characterize the performance surface of SNR_{eff} by taking into account the fact that the dominant error event may change depending on the choice of the target. Finally, the results of numerical search

for optimum target based on SNR_{eff} are presented in Section 4.3. We show that these results corroborate the findings of our analytical characterization work.

4.1 Clarification of the Global Optima

In the development of the proposed analytical approach for optimum target design in Chapter 3, we used the effective detection SNR as the cost function. We found that the optimum equalizer that maximizes SNR_{eff} is the same as the solution of unconstrained MMSE equalizer. With this optimum equalizer, the SNR_{eff} can be expressed as (see 3.11))

$$SNR_{eff} = \frac{1}{4} \cdot \frac{\left(\int_{-0.5}^{0.5} |G|^2 |E^d|^2 \, d\Omega \right)^2}{\int_{-0.5}^{0.5} \left[|G|^4 |E^d|^2 \, \mathrm{P}_a \Big/ \left(1 + \frac{\mathrm{P}_a |R|^2}{\mathrm{P}_n} \right) \right] d\Omega}, \tag{3.11}$$

where $G,$, E^d and R are the Fourier transforms of target, assumed dominant error event and natural channel bit response, respectively, P_a is the PSD of input data and P_n is the PSD of overall channel noise (i.e. electronics noise and medium noise) at equalizer input. As was shown in (3.11), the SNR_{eff} is related to $|G|^2$ instead of G. This motivated us to design optimum magnitude frequency response $|G_o|^2$ of the target based on SNR_{eff} . To solve this optimization problem, we replaced $|G|^2$ with $X = 1 + 2\sum_{i=1}^{N-1} x_i \cos(i\, 2\pi\Omega)$ (N is the length of target response) resulting in (see (3.12))

$$J(X) = \frac{1}{4} \cdot \frac{\left(\int_{-0.5}^{0.5} X |E^d|^2 \, d\Omega \right)^2}{\int_{-0.5}^{0.5} \left[X^2 |E^d|^2 \, \mathrm{P}_a \mathrm{P}_n \Big/ \left(\mathrm{P}_n + \mathrm{P}_a |R|^2 \right) \right] d\Omega}. \tag{3.12}$$

We may refer to the space of all possible vectors $\mathbf{x} = [x_1, x_2, \cdots, x_{N-1}]^T$ as X -domain. It was found in Chapter 3 that $J(X)$ has a single maximum at $X = X_o$, which is uniquely determined by (3.15) (if E^d is a single-bit error event) or (3.17) (if E^d is multi-bit error event). The performance surface of SNR_{eff} is part of the surface of $J(X)$ over the feasible region $\tilde{R}$ (in X domain) wherein the $\mathbf{x}$ can be de-convoluted into target response $\mathbf{g}$ with real-valued coefficients, i.e. X can be spectral factorized into a valid target response[1] G. If the unique maximizer X_o of $J(X)$ lies inside the feasible region $\tilde{R}$, then clearly, X_o is also the unique optimum solution that maximizes SNR_{eff}, i.e. $|G_o|^2 = X_o$. If X_o is outside $\tilde{R}$, then the optimum solution $|G_o|^2$ of SNR_{eff} must be located on the boundary of $\tilde{R}$. In this case, it is not clear whether the optimum solution $|G_o|^2$ of SNR_{eff} is unique or not.

In this section, using proof by contradiction, we show the uniqueness of the optimum $|G_o|^2$ that maximizes SNR_{eff} given by (3.11). In the development of the proof, we need to use the equations and inequalities listed below.

1. If $\frac{b}{a} = \frac{d}{c}$ with $a, b, c, d > 0$, then $\frac{b}{a} = \frac{d}{c} = \frac{b+d}{a+c} = \frac{\sqrt{bd}}{\sqrt{ac}}$. (4.1a)

2. If $\frac{b}{a} \le \frac{d}{c}$ with $a, b, c, d > 0$, then $\frac{b}{a} \le \frac{b+d}{a+c} \le \frac{d}{c}$. (4.1b)

3. $\left(\int_a^b f(x)\, g(x)\, dx\right)^2 \le \int_a^b [f(x)]^2 dx \int_a^b [g(x)]^2 dx$ for real-valued functions $f(x)$ and $g(x)$. (4.1c)

[1] Since $\mathbf{x}$ and X are uniquely related, henceforth, we shall use $\mathbf{x}$ and X interchangeably, and also $\mathbf{g}$ and G, and $\boldsymbol{\varepsilon}$ and E. Further, in this chapter, we strictly refer to the notation G as a target response with real-valued coefficients, and thus $|G|^2$ is inside the region $\tilde{R}$.

It is easy to verify (4.1a) and (4.1b). And (4.1c) is the well-known Schwartz inequality, where the equality holds only when $f(x)=\varphi g(x)$ for $x\in[a,b]$ where φ is an arbitrary real-valued constant.

Now, let us suppose that there exist two distinct and equivalent global optima, $|G_{o,1}|^2$ and $|G_{o,2}|^2$ ($|G_{o,1}|^2 \neq |G_{o,2}|^2$), for SNR_{eff} such that

$$M \triangleq SNR_{eff}\left(|G_{o,1}|^2\right) = SNR_{eff}\left(|G_{o,2}|^2\right) = \max_{\{|G|^2\}}\left(SNR_{eff}\left(|G|^2\right)\right). \tag{4.2}$$

Hence, by using (4.1a), we can obtain the following from (4.2) and (3.11):

$$\begin{aligned} M &= \frac{\left(\int_{-0.5}^{0.5}|G_{o,1}|^2\left|E^d\right|^2 d\Omega\right)^2 + k^2\left(\int_{-0.5}^{0.5}|G_{o,2}|^2\left|E^d\right|^2 d\Omega\right)^2}{\int_{-0.5}^{0.5}\left[|G_{o,1}|^4 H\right]d\Omega + k^2\int_{-0.5}^{0.5}\left[|G_{o,2}|^4 H\right]d\Omega} \\ &= \frac{k\left(\int_{-0.5}^{0.5}|G_{o,1}|^2\left|E^d\right|^2 d\Omega\right)\left(\int_{-0.5}^{0.5}|G_{o,2}|^2\left|E^d\right|^2 d\Omega\right)}{k\sqrt{\int_{-0.5}^{0.5}\left[|G_{o,1}|^4 H\right]d\Omega\int_{-0.5}^{0.5}\left[|G_{o,2}|^4 H\right]d\Omega}}, \end{aligned} \tag{4.3}$$

where $H = 4\left|E^d\right|^2 \mathrm{P}_a\mathrm{P}_n \Big/ \left(\mathrm{P}_n + \mathrm{P}_a|R|^2\right)$ and k is an arbitrary positive constant. According to (4.1c), we have the inequality given by

$$\int_{-0.5}^{0.5}\left[|G_{o,1}|^2|G_{o,2}|^2 H\right]d\Omega < \sqrt{\int_{-0.5}^{0.5}\left[|G_{o,1}|^4 H\right]d\Omega\int_{-0.5}^{0.5}\left[|G_{o,2}|^4 H\right]d\Omega}\,. \tag{4.4}$$

Different from (4.1c), a strict inequality is used in (4.3), because we supposed that $|G_{o,1}|^2 \neq |G_{o,2}|^2$ (thus, $|G_{o,1}|^2\sqrt{H} \neq |G_{o,2}|^2\sqrt{H}$). Applying (4.4) to (4.3), we find that

$$\begin{aligned} M &= \frac{\left(\int_{-0.5}^{0.5}|G_{o,1}|^2\left|E^d\right|^2 d\Omega\right)^2 + k^2\left(\int_{-0.5}^{0.5}|G_{o,2}|^2\left|E^d\right|^2 d\Omega\right)^2}{\int_{-0.5}^{0.5}\left[|G_{o,1}|^4 H\right]d\Omega + k^2\int_{-0.5}^{0.5}\left[|G_{o,2}|^4 H\right]d\Omega} \\ &< \frac{2k\left(\int_{-0.5}^{0.5}|G_{o,1}|^2\left|E^d\right|^2 d\Omega\right)\left(\int_{-0.5}^{0.5}|G_{o,2}|^2\left|E^d\right|^2 d\Omega\right)}{2k\int_{-0.5}^{0.5}\left[|G_{o,1}|^2|G_{o,2}|^2 H\right]d\Omega}\,. \end{aligned} \tag{4.5}$$

Then, with (4.1b) and (4.5), we reach the inequity given by

$$M < \frac{\left(\int_{-0.5}^{0.5}\left(|G_{o,1}|^2 + k|G_{o,2}|^2\right)|E^d|^2\, d\Omega\right)}{\int_{-0.5}^{0.5}\left[\left(|G_{o,1}|^2 + k|G_{o,2}|^2\right)^2 H\right] d\Omega} = SNR_{eff}\left(|G'_o|^2\right), \tag{4.6}$$

where $|G'_o|^2 = \left(|G_{o,1}|^2 + k|G_{o,2}|^2\right)/(1+k)$ is also a squared magnitude frequency response of a target response with unit energy, and it corresponds to a point in between $|G_{o,1}|^2$ and $|G_{o,2}|^2$ in X domain, since $k > 0$. Obviously, the derived inequality shown in (4.6) contradicts with the assumption that $|G_{o,1}|^2$ and $|G_{o,2}|^2$ are equivalent and distinct global optima that maximize SNR_{eff}. Thus, the uniqueness of the global optimum $|G_o|^2$ based on SNR_{eff} is proved.

In a similar way, we can also prove that for an arbitrary $|G'|^2$ different from the global optimum $|G_o|^2$ of SNR_{eff} (i.e. $SNR_{eff}\left(|G|^2\right) \le SNR_{eff}\left(|G_o|^2\right)$), any point in between $|G'|^2$ and $|G_o|^2$ in X domain results in a value of SNR_{eff} greater than $SNR_{eff}\left(|G'|^2\right)$. This indicates that there are no local optima on the performance surface of SNR_{eff}, and SNR_{eff} has a single maximum at $|G|^2 = |G_o|^2$. It also follows that the performance surface of SNR_{eff} is a concave surface.

Although $|G_o|^2$, the optimum magnitude frequency response of target based of SNR_{eff} is found unique, there are usually more than one target responses obtained by spectral factorization, with different phases but having the same optimum magnitude frequency response $|G_o|^2$. Further, if we have optimum target $\mathbf{g}_o$ then $-\mathbf{g}_o$ is also an optimum target for the same PRML system. All the target responses corresponding to $|G_o|^2$ are global optimizers of SNR_{eff}, since they result in the same maximum effective detection SNR. Figure 4.1(a) illustrates an example where there are four global

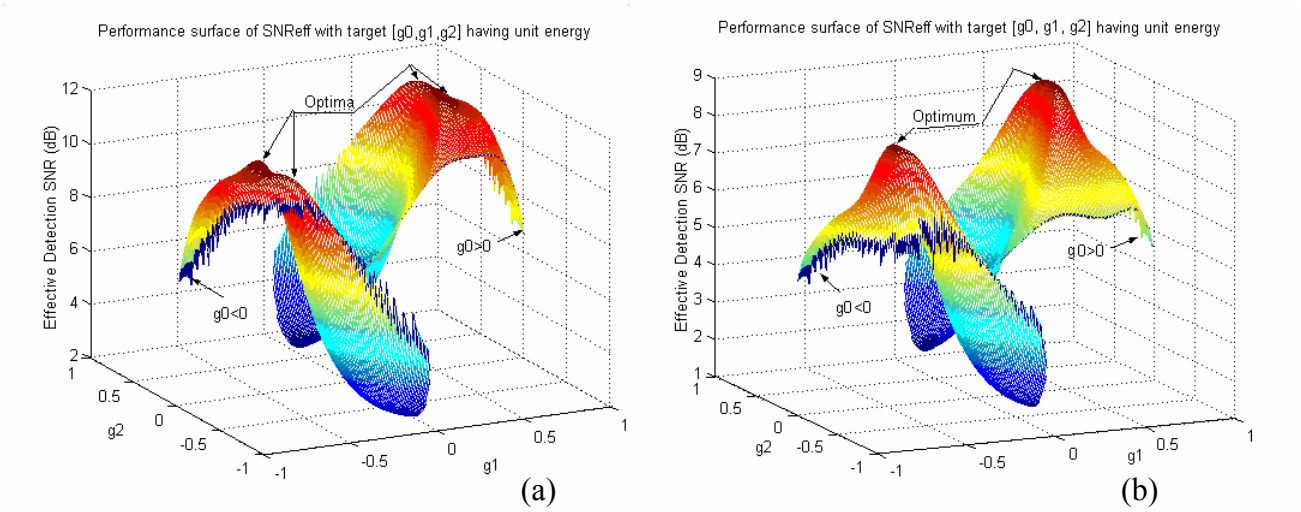

Figure 4.1: Performance surface of effective detection SNR with 3-tap target, $[g_0, g_1, g_2]$ over the region where the error event [+2 –2] dominates the bit error probability. The target energy is normalized to be unity and linear density is 2.5. (a) perpendicular recording channel modeled by arctangent function in (2.5a) with electronics noise at SNR of 27dB and 0% jitter, (b) perpendicular recording channel modeled by hyperbolic tangent function in (2.5b) with electronics noise at SNR of 30 dB and 3% jitter.

optimizers given by $\mathbf{g}_{o,1} = [0.6172, 0.7021, 0.3551]^T$, $\mathbf{g}_{o,2} = [0.3551, 0.7021, 0.6173]^T$, $\mathbf{g}_{o,3} = -\mathbf{g}_{o,1}$ and $\mathbf{g}_{o,4} = -\mathbf{g}_{o,2}$. Unique pair of optimum target responses $\{\mathbf{g}_o, -\mathbf{g}_o\}$ based on SNR_{eff} is found if all the zeros of the D transform of $|G_o|^2$ are on the unit circle. See the example illustrated in Figure 4.1(b), where there is a pair of global optimum target responses given by $\mathbf{g}_{o,1} = [0.5278, 0.6655, 0.5278]^T$ and $\mathbf{g}_{o,2} = -\mathbf{g}_{o,1}$. The above findings imply that numerical search for optimum target response based on SNR_{eff} can always lead to a global optimum, no matter which point the search starts with.

4.2 Discussion on Dominant Error Event

Throughout the above discussion on the uniqueness of the optimum target based on effective detection SNR, we assumed that the dominant error event E^d remains

unchanged with target. In fact, however, different targets may result in different dominant error events. Further, we may find that with a certain choice of target, there are multiple error events dominating the bit error probability. Hence, it would be better that we design optimum target based on an overall effective detection SNR defined by

$$\overline{SNR}_{eff}\left(|G|^2\right) = \min_{\{E\in\Psi\}}\left(S_E\left(|G|^2\right)\right), \tag{4.7}$$

where Ψ is the set of all possible patterns of error event E and S_E given by

$$S_E\left(|G|^2\right) = \frac{1}{4}\cdot\frac{\left(\int_{-0.5}^{0.5}|G|^2|E|^2\,d\Omega\right)^2}{\int_{-0.5}^{0.5}\left[|G|^4|E|^2\,\mathrm{P}_a\mathrm{P}_n\Big/\left(\mathrm{P}_n+\mathrm{P}_a|R|^2\right)\right]d\Omega}.$$

Note that the error event E used in S_E is independent of the target G. If we change notation E to be E^d, then S_{E^d} is exactly the SNR_{eff} given by (3.11). In this section, we determined the dominant error event as $\overline{E}^d = \arg\min_{\{E\in\Psi\}}\left(S_E\left(|G|^2\right)\right)$. Apparently, $\overline{E}^d$ changes depending upon which target G is used for evaluating $\overline{SNR}_{eff}$. Thus far, an explicit function reflecting the relationship between target and dominant error event has not yet been reported. Therefore, analytical approach for optimizing $\overline{SNR}_{eff}$ given by (4.7) will be impeded by great mathematical difficulty. In this section, we discuss the effectiveness of target design based on SNR_{eff} that accounts for only a single dominant error event.

Since the data sequence input to magnetic recording channel is binary, the elements of the error event pattern are constrained to be ternary $\{+2,-2,0\}$. Hence, the dominant error event does not continuously change with target G. In other words, we can divide the target coefficient domain into continuous regions $\overline{r}_1,\overline{r}_2,\cdots,\overline{r}_n$ such that all the targets inside the region $\overline{r}_i$ result in the same dominant error event E_i

($i = 1, 2, \cdots, n$), i.e. $E_i = \arg\min_{\{E \in \Psi\}} (S_E)$ for $\mathbf{g} \in \overline{r}_i$. Mapping $\overline{r}_1, \overline{r}_2, \cdots, \overline{r}_n$ into X–domain, we get corresponding regions $\overline{R}_1, \overline{R}_2, \cdots, \overline{R}_n$, which are continuous too. Note that $\tilde{R} = \overline{R}_1 \bigcup \overline{R}_2 \bigcup \cdots \bigcup \overline{R}_n$ is the region of all possible $|G|^2$ (squared magnitude frequency responses of targets) in X–domain. Having all the possible dominant error events $E_1, E_2, \cdots, E_n$ for given channel conditions, we may rewrite (4.7) as

$$\overline{SNR}_{eff}\left(|G|^2\right) = \min_{E \in \{E_1, E_2, \cdots, E_n\}} \left(S_E\left(|G|^2\right)\right),$$

or equivalently,

$$\overline{SNR}_{eff}\left(|G|^2\right) = S_{E_i}\left(|G|^2\right) \text{ for } |G|^2 \in \overline{R}_i,\ i = 1, 2, \cdots, n .$$

We now show that the performance surface of $\overline{SNR}_{eff}\left(|G|^2\right)$ is concave over the region $\tilde{R}$ for all possible $|G|^2$ and has a unique optimum. To begin with, observe the similarity between S_E and SNR_{eff} given by (3.11). Therefore, based on the analysis on characterization of SNR_{eff} in Section 4.1, we can conclude that S_E with any error event E is a concave surface over the region $\tilde{R}$ in X-domain. Let $|G_1|^2$ and $|G_2|^2$ denote any two distinct squared magnitude frequency responses of targets that result in the same value of $\overline{SNR}_{eff}$, i.e. $|G_1|^2 \neq |G_2|^2$ and $\overline{SNR}_{eff}\left(|G_1|^2\right) = \overline{SNR}_{eff}\left(|G_2|^2\right) \triangleq M$. Since $\overline{SNR}_{eff}\left(|G|^2\right) = \min\left(S_{E_1}\left(|G|^2\right), S_{E_2}\left(|G|^2\right), \cdots, S_{E_n}\left(|G|^2\right)\right)$, we get $S_{E_i}\left(|G_1|^2\right) \geq M$ and $S_{E_i}\left(|G_2|^2\right) \geq M$ for $i = 1, 2, \cdots, n$. Hence, for any point $|G'|^2$ in between $|G_1|^2$ and $|G_2|^2$, we have

$$S_{E_1}\left(|G'|^2\right) > M,\ \ S_{E_2}\left(|G'|^2\right) > M, \cdots, S_{E_n}\left(|G'|^2\right) > M ,$$

because $S_{E_1}, S_{E_2}, \cdots, S_{E_n}$ are all concave surfaces over the region $\tilde{R}$ in X-domain. As a result, $\overline{SNR}_{eff}\left(|G'|^2\right) = \min\left(S_{E_1}\left(|G'|^2\right), S_{E_2}\left(|G'|^2\right), \cdots, S_{E_n}\left(|G'|^2\right)\right) > M.$ Based on the

above analysis, we can conclude that $\overline{SNR}_{eff}$ is also a concave surface over the region $\tilde{R}$. Consequently, $\overline{SNR}_{eff}$ has a unique optimum $|G_o|^2$ (i.e. maximum).

Let $|G_{o,1}|^2, |G_{o,2}|^2, \cdots, |G_{o,n}|^2$ denote the optimizers (i.e. maximizers) of $S_{E_1}, S_{E_2}, \cdots, S_{E_n}$, respectively, and $|\bar{G}_o|^2$ denote the optimizer of $\overline{SNR}_{eff}$. If the optimizer $|G_{o,k}|^2$ of S_{E_k} lies inside the region $\bar{R}_k$ where $\overline{SNR}_{eff} = S_{E_k}$ for $|G|^2 \in \bar{R}_k$, then obviously, the optimizer $|G_{o,k}|^2$ is also the optimum solution for $\overline{SNR}_{eff}$ (i.e. $|\bar{G}_o|^2 = |G_{o,k}|^2$). In such case, there must be no other optimizer $|G_{o,i}|^2$ ($|G_{o,i}|^2 \neq |G_{o,k}|^2$) for S_{E_i} to be located inside the corresponding region $\bar{R}_i$ where $\overline{SNR}_{eff} = S_{E_i}$, since $\overline{SNR}_{eff}$ has a unique optimum. As $|\bar{G}_o|^2 = |G_{o,k}|^2$, optimizing $\overline{SNR}_{eff}$ is equivalent to optimizing S_{E_k} based on the single error event E_k. Having the dominant error event $\bar{E}^d = E_k$, we can obtain the optimum solution $|G_{o,k}|^2$ of S_{E_k}, i.e. the optimum solution $|\bar{G}_o|^2$ of $\overline{SNR}_{eff}$, by the analytical approach developed in Chapter 3. Furthermore, in Chapter 3, we also obtained the optimum solution (3.26) for infinitely long target based on SNR_{eff}, that is $|G_{o,\inf}|^2 = \varphi\left(\mathrm{P}_n + \mathrm{P}_a|R|^2\right)\big/\mathrm{P}_a\mathrm{P}_n$, which is independent of error event pattern. This implies that $|G_{o,\inf}|^2$ is also the optimum solution for $\overline{SNR}_{eff}$ with infinitely long target, because all the S_E with different error events are maximized by $|G_{o,\inf}|^2$. The optimized $\overline{SNR}_{eff}$ with $|G_{o,\inf}|^2$ is given by

$$\overline{SNR}_{eff}\left(\left|G_{o,\inf}\right|^2\right) = \min_{\{E\in\Psi\}}\left(\frac{1}{4}\int_{-0.5}^{0.5}\left(\frac{1}{\mathrm{P}_a}+\frac{|R|^2}{\mathrm{P}_n}\right)|E|^2 d\Omega\right). \tag{4.8}$$

The dominant error event $\bar{E}^d$ is the error pattern that minimizes the argument of $\min(\bullet)$ function in (4.8). Since the dominant error event pattern is not sensitive to minor changes in target response, dominant error event for the infinitely long optimum

solution $\left|\overline{G}_{o,\inf}\right|$ is usually also the dominant error event for the optimum $\left|\overline{G}_o\right|^2$ of finite-length target, whose spectral characteristics are similar to that of $\left|\overline{G}_{o,\inf}\right|$. Use of (4.8) to find dominant error event $\overline{E}^d$, or at least the candidates most likely to be E^d, facilitates our approach for designing the optimum target based on the $\overline{SNR}_{eff}$ criterion.

If every S_{E_i} $(i = 1, 2, \cdots, n)$ has its optimizer outside the region $\overline{R}_i$ over which E_i is the resulting dominant event, then the maximum of each sub-surface $\overline{SNR}_{eff}\left(|G|^2\right) = S_{E_i}\left(|G|^2\right)$ for $|G|^2 \in \overline{R}_i$ must appear on the boundary of $\overline{R}_i$ joining with other region(s) adjacent to $\overline{R}_i$. Consequently, the optimizer $\left|\overline{G}_o\right|^2$ that maximizes $\overline{SNR}_{eff}$ must be located on a joint boundary of two or more adjacent regions, for example, $\overline{R}_{\mathrm{I}}, \overline{R}_{\mathrm{II}}, \cdots, \overline{R}_{\mathrm{L}}$ that correspond to the dominant error events $E_{\mathrm{I}}, E_{\mathrm{II}}, \cdots, E_{\mathrm{L}}$, respectively. That is,

$$\overline{SNR}_{eff,o} = S_{E_{\mathrm{I}}}\left(\left|\overline{G}_o\right|^2\right) = S_{E_{\mathrm{II}}}\left(\left|\overline{G}_o\right|^2\right) = \cdots = S_{E_{\mathrm{L}}}\left(\left|\overline{G}_o\right|^2\right). \tag{4.9}$$

We see from (4.9) that $\left|\overline{G}_o\right|^2$ results in multiple dominant error events $E_{\mathrm{I}}, E_{\mathrm{II}}, \cdots, E_{\mathrm{L}}$ from the viewpoint of SNR_{eff} criterion. Defining $\overline{S} = \min\left(S_{E_{\mathrm{I}}}, S_{E_{\mathrm{II}}}, \cdots, S_{E_{\mathrm{L}}}\right)$ and $\overline{R}' = \overline{R}_{\mathrm{I}} \bigcup \overline{R}_{\mathrm{II}} \bigcup \cdots \bigcup \overline{R}_{\mathrm{L}}$, we have $\overline{SNR}_{eff}\left(|G|^2\right) = \overline{S}\left(|G|^2\right)$ for $|G|^2 \in \overline{R}'$. Similar to the analysis in the last paragraph, it can be verified that $\overline{S}$ is a concave surface with its unique optimizer inside the region $\overline{R}'$, which is also the optimizer $\left|\overline{G}_o\right|^2$ of $\overline{SNR}_{eff}$. In such a case, optimizing $\overline{SNR}_{eff}$ is equivalent to optimizing $\overline{S}$ based on much fewer error events, namely, $E_{\mathrm{I}}, E_{\mathrm{II}}, \cdots, E_{\mathrm{L}}$. The candidates of these multiple dominant error events $E_{\mathrm{I}}, E_{\mathrm{II}}, \cdots, E_{\mathrm{L}}$ can be found by making use of (4.8). We may also use numerical search methods to find the optimum $\left|\overline{G}_o\right|^2$ that maximizes $\overline{S}$ (and equivalently

maximizes $\overline{SNR}_{eff}$), since $\overline{S}$ is characterized as a concave surface with a unique maximum. On the other hand, as concluded in the last paragraph, the optimizer $\left|\overline{G}_o\right|^2$ of $\overline{SNR}_{eff}$ and the optimizers of $S_{E_{\mathrm{I}}}, S_{E_{\mathrm{II}}}, \cdots, S_{E_{\mathrm{L}}}$ approach closer to each other with increase in target length, and become the same solution as $\left|G_{o,\inf}\right|^2$ given by (3.26) when the target length approach infinity. Therefore, with reasonably long target length, the optimizers $\left|G_{o,\mathrm{I}}\right|^2, \left|G_{o,\mathrm{II}}\right|^2, \cdots, \left|G_{o,\mathrm{L}}\right|^2$ of $S_{E_{\mathrm{I}}}, S_{E_{\mathrm{II}}}, \cdots, S_{E_{\mathrm{L}}}$, respectively, are close enough to $\left|\overline{G}_o\right|^2$ such that

$$\overline{SNR}_{eff,o} = \overline{S}\left(\left|\overline{G}_o\right|^2\right) \approx S_{E_{\mathrm{I}}}\left(\left|G_{o,\mathrm{I}}\right|^2\right) \approx S_{E_{\mathrm{II}}}\left(\left|G_{o,\mathrm{II}}\right|^2\right) \approx \cdots \approx S_{E_{\mathrm{L}}}\left(\left|G_{o,\mathrm{L}}\right|^2\right). \tag{4.10}$$

Eqn. (4.10) shows that any of the optimizers $\left|G_{o,\mathrm{I}}\right|^2, \left|G_{o,\mathrm{II}}\right|^2, \cdots, \left|G_{o,\mathrm{L}}\right|^2$, which can be obtained by the analytical approach developed in Section 3, will result in almost equivalent optimum performance in terms of $\overline{SNR}_{eff}$.

In Figure 4.2(a), we plot several performance surfaces of SNR_{eff} based on different assumed dominant error events. As shown in Figure 4.2(b), the pattern of dominant error event changes over different regions in X -domain. However, as shown in Figure 4.2(a), every SNR_{eff} with different assumed dominant error event reaches its maximum within the same region where the error event $[+2\ -2]$ is the resulting dominant error event (see the dark shaded area in Figure 4.2(b)). In Figure 4.3, we illustrate the performance surface of the $\overline{SNR}_{eff}$ defined by (4.7) (for the same channel conditions as in Figure 4.1(b)). As can be observed from Figure 4.3, the global optimum of the $\overline{SNR}_{eff}$ occurs within the region where the error event $[+2\ -2]$ is the dominant error event, and there are no local optima.

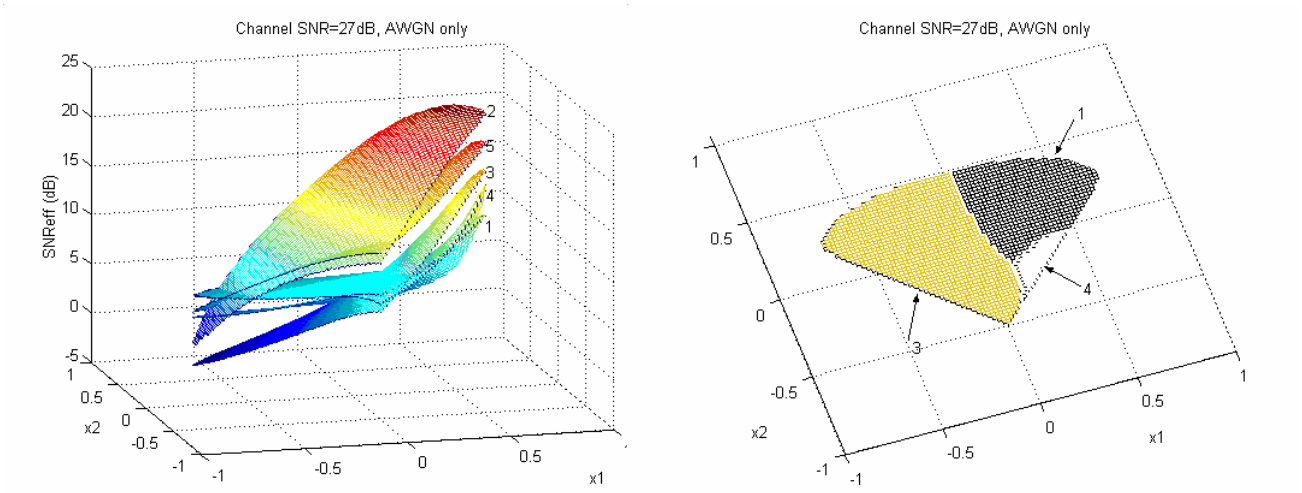

(a) (b)

Figure 4.2: Comparison of SNR_{eff} with 3-tap unit-energy target based on different assumed dominant error events for the perpendicular recording channel with electronics noise only at SNR of 27dB and channel linear density of 2.5. a) SNR_{eff} based on different assumed dominant error events in X-domain, b) regions in X-domain where a certain error event dominates BER. (Error event patterns: 1 → [+2 –2], 2 → [+2 +2], 3 → [+2], 4 → [+2 –2 +2] and 5 → [+2 -2 +2 -2 +2].)

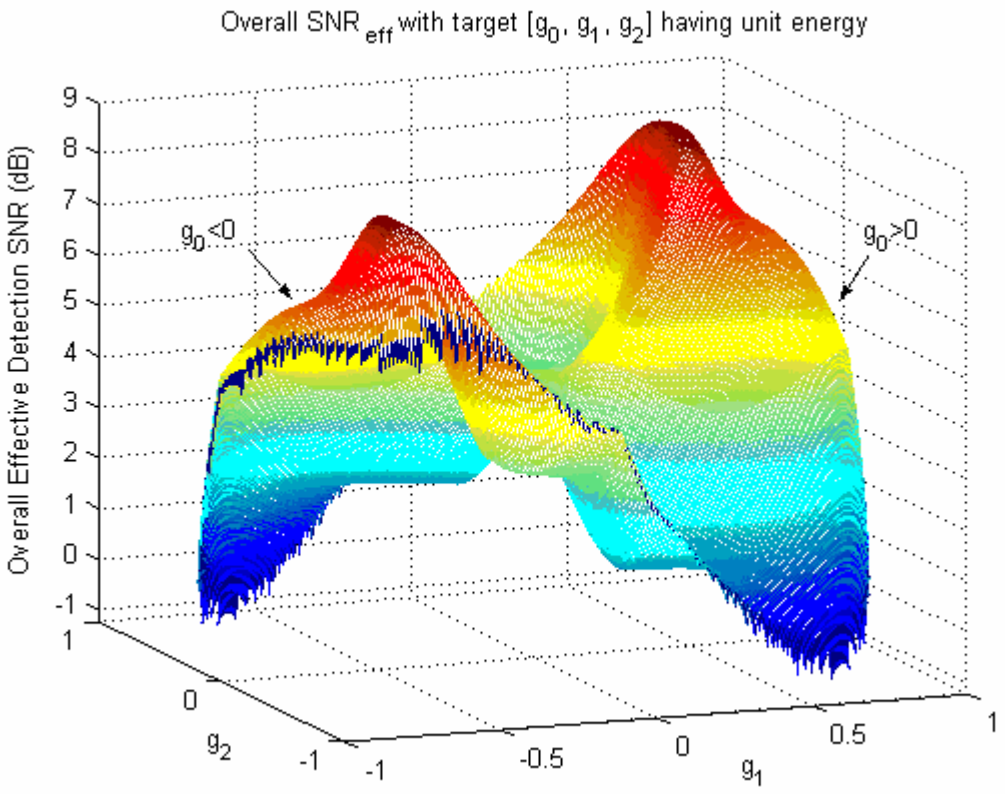

Figure 4.3: Performance surface of $\overline{SNR_{eff}}$ with 3-tap unit-energy target.

4.3 Numerical Search Results

In this section, we conduct numerical search for finding optimum targets based on the SNR_{eff} criterion with a given dominant error event. To verify the effectiveness of the SNR_{eff} criterion, we also perform the numerical search based on the theoretical expression for BER, which takes into account several error event patterns. The numerical search results obtained from these search approaches corroborate the characterization of the performance surface of SNR_{eff} we provided in the previous two sections. The channel used for this study is perpendicular recording channel at linear density of 2.5.

4.3.1 Search Based on Effective Detection SNR

The cost function of SNR_{eff} used in the numerical search is defined by (3.8), i.e.

$$SNR_{eff} = \frac{1}{4}\frac{\left(\left(\tilde{\boldsymbol{\varepsilon}}^d\right)^T \tilde{\boldsymbol{\varepsilon}}^d\right)^2}{\left(\left(\tilde{\boldsymbol{\varepsilon}}^d\right)^T \mathbf{R}_{ee}\tilde{\boldsymbol{\varepsilon}}^d\right)}, \tag{3.8}$$

where $\tilde{\boldsymbol{\varepsilon}}^d$ is obtained by filtering the dominant error event $\tilde{\boldsymbol{\varepsilon}}^d$ by the target $\mathbf{g}$, and $\mathbf{R}_{ee}$ is the autocorrelation matrix of the total noise at equalizer output. We use the conventional steepest descent (SD) algorithm [57] to update the tap weights of target and equalizer (the length of equalizer is set long enough) in each iteration of the search. The SNR_{eff} employed in the search practice is computed based on the error event $[+2-2]$. BER simulations are also conducted using the targets obtained from the numerical search.

It is known that the numerical search using SD method may lead to local optima.

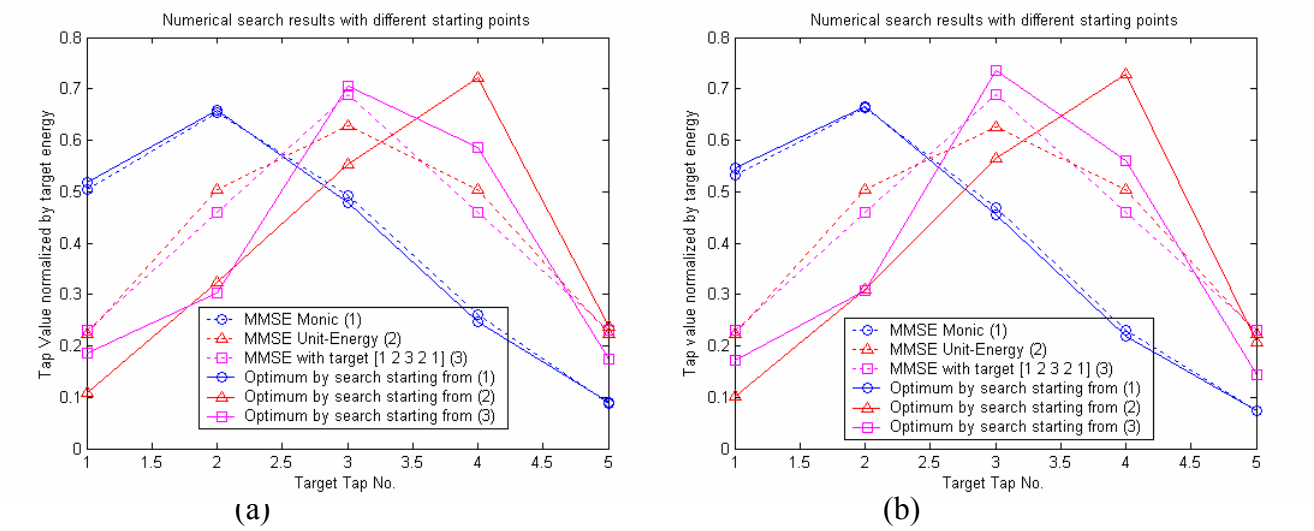

Figure 4.4: Starting points and ending points in the numerical searches for optimum target based on SNR_{eff} in the perpendicular recording channel at linear density of 2.5 and channel SNR of 27dB with (a) 0% jitter, and (b) with 3% jitter.

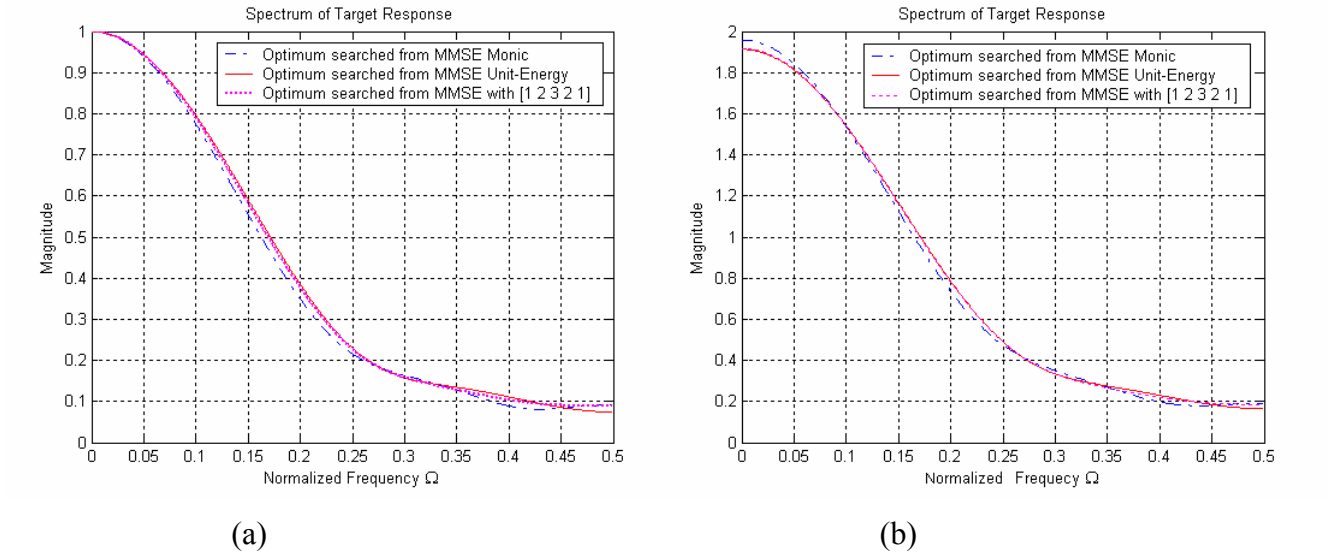

Figure 4.5: Magnitude frequency responses of the optimum targets obtained in the numerical searches based on SNR_{eff} in the perpendicular recording channel at linear density of 2.5 and channel SNR of 27dB with (a) 0% jitter, and (b) 3% jitter.

In order to find the global optimum, we may repeat the numerical search by SD with different starting points to see whether each search converges to the same optimum. In the case of SNR_{eff} based search, we find that different starting points usually result in

different optimum targets. However, these different optimum targets produce similar BER performances in simulations. Figures 4.4(a) and 4.4(b) illustrate the search results in the absence and presence of media noise, respectively. The SNR with respect to electronics noise is set to be 27 dB. The broken lines with marks represent the three different starting targets used in the search. As indicated, these starting targets are given by the standard PR target [1 2 3 2 1], monic constrained MMSE target, and unit-energy constrained MMSE target, respectively. The equalizers for these three cases are initialized with the solutions of MMSE PR equalizers given by (2.29) based on these three targets, respectively. The search interations from the three different starting points lead to quite different optimum target responses, which are indicated by the solid lines in Figures 4.4(a) and 4.4(b). All the searched target responses resulted in similar BER performances (not shown here): in the order of 10^{-5} without media noise and 10^{-4} with media noise. Further, as shown in Figure 4.5, these different optimum targets obtained by numerical search have almost equal magnitude frequency responses. These results corroborate our analytical results given in Section 4.1 that the optimum targets based on the SNR_{eff} criterion for a given dominant error event are global optimizers of SNR_{eff} and all these optimum targets have the same magnitude frequency response.

4.3.2 Search Based on BER Expression

The numerical results in Section 4.3.1 are based on a single dominant error event. In order to account for the fact that dominant error event is dependent on target, we may consider the numerical search based on the overall SNR_{eff} criterion given by (4.7).

However, in order to use the simple SD algorithm, here, we conduct the numerical search based on the tight upper bound of BER given by (3.6), i.e.

$$P_b \approx \sum_{\boldsymbol{\varepsilon}\in\Psi} W_H(\boldsymbol{\varepsilon}) 2^{-W_H(\boldsymbol{\varepsilon})} Q\left(\frac{\tilde{\boldsymbol{\varepsilon}}^T\tilde{\boldsymbol{\varepsilon}}}{2\sqrt{\tilde{\boldsymbol{\varepsilon}}^T\mathbf{R}_{ee}\tilde{\boldsymbol{\varepsilon}}}}\right), \tag{3.6}$$

where Ψ denotes the set of all possible error events, $\tilde{\boldsymbol{\varepsilon}}$ is error event $\boldsymbol{\varepsilon}$ filtered by the target, and $W_H(\boldsymbol{\varepsilon})$ is the Hamming weight of $\boldsymbol{\varepsilon}$. At medium-to-high channel SNRs, P_b gives a reasonably accurate prediction of the BER performance of VA detector. As the $Q(\bullet)$ function exponentially decreases with its argument, the cost function given by (3.6) is almost equivalent to $\overline{SNR}_{eff}$ given by (4.7). Since the quantity $W_H(\boldsymbol{\varepsilon})2^{-W_H(\boldsymbol{\varepsilon})}$ exponentially decreases with $W_H(\boldsymbol{\varepsilon})$, we can limit Ψ in (3.6) to the set of error events having small Hamming weights.

Table 4.1 lists the numerical search results obtained from SNR_{eff} based search and BER prediction based search with SNR of 27 dB and 0%, 3% and 6% jitter,

Table 4.1: Targets obtained by numerical search and BER simulation results (SNR=27 dB).

Jitter	Cost function: SNR_{eff}		Cost function: BER prediction	
	Searched target response	BER (simu.) $\times 10^{-4}$	Searched target response	BER (simu.) $\times 10^{-4}$
0%	[0.186, 0.301, 0.703, 0.591, 0.178]	0.567	[0.186, 0.304, 0.706, 0.587, 0.175]	0.604
3%	[0.172, 0.309, 0.738, 0.557, 0.141]	1.33	[0.172, 0.307, 0.737, 0.559, 0.143]	1.39
6%	[0.100, 0.393, 0.819, 0.392, 0.104]	8.83	[0.106, 0.392, 0.818, 0.396, 0.100]	8.11

Table 4.2: Targets obtained by numerical search and BER simulation results (SNR=30.5 dB and 8% jitter).

Cost function	Searched target response	BER (simu.) $\times 10^{-4}$
SNR_{eff} with error event [2 –2]	[0.6554, 0.6984, 0.2844, 0.0424, –0.0047]	3.356
SNR_{eff} with error event [2 –2 2]	[0.6560, 0.6977, 0.2823, 0.0425, -0.0038]	3.337
BER prediction	[0.6559, 0.6984, 0.2834, 0.0417, –0.0045]	3.347

respectively. Under these channel conditions, single dominant error [+2 –2] is found. The results shown in Table 4.1 correspond to the search that starts with the standard target [1 2 3 2 1] and the MMSE PR equalizer obtained for this target. As observed from the tabulated data, the searches for optimum target based on the two cost functions, SNR_{eff} and BER, lead to quite similar results, in terms of target coefficients and the BER performances with the searched targets. Table 4.2 lists the search results with SNR of 30.5 dB and 8% jitter such that there exist two dominant error events [+2 –2] and [+2 –2 +2]. The searches start with the target and PR equalizer designed by the monic constrained MMSE criterion. As shown in the table, the results (i.e. the searched target coefficients and the BER performances with the searched targets) from SNR_{eff} based searches with error event [+2 –2] only and with error event [+2 –2 +2] only are quite similar to the results from BER prediction based search that takes into account multiple error events. These numerical results corroborate our analytical results given in Section 4.2 that optimizing $\overline{SNR}_{eff}$ with the dominant error event

dependent on the target (or equivalently, the BER expression we used here) is equivalent to optimizing SNR_{eff} with a single dominant error event.

4.4 Conclusion

In this Chapter, we proved the uniqueness of the optimum magnitude frequency response of target based on the SNR_{eff} criterion, with and without the consideration of the dependence of the dominant error event on the target. Results from numerical approach corroborated with the findings based on our analysis work. Throughout the analysis in Chapters 3 and 4, we considered that channel noises to be stationary and Gaussian distributed. However, the media noise, which becomes the dominant noise source on high-density recording channels, is actually data-dependent and thus, non-stationary and non-Gaussian. In the next chapter, we are going to modify the SNR_{eff} criterion that takes into account the data-dependence of media noise.

Chapter 5

Optimum Target Design to Combat Media Noise

In this chapter, we investigate the target design problem with emphasis on combating media noise, which is the dominant noise source in high-density magnetic recording channels. Since media noise is not only correlated but also data-dependent, the detector needs to become data-dependant too. Proposals for modifying the branch metrics of VA detector according to the data-dependent correlation, variance and/or mean of media noise have been reported in [42, 43, 44, 45, 46, 58]. In this chapter, we propose to compute the branch metrics of VA detector with data-dependent GPR target designed by a modified effective detection SNR criterion that accounts for the data-dependence of media noise. We start Section 5.1 with formulation of the modified SNR_{eff} criterion that incorporates the data-dependence nature of media noise. In Section 5.2, we develop the approach for finding the data-dependent optimum target based on this modified SNR_{eff} criterion. The modified VA detector tuned to the designed data-dependent optimum targets is described in Section 5.3. Finally, we present in Section 5.4 the simulation results that illustrate the performance of our approach.

5.1 Modified Effective Detection SNR Criterion

In Chapters 3 and 4, we designed the optimum target based on the effective detection SNR criterion given by (3.8). This criterion is developed based on the assumption that the noise at VA detector input is stationary and Gaussian distributed. However, this assumption will be violated in the presence of media noise, since media noise is significantly data-dependent. In order to modify the effective detection SNR criterion to account for the data-dependence of media noise, we need to re-investigate the error analysis based on the underlying input data path $\mathbf{a} = [\cdots a_{k+1},, a_k, a_{k-1}, \cdots]$, as stated in Chapter 3, i.e.

$$\begin{aligned} P_r(\boldsymbol{\varepsilon}|\mathbf{a}) &= P_r\left(\frac{1}{2}\sum_{j=k_0}^{N_\varepsilon+N-2+k_0}\left(\sum_{i=0}^{N-1} g_i \varepsilon_{k-i-k_0+j}\right)^2 + \sum_{j=k_0}^{N_\varepsilon+N-2+k_0} e_{k+j}\left(\sum_{i=0}^{N-1} g_i \varepsilon_{k-i-k_0+j}\right) < 0 \middle| \mathbf{a}\right) \\ &= P_r\left(\frac{1}{2}\sum_{j=0}^{N_\varepsilon+N-2} \tilde{\varepsilon}_{k+j}{}^2 + \sum_{j=0}^{N_\varepsilon+N-2} e_{k+j+k_0}\tilde{\varepsilon}_{k+j} < 0 \middle| \mathbf{a}\right) \\ &= P_r\left(\frac{1}{2}d_\varepsilon^2 + u_k < 0 \middle| \mathbf{a}\right) = Q\left(\frac{d_\varepsilon^2}{2\sigma_{u,\varepsilon}}\right). \end{aligned} \tag{5.1}$$

In the absence of media noise, the data path $\mathbf{a}$ affects only the error sequence $\boldsymbol{\varepsilon}$, while the noise e_k at VA detector input is independent of $\mathbf{a}$. On the other hand, in the presence of media noise, the noise e_k also becomes dependent on $\mathbf{a}$. Consequently, the random quantity $u_k = \sum_{j=0}^{N_\varepsilon+N-2} e_{k+j+k_0}\tilde{\varepsilon}_{k+j}$ becomes even more data-dependent. To emphasize this data-dependence, we change the notation of the variance of u_k from $\sigma_{u,\varepsilon}^2$ to $\sigma_{u,\varepsilon}^2(\mathbf{a})$, where $\sigma_{u,\varepsilon}^2(\mathbf{a}) = E\left[u_k{}^2 \,|\, \mathbf{a}\right]$. Further, $P_r(\boldsymbol{\varepsilon}|\mathbf{a}) = Q\left(d_\varepsilon^2/(2\sigma_{u,\varepsilon}(\mathbf{a}))\right)$ becomes dependent on the assumed input data pattern. By averaging $P_r(\boldsymbol{\varepsilon}|\mathbf{a})$ over all possible data patterns supporting $\boldsymbol{\varepsilon}$, we have the probability of a single error event as

$$P_r(\boldsymbol{\varepsilon}) = \sum_{\mathbf{a}\in\Lambda_\varepsilon} P_r(\mathbf{a}) Q\left(\frac{d_\varepsilon^2}{2\sigma_{u,\varepsilon}(\mathbf{a})}\right), \tag{5.2}$$

where $\Lambda_{\boldsymbol{\varepsilon}}$ denotes the set of all the possible data patterns supporting the error event $\boldsymbol{\varepsilon}$ and $P_r(\mathbf{a})$ represents the probability that the data pattern $\mathbf{a}$ is transmitted/recorded. Consequently, at medium-to-high channel SNRs the BER performance can be predicted as

$$P_b \approx W_H(\boldsymbol{\varepsilon}^d) \sum_{\mathbf{a}\in\Lambda_{\boldsymbol{\varepsilon}^d}} P_r(\mathbf{a}) Q\left(\frac{d_{\boldsymbol{\varepsilon}^d}^2}{2\sigma_{u,\boldsymbol{\varepsilon}^d}(\mathbf{a})}\right), \tag{5.3}$$

where $\boldsymbol{\varepsilon}^d$ is the dominant error event that minimizes the argument of the $Q(\bullet)$ function in (5.2).

We now define the squared argument of the $Q(\bullet)$ function in (5.3) as the modified effective detection SNR, which is given by

$$SNR_{eff}^m(\mathbf{a}) = \frac{d_{\boldsymbol{\varepsilon}^d}^4}{4\sigma_{u,\boldsymbol{\varepsilon}^d}^2(\mathbf{a})}, \quad \text{for } \mathbf{a}\in\Lambda_{\boldsymbol{\varepsilon}}. \tag{5.4}$$

Clearly, the modified SNR_{eff} incorporates the data-dependent nature of media noise. The target optimized based on $SNR_{eff}^m(\mathbf{a})$ is expected to well combat media noise and produce the optimum BER performance for the particular input data pattern $\mathbf{a}$. Using the data-dependent optimum target designed by the modified SNR_{eff} criterion, the BER predicted by (5.3) is minimized as well.

5.2 Optimization Approach based on the Modified Criterion

Since the data-dependence of media noise is under consideration, we can no longer derive the expression of the modified SNR_{eff} in frequency domain by using the PSD of the noise alone. To find an analytical solution of the optimum target based on the

SNR_{eff}^{m} criterion, we first need to rewrite the criterion given by (5.4) as an explicit function of the target.

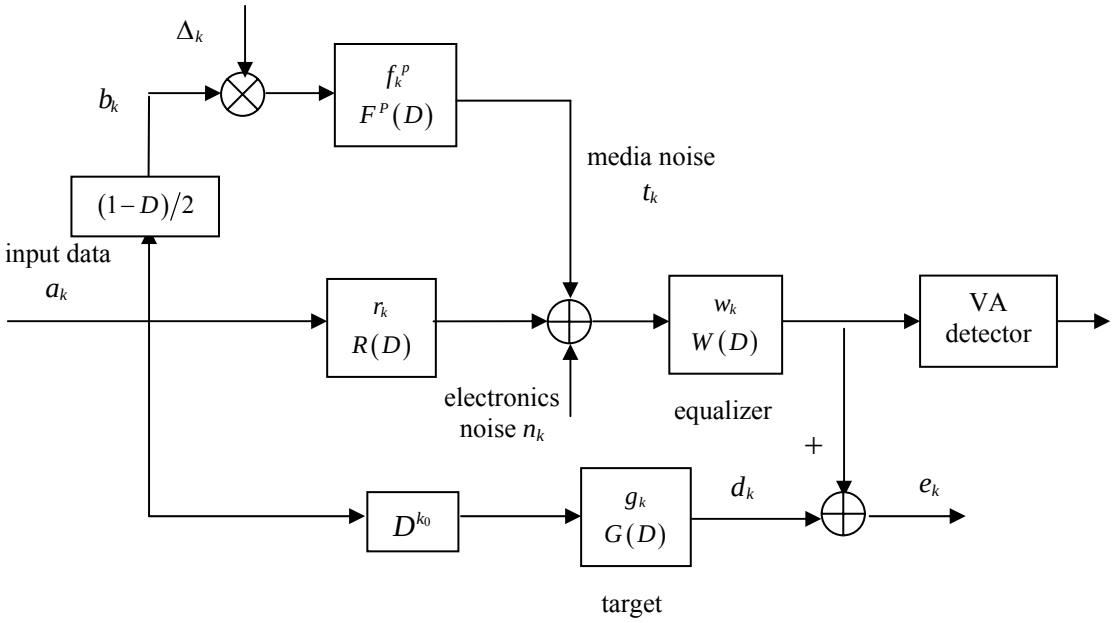

Figure 5.1: VA detector based magnetic recording channel with electronics noise and media noise.

Figure 5.1 illustrates a PRML channel model where the media noise is approximated by first-order transition jitter model[1]. As shown in Figure 5.1, there are two types of channel noises. One is the media noise t_k given by

$$t_k = \sum_i b_{k-i}\Delta_{k-i} f_i^p = \frac{1}{2}\sum_i (a_{k-i} - a_{k-i-1})\Delta_{k-i} f_i^p , \tag{5.5}$$

where f_k^p denotes the first-order derivative jitter path and Δ_k is the random transition jitter that is modeled as a white Gasussian random variable with zero mean and variance σ_t^2. Eqn. (5.5) indicates that the media noise has Gaussian distribution when conditioned on the input data pattern. Another channel noise is electronics noise n_k, which is modeled as an AWGN with variance σ_n^2. The estimation error e_k, which

[1] This figure is the same as Figure 3.4 and it is repeated here for the sake of convenience.

represents the total noise at VA detector input, includes media noise t_k, electronics noise n_k and residual ISI, i.e.

$$e_k = (n_k + t_k) \otimes w_k + a_k \otimes \eta_k , \tag{5.6}$$

where $\otimes$ denotes the convolution operator, $\{w_i\}$ are the equalizer tap weights, $a_k \otimes \eta_k$ represents the residual ISI, and $\{\eta_k\}$ denote the coefficients of the transfer function given by $\mathrm{I}(D) = R(D)W(D) - G(D)D^{k_0}$, i.e. the residual ISI channel. Here, we consider the equalizer to be the unconstrained MMSE PR equalizer given by

$$W = \frac{\mathrm{P}_a R^* e^{-j2\pi k_0}}{\mathrm{P}_{\bar{n}} + \mathrm{P}_a |R|^2} G = VG , \tag{5.7}$$

where $V = \left(\mathrm{P}_a R^* e^{-j2\pi k_0}\right) \Big/ \left(\mathrm{P}_{\bar{n}} + \mathrm{P}_a |R|^2\right)$, $\mathrm{P}_{\bar{n}} = \sigma_n^2 + E\left[b_k^2\right]\sigma_t^2 \left|F^p\right|^2$ denotes the effective PSD of the overall channel noise at equalizer input, P_a is the PSD of input data sequence. Letting $\{v_k\}$ denote the coefficients of V, we may rewrite (5.6) as

$$e_k = ((n_k + t_k) \otimes v_k + a_k \otimes \eta'_k) \otimes g_k ,$$

where $\{\eta'_k\}$ are the coefficients of the transfer function given by $\mathrm{I}'(D) = R(D)V(D) - D^{k_0}$. Consequently, the output of the equalizer can be expressed as

$$y_k = a_{k-k_0} \otimes g_k + e_k = (a_{k-k_0} + n_k \otimes v_k + t_k \otimes v_k + a_k \otimes \eta'_k) \otimes g_k . \tag{5.8}$$

We also note that the random quantity u_k in (5.1) is given by

$$u_k = e_{k+k_0} \otimes \varepsilon^d_{-k} \otimes g_{-k} , \tag{5.9}$$

where $\left\{\varepsilon_i^k\right\}$ are the elements of the dominant error event $\boldsymbol{\varepsilon}^d$. By incorporating (5.8) and (5.9) in Figure 5.1, a channel model equivalent to (5.8) results as shown in Figure 5.2, where $E^d(D)$ is the D transform of the dominant error event $\boldsymbol{\varepsilon}^d$ and '*' denotes complex conjugation.

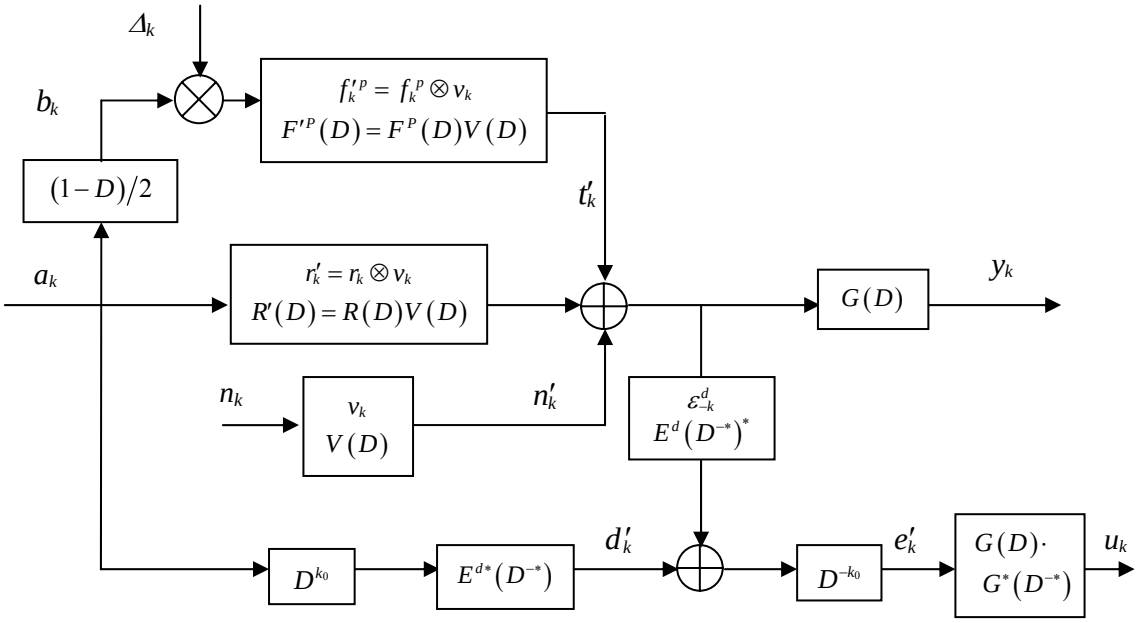

Figure 5.2: Channel model equivalent to the model given by (5.5).

From the channel model shown in Figure 5.2, the effective estimation error e_k' is expressed as

$$e_k' = (n_{k+k_0}' + t_{k+k_0}') \otimes \varepsilon_{-k}^d + a_{k+k_0} \otimes \bar{\eta}_k ,$$

where $t_k' = \sum_i b_{k-i}\Delta_{k-i} f_i'^p = \frac{1}{2}\sum_i (a_{k-i} - a_{k-i-1})\Delta_{k-i} f_i'^p$, $n_k' = n_k \otimes v_k = \sum_i n_{k-i} v_i$ (n_k' is independent of data pattern), $\{\bar{\eta}_k\}$ denote the coefficients of an effective residual ISI channel whose transfer function is given by $\bar{\mathrm{I}}(D) = (R(D)V(D) - D^{k_0})E^{d*}(D^{-*})$, and $f_k'^p = f_k^p \otimes v_k$. Letting $\bar{f}_k^p = f_k'^p \otimes \varepsilon_{-k}^d = f_k^p \otimes v_k \otimes \varepsilon_{-k}^d$ and $\bar{w}_k = v_k \otimes \varepsilon_{-k}^d$, we have $t_k'' = t_k' \otimes \varepsilon_{-k}^d = \frac{1}{2}\sum_i (a_{k-i} - a_{k-i-1})\Delta_{k-i}\bar{f}_i^p$, $n_k'' = n_k' \otimes \varepsilon_{-k}^d = n_k \otimes \bar{w}_k = \sum_i n_{k-i}\bar{w}_i$ and $e_k' = n_{k+k_0}'' + t_{k+k_0}'' + a_{k+k_0} \otimes \bar{\eta}_k$. Then, the conditional autocorrelation function of e_k' can be computed as

$$
\begin{aligned}
r_{e'}(k,m,\mathbf{a}) &\triangleq E\left[e'_k e'_m \middle| \mathbf{a}\right] \\
&= E\left[n''_{k+k_0} n''_{m+k_0} \middle| \mathbf{a}\right] + E\left[t''_{k+k_0} t''_{m+k_0} \middle| \mathbf{a}\right] + E\left[\sum_i a_{k+k_0-i}\overline{\eta}_i \sum_i a_{m+k_0-i}\overline{\eta}_i \middle| \mathbf{a}\right] \\
&= \sigma_n^2 \sum_i \overline{w}_i \overline{w}_{i+m-k} + \frac{\sigma_t^2}{4}\sum_i \left(a_{k+k_0-i} - a_{k+k_0-i-1}\right)^2 \overline{f}_i^{\,p}\, \overline{f}_{i+m-k}^{\,p} + \sum_i \sum_j \overline{\eta}_i \overline{\eta}_j a_{k+k_0-i} a_{m+k_0-j}\,,
\end{aligned}
$$

since the input data, transition jitter shift Δ_k and electronics noise n_k are independent of each other, and n_k and Δ_k are white Gaussian processes with variances σ_n^2 and σ_t^2, respectively. Apparently, $r_{e'}(k,m,\mathbf{a}) = r_{e'}(m,k,\mathbf{a})$.

With N –tap target, the random quantity u_k shown in Figure 5.2 is then given by

$$
u_k = \sum_{i=-N+1}^{N-1} (g_i \otimes g_{-i})\, e'_{k-i} = x_0 e'_k + \sum_{i=1}^{N-1} x_i \left(e'_{k-i} + e'_{k+i}\right),
$$

where $x_k = g_k \otimes g_{-k}$ for $-N+1 \le k \le N-1$ and $x_k = x_{-k}$. With the given dominant error event $\boldsymbol{\varepsilon}^d$, the variance of u_k conditioned on input data pattern $\mathbf{a}$ that supports $\boldsymbol{\varepsilon}^d$ is computed as

$$
\begin{aligned}
\sigma^2_{u,\boldsymbol{\varepsilon}^d}(\mathbf{a}) &= E\left[{u_k}^2 \middle| \mathbf{a}\right] \\
&= x_0^2 E\left[{e'_k}^2 \middle| \mathbf{a}\right] + 2x_0 \sum_{i=1}^{N-1} x_i E\left[e'_k \left(e'_{k-i} + e'_{k+i}\right) \middle| \mathbf{a}\right] \\
&\qquad + \sum_{i=1}^{N-1}\sum_{j=1}^{N-1} x_i x_j E\left[\left(e'_{k-i} + e'_{k+i}\right)\left(e'_{k-j} + e'_{k+j}\right) \middle| \mathbf{a}\right] \\
&= x_0 \tau_0(\mathbf{a}) + 4x_0 \mathbf{x}^T \boldsymbol{\tau}(\mathbf{a}) + 4\mathbf{x}^T \mathbf{T}(\mathbf{a})\,\mathbf{x}\,. \qquad (5.10)
\end{aligned}
$$

where $\mathbf{x} = \left[x_1, x_2, \cdots, x_{N-1}\right]^T$, $\tau_i(\mathbf{a}) = \frac{1}{2}\left(r_{e'}(k,k-i,\mathbf{a}) + r_{e'}(k,k+i,\mathbf{a})\right)$ for $0 \le i \le N-1$, $\mathrm{T}_{ij}(\mathbf{a}) = \left[r_{e'}(k-i,k-j,\mathbf{a}) + r_{e'}(k-i,k+j,\mathbf{a}) + r_{e'}(k+i,k-j,\mathbf{a}) + r_{e'}(k+i,k+j,\mathbf{a})\right]/4$ for $1 \le i, j \le N-1$, $\boldsymbol{\tau}(\mathbf{a}) = \frac{1}{2}\left[\tau_1(\mathbf{a}), \tau_2(\mathbf{a}), \cdots, \tau_{N-1}(\mathbf{a})\right]^T$, and $\mathbf{T}(\mathbf{a})$ is a $(N-1)\times(N-1)$ matrix with $\mathrm{T}_{ij}(\mathbf{a})$ being its $(i,j)^{\text{th}}$ element for $1 \le i, j \le N-1$. Clearly, $\mathbf{T}(\mathbf{a})$ is a symmetric matrix. It is also a positive definite matrix, since $\sigma^2_{u,\boldsymbol{\varepsilon}^d}(\mathbf{a})$ in (5.10) is the

conditional variance of the random variable u_k. In addition, the numerator of (5.4) is also a function of $\mathbf{x}$, i.e.

$$d_{\varepsilon^d}^4 = p_0^2 + 4p_0\mathbf{x}^T\mathbf{p} + 4\mathbf{x}^T\mathbf{B}\mathbf{x}, \tag{5.11}$$

where $p_i = \int_{-0.5}^{0.5} \left|E^d\right|^2 \cos(i2\pi\Omega)\, d\Omega$ for $0 \le i \le N-1$, $\mathbf{p} = [p_1, \ldots, p_{N-1}]^T$ and $\mathbf{B} = \mathbf{p}\mathbf{p}^T$.

With (5.10) and (5.11), we change the modified SNR_{eff} defined by (5.4) into

$$J_{\mathbf{a}}(\mathbf{x}) = \frac{1}{4} \cdot \frac{p_0^2 + 4p_0\mathbf{x}^T\mathbf{p} + 4\mathbf{x}^T\mathbf{B}\mathbf{x}}{\tau_0(\mathbf{a}) + 4\mathbf{x}^T\boldsymbol{\tau}(\mathbf{a}) + 4\mathbf{x}^T\mathbf{T}(\mathbf{a})\mathbf{x}}, \tag{5.12}$$

which is an explicit function of auto-correlated target coefficient vector $\mathbf{x}$. When the convolution feature of $\mathbf{x}$ is kept, $J_{\mathbf{a}}(\mathbf{x})$ given by (5.12) is equivalent to the modified SNR_{eff} defined by (5.4). Due to the similarity between (5.12) and (3.14), the analytical approach developed in Chapter 3 can be directly applied for solving the optimization problem given by the modified SNR_{eff}. Certainly, by this approach, we obtain the data-dependent optimum magnitude frequency response of target based on the modified SNR_{eff}.

5.3 Proposed Detector

In this section, we develop a modified VA detector to combat media noise. The branch metric of the modified VA detector is computed with the data-dependent optimum target based on the modified SNR_{eff} criterion. Since the modified SNR_{eff} criterion only defines the optimum magnitude frequency response of target, we select the minimum-phase target having this optimum magnitude frequency response to compute the VA branch metrics. In order to emphasize the data-dependence of the selected

optimum target, we denote its tap weights and D transform as $\{g_{o,i}(\mathbf{a})\}$ and $G_{\mathbf{a}}(D)$, respectively, where $\mathbf{a}$ represents the data pattern under consideration.

5.3.1 Modified VA Detector

In the approach for designing optimum target based on the modified SNR_{eff} criterion, the equalizer is obtained as the unconstrained MMSE PR equalizer for the data-dependent optimum target, i.e.

$$W_{\mathbf{a}} = \frac{\mathrm{P}_a R^* e^{-j2\pi k_0}}{\mathrm{P}_{\bar{n}} + \mathrm{P}_a |R|^2} G_{\mathbf{a}} = V G_{\mathbf{a}} .$$

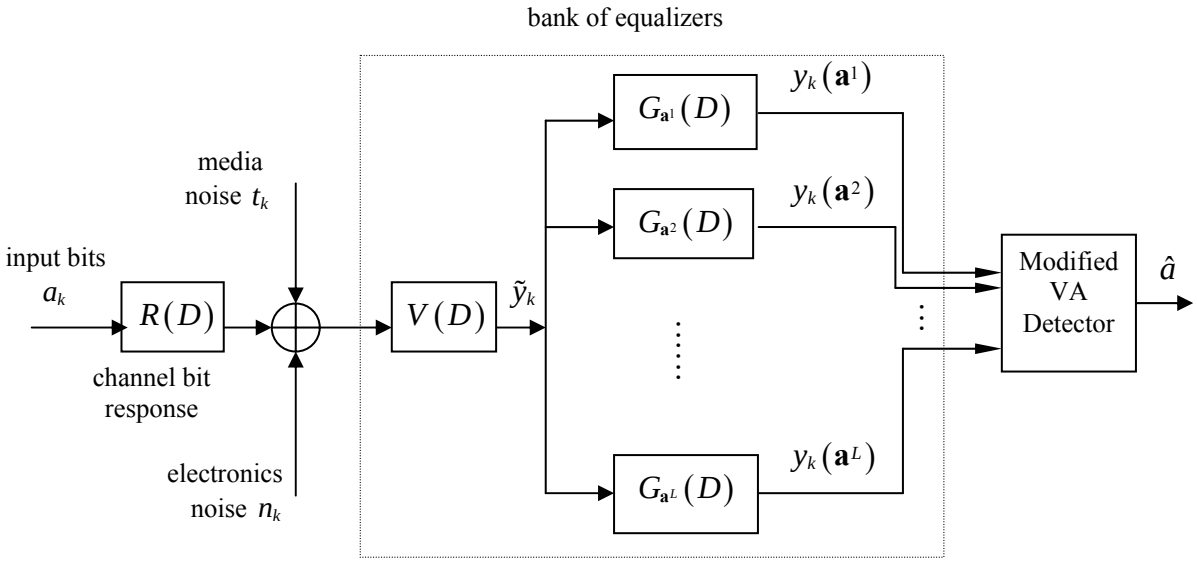

Figure 5.3: PRML system using data-dependent equalizer and data-dependent target designed by the modified SNR_{eff} criterion.

Here, the equalizer $W_{\mathbf{a}}(D)$ is data-dependent since the target $G_{\mathbf{a}}(D)$ is data-dependent. The straightforward way to implement the data-dependent PR equalizer is illustrated in Figure 5.3, where $\{\mathbf{a}^1, \mathbf{a}^2, \cdots, \mathbf{a}^L\}$ denote the data patterns under consideration.

We propose to modify the VA detector by adjusting its branch metrics computation to incorporate the data-dependent optimum target. For a normal full-state VA detector, for example, a branch metric at instant k is computed as

$$\left(y_k - \sum_i g_i a_{k-i-k_0} \right)^2 ,$$

where y_k is the equalizer output and $\{g_k\}$ denote the target tap weights. Different from the normal VA detector, the modified VA detector computes its branch metric as

$$\left(y_k(\mathbf{a}^n) - \sum_i g_{o,i}(\mathbf{a}^n) a^n_{k-i-k_0} \right)^2 ,$$

where $\{a_k^n\}$ are the data from the data pattern $\underline{a}^n$, $\{g_{o,i}(\mathbf{a}^n)\}$ are the tap weights of the optimum target $G_{\mathbf{a}^n}(D)$, and $y_k(\mathbf{a}^n)$ is the output of the equalizer obtained for the target $G_{\mathbf{a}^n}(D)$,.

If the first tap of $G_{\mathbf{a}}(D)$ is normalized to unity, we may re-express the computation of the modified branch metric as

$$\begin{aligned} \left(y_k(\mathbf{a}^n) - \sum_i g_{o,i}(\mathbf{a}^n) a^n_{k-k_0-i} \right)^2 &= \left(\sum_i \tilde{y}_{k-i} g_{o,i}(\mathbf{a}^n) - \sum_i g_{o,i}(\mathbf{a}^n) a^n_{k-k_0-i} \right)^2 \\ = \left(\tilde{y}_k - a^n_{k-k_0} + \sum_{i>1} (\tilde{y}_{k-i} - a^n_{k-k_0-i}) g_{o,i}(\mathbf{a}^n) \right)^2 &= \left(\tilde{y}_k - a^n_{k-k_0} - \sum_{i>1} \tilde{e}_{k-i}(-g_{o,i}(\mathbf{a}^n)) \right)^2 , \end{aligned} \quad (5.13)$$

where $\tilde{y}_k$ is the output of $V(D)$ and $\tilde{e}_k = \tilde{y}_k - a_k$. The RHS of the last equation in (5.13) resembles the branch metric computation in the data-dependent NPML system given in [58], with the primary target[2] as $G_r(D) = g_{o,0}(\mathbf{a}) = 1$ and the data-dependent noise predictor as $1 - G_{\mathbf{a}}(D)$, and $\tilde{e}_k$ is the estimation error at the output of the equalizer obtained for the primary target. Actually, the transfer function $V(D)$

[2] An approach that has been widely used for designing GPR target is to choose the overall target as the cascade of a primary target and secondary target. The primary target is usually chosen from a set of conventionally used targets and the equalizer is designed to shape the channel to the primary target. Thereafter, the secondary target is designed to achieve noise whitening at the VA detector input. The NPML scheme is an example of this approach

happens to be the MMSE equalizer for the target $G_r(D)$. Hence, we have an alternative way to implement the system shown in Figure 5.2 like a NPML system that embeds the data-dependent noise predictor $1-G_{\mathbf{a}}(D)$ in the VA trellis. The difference between our approach and the data-dependent NPML system proposed in [58] is that the latter designs the data-dependent noise predictor based on the MMSE criterion while we use the modified SNR_{eff} criterion. The resulting NPML-type implementation of our approach is shown in Figure 5.4.

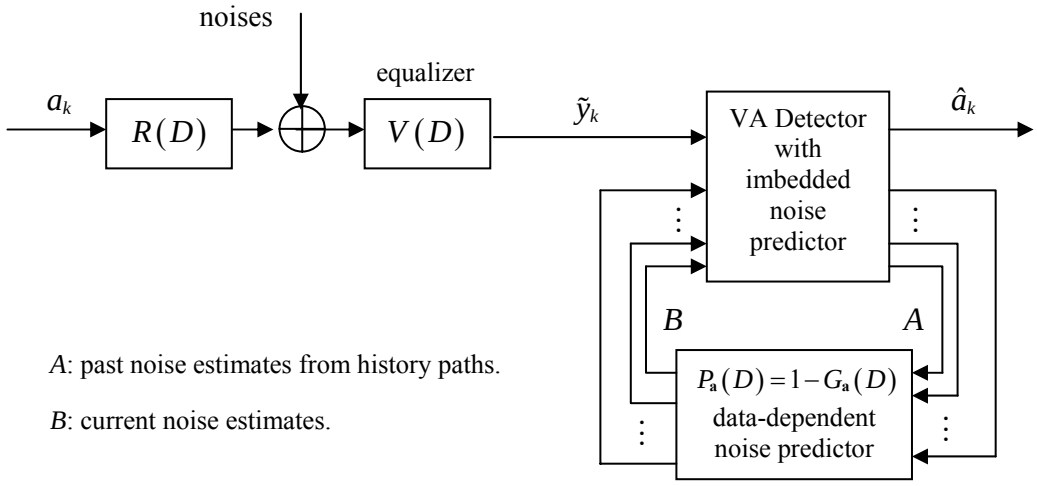

Figure 5.4: Alternative NPML-type implementation of the system using data-dependent equalizer and target designed by the modified SNR_{eff} criterion.

5.3.2 Estimation of Noise Correlation

To compute the modified SNR_{eff} given by (5.4), we need the knowledge of the noise correlation conditioned on the data pattern. For the media noise modeled by (5.5):

$$t_k = \sum_i b_{k-i}\Delta_{k-i} f_i^{\,p} = \frac{1}{2}\sum_i (a_{k-i} - a_{k-i-1})\Delta_{k-i} f_i^{\,p},$$

its autocorrelation is computed as

$$r_t(k,m,\mathbf{a}) \triangleq E\left[t_k t_m \middle| \mathbf{a}\right] = \frac{\sigma_t^2}{4} \sum_{i=-I_1}^{I_2-m+k} \left(a_{k-i} - a_{k-i-1}\right)^2 f_i^{\,p} f_{i+m-k}^{\,p}, \tag{5.14}$$

where I_1 and (I_2+1) are the number of anti-causal and causal taps, respectively, of the jitter path $F^P(D)$. As indicated in (5.14), the calculation of $r_t(k,m,\mathbf{a})$ depends on the input data over the span of (I_1+I_2+2) bits. This span is usually quite large, and hence calculation of $r_t(k,m,\mathbf{a})$ over all possible data patterns **a** becomes a very tedious computational task. Further, the fact that the span includes future data bits (i.e. $a_{k+1}, a_{k+2}, \cdots, a_{k+I_1}$) makes branch metric computations impractical in VA detector. Hence, we have to restrict to a shorter span of the data pattern, which accounts for the significant part of the data-dependence. Keeping this in mind and noting that the VA branch metrics computation at instant k involves the data bits $\{a_{k-k_0-N+1}, a_{k-k_0-N+2}, \cdots, a_{k-k_0-1}, a_{k-k_0}\}$ (N is the target length), we may estimate the conditional noise correlation at instant k based on the input data from instant $k-k_0-N_a+1$ ($N_a \le N$) to instant $k-k_0-N_b$ ($N_b \ge 0$), i.e.

$$\tilde{r}_t\left(k,m,\mathbf{a}_{k-k_0-N_a+1}^{k-k_0-N_b}\right) \triangleq E\left[r_t(k,m,\mathbf{a}) \middle| \mathbf{a}_{k-k_0-N_a+1}^{k-k_0-N_b}\right], \tag{5.15}$$

where $\mathbf{a}_{k-k_0-N_a+1}^{k-k_0-N_b} = \left[a_{k-k_0-N_a+1}, \cdots, a_{k-k_0-N_b}\right]$ denotes the shortened data pattern and the expectation $E[\bullet]$ is taken over the data excluded by $\mathbf{a}_{k-k_0-N_a+1}^{k-k_0-N_b}$. If we use longer data patterns, for example, $\mathbf{a}_{k-k_0-N_a+1}^{k-k_0-N_b}$ with $N_a > N$ and/ or $N_b < 0$, the estimation given by (5.15) can be more accurate. To implement the design with longer data patterns, we can either increase the number of states in VA detector, or use the data bits from the survivor paths [58]. The former approach results in exponential increase in the complexity, and the latter results in error propagation. Therefore, we need to find an acceptable trade-off between implementation complexity and accuracy when determining the span of data pattern used in (5.15).

5.4 Simulation Results

Simulations are conducted to investigate the performance of our proposed approach based on the channel model shown in Figure 5.1. Uncoded input data and the perpendicular recording channels at linear density of 2.5 with 3% jitter and 6% jitter, respectively, are used for our studies in this section. Under the same channel conditions, we also investigate the performance of other approaches designed based on stationary noise environment and those designed for combating media noise. They are normal SNR_{eff} approach and NPML with data-dependent predictor. To make the complexity of VA detector for all the approaches, we consider 5-tap targets for normal and modified SNR_{eff} approaches, respectively, PR2 target $(1+D)^2$ with 2-tap noise predictor, and 3-tap monic constrained MMSE target with 2-tap noise predictor. For the sake of convenience, we use abbreviations SNR_{eff}, modified SNR_{eff}, PR2NP2 and GPR3NP2 to refer to these approaches in the rest of this section. To avoid error propagation due to the use of local decision feedback, we set the VA detector to have 4-bit states, and short spans of the data patterns ($N_a = 2,3$ and $N_b = 0$). The channel used in this study is perpendicular recording channel at linear density of 2.5.

From the BER plots shown in Figure 5.5, we see that the proposed modified SNR_{eff} conditioned on 3-bit data pattern outperforms other data-dependent designs by 0.5 dB at BER of 10^{-4} with 3% jitter and 6% jitter, respectively, although some of them use longer data patterns. Since the modified SNR_{eff} approach aims to deal with data-dependent media noise, it does not show advantage over normal SNR_{eff} approach with low media noise, i.e. 3% jitter (see Figure 5.5(a)). However, as shown in Figure 5.5(b), when media noise increases to 6% jitter, the modified SNR_{eff} approach achieves about 0.2 dB performance gain over the normal SNR_{eff} approach at BER of 10^{-4}. It is

also observed from Figure 5.5(b) that the performance of the modified SNR_{eff} approach is improved by increasing the span of the data patterns from 2 bits to 3 bits. Intuitively, if we use long enough data pattern, the modified SNR_{eff} approach will achieve even more significant performance improvement, but the implementation complexity will increase significantly too.

5.5 Conclusion

In this chapter, we proposed a modified SNR_{eff} criterion that takes into account the data-dependence nature of media noise, and designed data-dependent GPR targets based on the modified SNR_{eff} criterion. We also proposed modified VA detector that employs the data-dependent GPR targets. Simulation results show that our modified SNR_{eff} approach achieves performance gain compared to the existing approaches that have been developed to combat media noise.

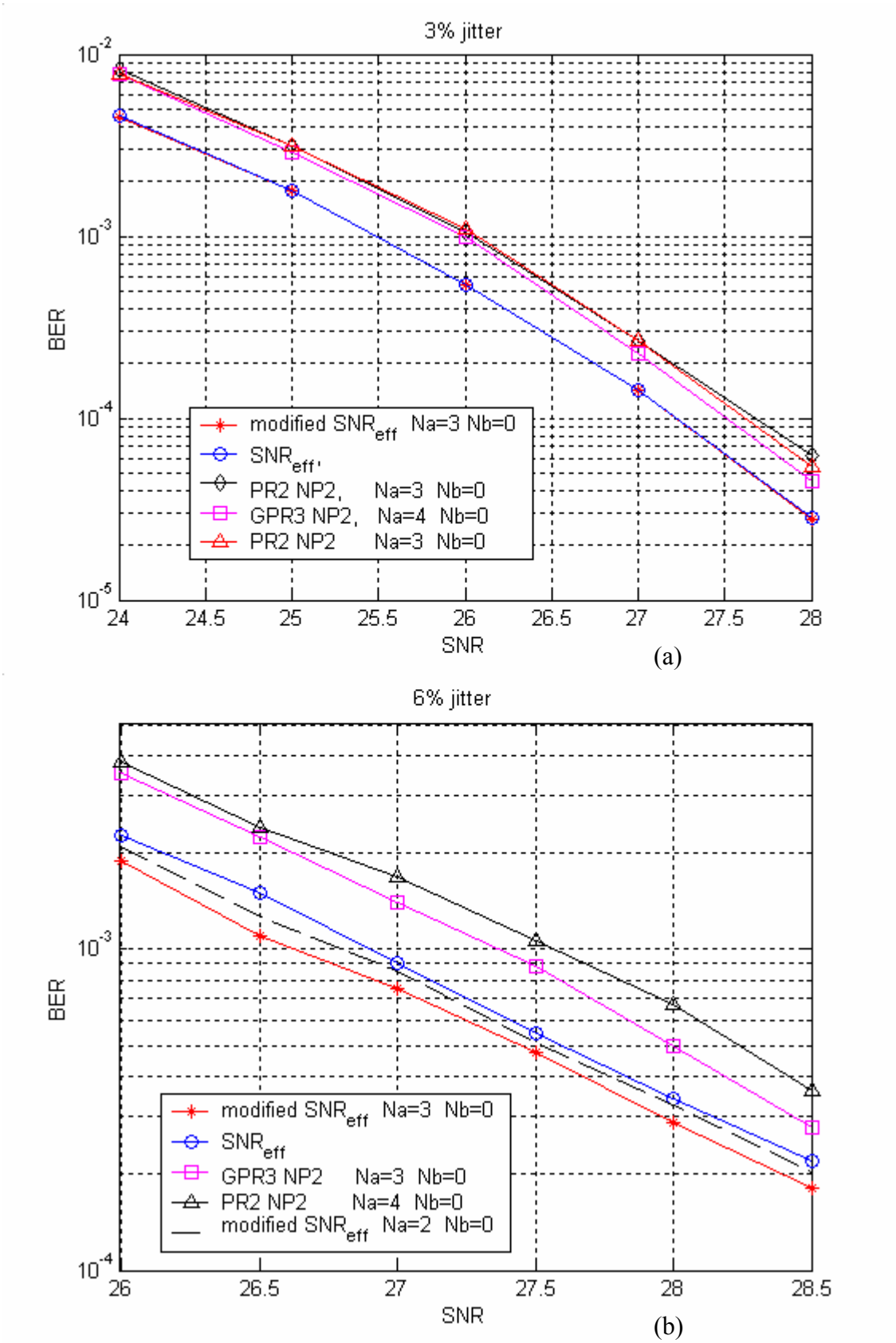

Figure 5.5: BER performances of different detection approaches for the perpendicular recording channel at linear density of 2.5 with media noise. (a) 3% jitter, and (b) 6% jitter.

Chapter 6

Conclusions and Future Work

In this thesis, we investigated the partial-response maximum-likelihood (PRML) detection strategy for perpendicular magnetic recording channels at high recording densities. In particular, we developed a novel analytical approach to design optimum generalized partial-response (PR) target response for PRML systems. We also proposed an approach to design target for combating media noise.

The thesis can be divided into three parts. The first part includes Chapters 1 and 2, where we briefly surveyed the existing techniques on the related topics and introduced background knowledge of modeling magnetic recording channel, linear PR equalization and Viterbi algorithm detection. In the second part, which consists of Chapters 3 and 4, we developed a novel analytical approach for finding optimum target based on a cost function that is closely related to the performance of Viterbi detector (VD), and then characterized the performance surface of this cost function. In the last part, which is Chapter 5, we proposed the method of designing target to deal with data-dependant media noise. The work reported in Parts 2 and 3 are elaborated below.

The effective detection signal-to-noise ratio (SNR_{eff}) is an equivalent measure of the bit-error-rate (BER) performance of VD. Hence, it is reasonable to claim that the target designed by the SNR_{eff} criterion can achieve the optimum performance of VD.

However, compared to the mean square error (MSE) criterion that is the widely used cost function for target design, SNR_{eff} appears so complicated that its optimum target solution is not yet available. On recognizing that the SNR_{eff} is related to the magnitude frequency response of the target and is independent of the target phase, a novel approach is proposed in this thesis (Chapter 3) for finding analytical solution of the optimum magnitude frequency response of the target that maximizes SNR_{eff}. Besides the analytical approach, this thesis (Chapter 4) is also the first to report the characterization of the performance surface of SNR_{eff}. The characterization indicates that all the optima of SNR_{eff} are global optima and take the same magnitude frequency response, which is uniquely provided by our analytical solution. Numerical search results corroborate the analytical results. Further, simulation results show that the BER results correlate well with the trends in SNR_{eff}, Simulation results also show that the targets based on the SNR_{eff} criterion achieves the best performance compared to the targets from non-SNR_{eff} approaches. With 6-tap target, for example, the SNR_{eff} approach results in gains of at least 1 dB in terms of effective detection SNR at high channel densities over most of the existing approaches, and maximum 0.024 dB over the monic constrained MMSE approach. In some sense, the SNR_{eff} approach produces a reasonable upper bound for the performance of PRML systems using VD, and the monic constrained MMSE approach achieves the near-optimum performance.

In order to combat media noise that bears significant data-dependence nature, a modified SNR_{eff} criterion is proposed in Chapter 5 by incorporating noise statistics conditioned on data patterns. Consequently, the VD that uses these GPR targets designed by the modified SNR_{eff} criterion is expected to result in the optimum performance for all the data patterns. Simulation results show that in media noise environment, our approach of using VD tuned to the proposed data-dependent GPR

target yields a gain of about 0.5 dB at a BER of 10^{-4} over the existing approaches that aim to deal with media noise, and 0.2 dB over the normal SNR_{eff} approach.

Directions for Future Work

There are several issues that remain to be solved to make the reported work more complete and effective for signal detection in high-density perpendicular recording channels. The issues concerning the problems attempted in this thesis, are listed as below.

- Development of an efficient adaptive algorithm to implement the target design based on the SNR_{eff} criterion without requiring the knowledge of channel characteristics.
- Development of a more accurate model of media noise that can accommodate large percentages of transition jitter.
- Development of a more accurate algorithm for estimating the data-dependent noise statistics.
- Investigation of the PRML detection strategy with timing recovery for channels with media noise.
- Investigating the equalizer and target design that exploits the modulation code properties.
- Investigating the application of the proposed approach in other type of channels, for example, optical recording channels.

We believe that serious attempts on the issues listed above will help to make our work more useful and extend it to address the problem of signal detection in recording channels in a holistic manner.

Bibliography

[1] J. Moon, "The role of SP in data-storage," *IEEE Signal Processing Magazine*, vol. 15, no. 4, pp. 54-72, Jul. 1998.

[2] J.G. Proakis, "Equalization techniques for high-density magnetic recording," *IEEE Signal Processing Magazine*, vol. 15, no. 4, pp. 73-82, Jul. 1998.

[3] R.D. Cideciyan, *et al*., "A PRML system for digital magnetic recording," *IEEE J. Select Areas Commun.*, vol. 10, no. 1, pp. 38-56, Jan. 1992.

[4] S. Iwasaki and Y. Nakamura, "An analysis for the magnetization mode for high density magnetic recording," *IEEE Trans. Magn.*, vol. 13, no. 5, pp. 1272-1277, Sep. 1977.

[5] S. Iwasaki, "Discoveries that guided the beginning of perpendicular magnetic recording," *J. Magn. and Magn. Mater.*, vol. 235, pp. 227-234, Oct. 2001.

[6] A. Taratorin, D. Cheng, and E. Marinero, "Media noise, nonlinear distortion, and thermal stability in high-density recording," *IEEE Trans. Magn.*, vol. 36, no. 1, pp. 80-85, Jan. 2000.

[7] D. Weller and A. Moser, "Thermal effect limits in ultrahigh-density magnetic recording," *IEEE Trans. Magn.*, vol. 35, no. 6, pp. 4423-4439, Nov. 1999.

[8] R. Wood, Y. Sonobe, Z. Jin, and B. Wilson, "Perpendicular recording: The promise and the problems," *J. Magn. and Magn. Mater.*, vol. 235, pp. 1-9, Oct. 2001.

[9] "Seagate 'gets vertical' and demonstrates record storage areal and performance," Seagate Technology News Release (online) Silicon Valley, Nov. 12, 2002. Available at http://www.seagate.com/cda/newsinfo/newsroom/releases/article/0,1121,1555,00.html

[10] G.J. Tarnopolsky, "Hard disk drive capacity at high magnetic areal density," *IEEE Trans. Magn.*, vol. 40, no. 1, pp. 301-306, Jan. 2004.

[11] "Read-Rite says they, not Seagate, are top in vertical recording density," Enterprise Storage Forum (online), Nov. 15, 2002. Available at http://www.enterprisestorageforum.com/technology/news/article.php/1501631

[12] Z. Zhang *et al.*, "Magnetic recording demonstration over 100 Gb/in^2," *IEEE Trans. Magn.*, vol. 38, no. 5, pp. 1861-1866, Sep. 2002.

[13] K. Ouchi, "Recent advancements in perpendicular magnetic recording," *IEEE Trans. Magn.*, vol. 37, no. 4, pp. 1217-1222, Jul. 2001.

[14] H. Melbye and C. Chi, "Nonlinearities in high density digital recording," *IEEE Trans. Magn.*, vol. 15, no. 5, pp. 746-748, Sep. 1978.

[15] J.W.M. Bergmans, J.O. Voorman, and H.W. Wong-Lam, "Structure and adjustment of a novel write-precompensation scheme," *IEEE Trans. Magn.*, vol. 35, no. 3, pp. 2053-2059, May 1999.

[16] B. Brickner and J. Moon, "Combating partial erasure and transition jitter in magnetic recording," *IEEE Trans. Magn.*, vol. 36, no. 2, pp. 532-536, Mar. 2000.

[17] S.X. Wang and A.M. Taratorin, *Magnetic Information Storage Technology*. Boston: Academic Press, 1998, chaps. 3, 9.

[18] A.M. Baran and H. N. Bertram, "Transition position and amplitude fluctuation noise model for longitudinal thin film media," *IEEE Trans. Magn.*, vol. 23, no. 5, pp. 2374-2376, Sep. 1987.

[19] R.A. Baugh, E.S. Murdock, and B.R. Natarajan, "Measurement of noise in magnetic media," *IEEE Trans. Magn*., vol. 19, no. 5, pp. 1722-1724, Sep. 1983.

[20] N. Honda and K. Ouchi, "Low noise design of perpendicular magnetic recording media," *J. Magn. and Magn. Mater*., vol. 235, pp. 289-296, Jun. 2001.

[21] D.J. Tyner and J.G. Proakis, "Partial response equalizer performance in digital magnetic recording channels," *IEEE Trans. Magn*., vol. 29, no. 6, pp. 4194-4208, Nov. 1993.

[22] G.D. Forney, Jr., "Maximum-likelihood sequence estimation of digital sequences in the presence of intersymbol interference," *IEEE Trans. Inform. Theory*, vol. 18, no. 3, pp. 363-378, May 1972.

[23] G.D. Forney, Jr., "The Viterbi algorithm, " *Proc. IEEE*, vol. 61, no. 3, pp. 268-278, Mar. 1973.

[24] H. Kobayashi, "Application of probabilistic decoding to digital magnetic recording systems," *IBM J. Res. Develop*., vol., 15, pp. 65-74, Jan. 1971.

[25] H. K. Thapar and A.M. Patel, "A class of partial response systems for increasing storage density in magnetic recording," *IEEE Trans. Magn*., vol. 23, no. 5, pp. 3666-3668, Sep. 1987.

[26] Y. Okamoto, et al., "A study of PRML systems for perpendicular recording using double layered medium," *IEEE Trans. Magn.*, vol. 36, no. 5, pp. 2164-2166, Sep. 2000.

[27] Y. Okamoto, H. Osawa, H. Saito, H. Muraoka, and Y. Nakmura, "Performance of PRML systems in perpendicular magnetic recording channel with jitter-like noise," *J. Magn. and Magn. Mater*., vol. 235, pp. 259-264, Oct. 2001.

[28] I. Lee, C. Modlin, and J.M. Cioffi, "Equalized maximum likelihood receiver in a magnetic recording channel," in *Proc. IEEE Intl. Conf. Global Telecommun. (GLOBECOM)*, Nov. 1993, pp. 1970-1973.

[29] I. Lee and J.M. Cioffi, "Equalized maximum likelihood receiver with a unit energy constraint," *IEEE Trans. Magn.*, vol. 33, no. 1, pp. 855-862, Jan. 1997.

[30] H. Sawaguchi, Y. Nishida, H. Takano, and H. Aoi, "Performance analysis of modified PRML channels for perpendicular recording systems," *J. Magn. and Magn. Mater.*, vol. 235, no. 1-3, pp. 265-272, Oct. 2001.

[31] J. Moon and W. Zeng, "Equalization for maximum likelihood detectors," *IEEE Trans. Magn.*, vol. 31, no. 2, pp. 1083-1088, Mar. 1995.

[32] J.W.M. Bergmans, "Density improvements in digital magnetic recording by decision feedback equalization," *IEEE Trans. Magn.*, vol. 22, no. 3, pp. 157-162, May 1986.

[33] N. Al-Dhahir and J.M. Cioffi, "MMSE decision-feedback equalizers: Finite-length results," *IEEE Trans. Inform. Theory*, vol. 41, no. 4, pp. 961-975, Jul. 1995.

[34] J. D. Coker, E. Eleftheriou, R. L. Galbraith, and W. Hirt, "Noise-predictive maximum likelihood (NPML) detection," *IEEE Trans. Magn.*, vol. 34, no. 1, pp. 110-117, Jan. 1998.

[35] S. Gopalaswamy and J. Bergmans, "Modified target and concatenated coding for d=1 constrained magnetic recording channels," in *Proc. IEEE Intl. Conf. Commun. (ICC)*, 2000, vol. 1, pp. 89-93.

[36] D.D. Falconer and F.R. Magee, Jr., "Adaptive channel memory truncation for maximum likelihood sequence estimation," *The Bell System Tech. Journal*, vol. 52, no. 9, pp. 1541-1562, Nov. 1973.

[37] S.K. Nair and J. Moon, "Nonlinear equalization for data storage channels," in *Proc. IEEE Intl. Conf. Global Telecommun. (GLOBECOM)*, May 1994, vol. 1, pp. 250-254.

[38] S.K. Nair and J. Moon, "Data storage channel equalization using neural networks," *IEEE Trans. Neural Networks*, vol. 8, no. 5, pp. 1037-1048, Sep. 1997.

[39] J-G. Zhu and X-G. Ye, "Impact of medium noise correlation on various partial response channels," *IEEE Trans. Magn.*, vol. 31, no. 6, pp. 3087-3089, Nov. 1995

[40] X. Che, L.C. Barbosa, and H.N. Bertram, "PRML performance estimation considering medium noise down track correlations," *IEEE Trans. Magn.*, vol. 29, no. 6, pp. 4062-4064, Nov. 1993.

[41] G.F. Hughes, X. Che, and R.S. Beach, "Time interval analysis errors in measuring recording media transition jitter," *IEEE Trans. Magn.*, vol. 33, no. 6, pp. 4475-4481, Nov. 1997.

[42] A. Kavčić and J.M.F. Moura, "Correlation-sensitive adaptive sequence detection," *IEEE Trans. Magn.*, vol. 34, no. 3, pp. 763-771, May 1998.

[43] J. Moon and J. Park, "Pattern-dependant noise prediction in signal dependent noise," *IEEE J. Select Areas Commun.*, vol. 19, no. 4, pp. 730-742, Apr. 2001.

[44] W. Zeng and J. Moon, "Modified Viterbi algorithm for a jitter-dominant $1-D^2$ channel," *IEEE Trans. Magn.*, vol. 28, no. 5, pp. 2895-2897, Sep. 1992.

[45] N.M. Zayed and L.R. Carley, "Equalization and detection for nonlinear recording channels with correlated noise," *IEEE Trans. Magn.*, vol. 35, no. 5, pp. 2295-2297, Sep. 1999.

[46] H. Sun, G. Mathew, and B. Farhang-Boroujeny, "Novel detection approach for high-density magnetic recording channels with data-dependent distortions," in *Proc. 9th Intl. Joint MMM/INTERMAG Conf.*, 2004, p. 450.

[47] J. Cioffi, W. Abbott, and K.D. Fisher, "A survey of adaptive equalization for magnetic-disk storage channels," in *Proc. 22nd Asilomar Conf. Signals, Systems and Computers*, Oct.-Nov. 1988, vol. 1, pp. 20-24.

[48] K.D. Fisher, J.M. Cioffi, and C.M. Melas, "An adaptive DFE for storage channels suffering from nonlinear ISI and transition dependent noise," in *Proc. IEEE Intl. Conf. Commun. (ICC), Boston, USA,* Jun. 1989, vol. 3, pp. 1638–1642.

[49] L.C. Barbosa, "Maximum likelihood sequence estimators: A geometric view," *IEEE Trans. Inform. Theory*, vol. 35, pp. 419-427, Mar. 1989.

[50] J. Moon and L.R. Carley, "Performance comparison of detection methods in magnetic recording," *IEEE Trans. Magn.*, vol. 26, no. 6, pp. 3155-3172, Nov. 1990.

[51] S. Gopalaswamy and P. McEwen, "Read channel issues in perpendicular magnetic recording," *IEEE Trans. Magn.*, vol. 37, no. 4, pp. 1929-1931, Jul. 2001.

[52] R. He and N. Nazari, "An analytical approach for performance evaluation of partial response systems in the presence of signal-dependant medium noise," in *Proc. IEEE Intl. Conf. Global Telecommun. (GLOBECOM)*, 1999, vol. 1b, pp. 939 –943.

[53] T. Oenning and J. Moon, "Modeling the Lorentzian magnetic recording channel with transition noise, " *IEEE Trans. Magn.*, vol. 37, no. 1, pp. 583-591, Jan. 2001.

[54] J.G. Proakis, *Digital Communications, 4th Edition*. Singapore: McGaw-hill Higher Education, 2001, chap. 5.

[55] J.W.M. Bergmans, *Digital Base-band Transmission And Recording*. Netherlands: Kluwer Academic Publishers, 1996, chaps. 5, 7, 6.

[56] K. Han and R. Spencer, "Comparison of different detection techniques for digital magnetic recording channels," *IEEE Trans. Magn*. vol. 31, no. 2, pp. 1128-1133, Mar. 1995.

[57] B. Farhang-Boroujeny, Adaptive Filters Theory and Applications. Singapore: John Wiley & Sons, 2000, chap. 5.

[58] J. Caroselli, S.A. Altekar, P. McEwen, and J.K. Wolf, "Improved detection for magnetic recording systems with media noise," *IEEE Trans. Magn*., vol. 33, no. 5, pp. 2779-2781, Sep. 1997.